



HAL
open science

Liquid alloys under electromagnetic fields seen at macroscale: transport processes, phase transition and behavior of free surface

Olga Budenkova

► **To cite this version:**

Olga Budenkova. Liquid alloys under electromagnetic fields seen at macroscale: transport processes, phase transition and behavior of free surface. Chemical and Process Engineering. Université Grenoble Alpes, 2022. tel-03593335

HAL Id: tel-03593335

<https://hal.science/tel-03593335>

Submitted on 7 Mar 2022

HAL is a multi-disciplinary open access archive for the deposit and dissemination of scientific research documents, whether they are published or not. The documents may come from teaching and research institutions in France or abroad, or from public or private research centers.

L'archive ouverte pluridisciplinaire **HAL**, est destinée au dépôt et à la diffusion de documents scientifiques de niveau recherche, publiés ou non, émanant des établissements d'enseignement et de recherche français ou étrangers, des laboratoires publics ou privés.

Université Grenoble Alpes

Laboratoire de Science et Ingénierie de Matériaux et Procédés
UMR CNRS 5266, Université de Grenoble Alpes

HABILITATION A DIRIGER DES RECHERCHES
Specialité: Mécanique des fluides énergétiques, Procédés

Olga Budenkova

**Liquid alloys under electromagnetic fields seen at
macroscale: transport processes, phase transition and
behavior of free surface**

Defended on 10 February 2022

devant le jury composé de:

Mr. Eric Beaugnon

Professor, Université Grenoble Alpes, Examiner

Mr. Gérard Berthiau

Professor, Université de Nantes, Reviewer

M^{me} Kerstin Eckert

Professor, Helmholtz-Zentrum Dresden-Rossendorf, Examiner

Mr. Dmitry Eskin

Professor, Brunel University, Reviewer

Mr. Alain Jardy

Director of research CNRS, Université de Lorraine, President of the jury

Mr. Joël Sommeria

Director of research CNRS, Université Grenoble Alpes, Reviewer

Mr. Piotr Zabinski

Professor, AGH University of Science and Technology, Examiner

Contents

Acknowledgments	4
Foreword	5
1 Introduction	8
1.1 Electromagnetic fields: basics	9
1.2 Expected effects of DC and AC magnetic fields	10
1.3 Summary	14
2 Solidification of alloys under the polyphase AC magnetic fields	15
2.1 Effect of RMF and TMF, columnar solidification, ternary alloys	19
2.1.1 Effect of RMF on solidification in microgravity	23
2.1.2 Effect of TMF on solidification in terrestrial conditions	26
2.2 Application of TMF and Equiaxed Growth in the AFRODITE benchmark	29
2.2.1 Estimation of the Lorentz force in the AFRODITE benchmark . . .	31
2.2.2 Equiaxed model for the AFRODITE benchmark	32
2.2.3 Application of the equiaxed model to the AFRODITE benchmark with TMF	34
2.3 Conclusion	35
2.3.1 The author contribution	36
3 Application of DC Magnetic Field in solidification of alloys	38
3.1 Experiments and theory of Magneto-Thermoelectric Force in application to solidification of alloys: state of art	39
3.2 Effect of the size and orientation of a solid particle on the intensity of the thermoelectric current	41
3.3 Intensity and configuration of the liquid flow around a spherical particle due to Magneto-ThermoElectric force	44
3.3.1 Analytical solution of an uncoupled convective magneto-thermo- electric problem for a spherical particle	45

3.3.2	Numerical solution for a coupled convective magneto - thermoelectric problem for a spherical particle and co-directed vectors \mathbf{B} and $\mathbf{G}_{T,\infty}$	47
3.3.3	Comparison of the analytical and numerical solution for a coupled magneto-thermoelectric problem	47
3.4	Conclusion	49
3.4.1	The author's contribution	50
4	Application of single-phase AC magnetic fields in processing of metallic alloys and measurements of their properties	51
4.1	Application of monophasic AC magnetic fields for nuclear waste treatment	51
4.2	Electromagnetic levitation: an environment and a measurement tool	55
4.2.1	Modeling of electromagnetic levitation in μg	56
4.2.2	Experimental set-up for the measurements of the thermophysical properties of the liquid metals in Terrestrial conditions	60
4.3	Conclusion	62
4.3.1	The author's contribution	62
5	Conclusion, ongoing projects and perspectives	63
5.1	Ongoing projects	65
5.2	More distant future...	67
	Bibliography	67
	A Curriculum Vitae	75
	B List of publications	81

Acknowledgments

I would like to express my deep gratitude to the jury membres, Prof. Eric Beaugnon, Prof. Gérard Berthiau, Prof. Kerstin Eckert, Prof. Dmitry Eskin, Dr. Alain Jardy, Dr. Joël Sommeria and Prof. Piotr Zabinski for their agreement to examine this work. The questions which I got regarding my Thesis and my oral presentation¹ of the work made me think again about all these phenomena which are waiting to be considered and to be taken into account. I have noted all of the remarks!

Organization of this great but unpredictable “COVID-type” defense was possible only due to our group manager Khadija Rassouli to whom I would like to express my special thanks.

I should recognize, of course, that a great part of the presented results would not be attained without the guidance of Prof. Yves Fautrelle, always available for the discussions. I deeply appreciate assistance and encouragement from Dr. Yves Du Terrail and Prof. Yves Delannoy. Not only they assured the possibility of the numerical modeling in EPM, but my acquaintance with the modeling of electromagnetic fields happened due to their competence and willingness to share their knowledge. In these days Dr. Annie Gagnoud explains me patiently and kindly the subtleties in numerical modeling of EPM, although I am certainly not (yet?) at the same level. And this is supported with passionate discussions and explanation coming from Dr Roland Ernst.

My actual work on levitation would hardly ever been started without my initiation to it by Dr. Jacqueline Etay and Christian Garnier. The help which I am getting now from Dr. Didier Chaussende and the technical team of SIMAP, Stephane Massucci, Benjamin Pichat, Ghatfan Hassan is precious.

I could continue this list of gratitude for several pages more since I got kind support and great collaborations from many people throughout (already) many years. Please be sure that this is memorized and deeply acknowledged!

To conclude, I thank my former colleagues from the Ioffe Institute for the permanent moral support, my friends and my parents.

¹I am writing this paragraph almost a week after the defense

Foreword

During my studies at Saint-Petersburg Polytechnic University², I acquired strong knowledge in thermal physics, a domain of physics which studies processes where temperature plays the important role. Yet, obviously, that spans from quantum physics to astrophysics... The thermal physics courses were accompanied by hydrodynamics courses. In my PhD thesis, carried out at the Ioffe Institute of the Russian Academy of Sciences³, I applied this knowledge to the numerical studies of heat transfer processes in the Czochralski growth of semi-transparent refractory crystals, which led me to the field of **Materials and Elaboration Processes**.

My research activity at the SIMAP laboratory⁴, where I arrived in 2007 as a PostDoc, started with the numerical studies of the effect of convection in solidification of binary alloys in columnar structure, i.e. for the immovable solid phase. Under terrestrial conditions, melt flow always exists during casting processes because of gravity and local thermal and concentration gradients inherent to solidification of multi-component materials. Convection is responsible for various kinds of defects, most important of which are macro and meso-segregations, i.e. non-uniform distribution of the components in the solidified samples. Meso-segregation that can be seen as channels or “spots” may form even if solidification conditions seem to be stabilizing, i.e. the flow does not spread over large distance and decays with time. Yet, more often the combination of the thermal and concentration gradients happens to have a destabilizing effect and intensifies natural convection that creates also macro-segregation (over the scale of the sample) while meso-segregation may be aggravated. On the other hand, some experimental observations reports that proportion of equiaxed grains increases in solidified samples if strong convection exist during solidification. Because of the strong coupling of heat and mass transfer processes at significantly different space scale, numerical modeling is probably the only way to understand the effect of convection. In particular, numerical studies that I performed, were intended to support experimental activity within the FP6 project IMPRESS⁵. In parallel, I participated in the numerical benchmark proposed in the framework of the ANR SMACS [1, 2]. Due to the latter benchmark, I implemented a lever-rule based model for solidification of the eutectic binary alloys in ANSYS[®] Fluent[®] and later extended it to the solidification of ternary alloys. For the sake of brevity, these works are not presented here but my further work on

²<https://english.spbstu.ru/>

³http://www.ioffe.ru/index_en.html

⁴Science et Ingénierie des Matériaux et Procédés <https://simap.grenoble-inp.fr/>

⁵Intermetallic Materials Processing in Relation to Earth and Space Solidification, <https://cordis.europa.eu/project/id/500635/reporting/fr>

solidification of alloys has been largely based on models and results of models validation that I got during the PostDoc period.

In 2011, I passed the CNRS⁶ competition and was recruited as researcher in the section 10 “Fluid and reactive media: transport, transfer, transformation processes” (“Milieux fluides et réactifs : transports, transferts, procédés de transformation”). My project was related to the solidification of the alloys under the action of the electromagnetic fields, denoted hereafter as EMF. Actually, electromagnetic fields have been used in metallurgy since a long time with various aims, for instance:

- to overcome the unstable natural convection with the structured forced flow;
- to increase the homogeneity of the components or of nucleants via better mixing of the melt;
- to enhance the heat transport due to convection and get more uniform temperature field;
- to increase fragmentation of the solid phase and produce solid phase in the form of equiaxed grains;
- to damp the flow and to assure diffuse growth regime.

However, mainly application of the EMF was based on trial and error methods and often lead to rather puzzling results. Consequently, it was supposed that numerical modeling of such processes with consistent comparison with experimental results would improve our understanding of the role of EMF fields in solidification processes. Following this idea, I continued my activity. A model for columnar solidification of ternary alloy that I developed during my PostDoc was applied to the simulation of on-ground experiments performed in University of Miskolc with traveling magnetic fields (Chapter 2 section 2.1 and 2.1.2). Then, the PhD work of Tao Wang allowed us to develop a numerical model for solidification of binary alloys in *equiaxed structure*, when solid phase is allowed to move. This model was used to perform numerical simulation of the AFRODITE benchmark on solidification of Sn-Pb alloys with electromagnetic stirring (Chapter 2, section 2.2) and further to the solidification of the large-size industrial ingot.

In parallel with modeling of the effect of AC magnetic fields on solidification, I was involved in the studies of the effect of the continuous magnetic field on the motion of the dendrites and liquid flow. Rather simple configuration of the set-up developed for these in-situ studies by the group MCA from IM2NP⁷ allowed mathematical formulations for which I obtained some analytic solutions and compared them with numerical computations realized with advanced numerical methods (Chapter 3).

Further, favorable environment and strong expertise accumulated in the group EPM allowed me to move deeper into the studies of the application of the electromagnetic fields. In particular, the PhD work of Rémi Bourrou allowed me to acquire knowledge about the applications and effects of monophasic AC fields, often referred to as inductive heating. The subject was actually opposite to the solidification since metallic and glass phases were supposed to be heated and held in the liquid state (Chapter 4, section 4.1).

⁶Centre National de la Recherche Scientifique <https://www.cnrs.fr/en>

⁷Equipe Microstructures de Croissance Auto-organisées de l’Institut Matériaux Microélectronique Nanosciences de Provence, <https://www.im2np.fr/equipe-microstructures-de-croissance-auto-organisees-mca>

Interestingly, in parallel, I have been studying the same kind of the electromagnetic field, monophasic AC, but of a significantly higher frequency and applied to an object of a completely different size. These studies, related to the measurements of the thermophysical properties of the liquid metals (Chapter 4, section 4.2) represent my actual field of interest. This activity continues in practical way with upgrading of the experimental set-up and implementation of revised measurement procedures.

Chapter 1

Introduction

Electromagnetic fields (EMF) offer a wide spectrum of possible manipulations over metallic materials in their liquid and solid phases during elaboration or recycling processes. Moreover, EMF can be used as the environment and also as the auxiliary tool in measurement procedures. Effective use of electromagnetic fields is related to a good electrical conductivity of metallic materials and is based on the phenomenon of electromagnetic induction that allows one to affect the process without having physical contact with materials. For further discussion, it is convenient to distinguish the use of *monophase* and *polyphase alternate current magnetic fields* (AC magnetic fields) and *continuous magnetic fields* (DC magnetic fields). Generally, polyphase AC magnetic fields are used to create driving forces which produce motion inside the load, i.e. so-called electromagnetic stirring in the liquid metals, while heating of the load is not aimed and might happen, but at the minor extent. Monophase AC fields, on the contrary, are used to perform intense heating of the load. The heating is accompanied by the appearance of magnetic pressure at the surface of metallic volume, which can lead to deformation of free surface of a large pool of liquid metal with formation of a dome and even levitation of the metallic sample. Finally, utilization of DC magnetic fields is mostly related to the damping of the convective transport inside the liquid metals.

It should be underlined that the classification of the electromagnetic fields given above according to the effects that they produce is applicable, actually, only to ideal cases, i.e. if infinitely long samples and inductors are considered and if some effects which are supposed to be of the second order are neglected. Once the real loads of finite sizes are considered, the resulting effect of application of a particular electromagnetic configuration can be different from that which is classically presented. Thus, for example, application of monophase AC fields results in creation of electromagnetic force which, depending on geometry of the liquid melt, may initiate liquid motion. Another, probably, more spectacular example is the appearance of the magneto-thermoelectric force when moderate and strong DC magnetic fields are applied to the solidification of alloys. This force is capable to alter the microstructure of the solid phase and the macro-segregation in the solidified alloys.

Because of the strong coupling between the electrical parameters and geometry of the electromagnetic coils with geometry, position and electromagnetic properties (generally

depending on temperature) of the loads and macroscopic motion of (or inside the) latter, numerical studies are usually required to reveal the effects of the EMF in a particular system.

1.1 Electromagnetic fields: basics

Before going to the examples of the role of electromagnetic fields in various engineering processes related to materials science, let us remind the basic notions and to outline the major effects that can be expected with applications of various EMF.

Generally, application of electromagnetic fields is based on the two effects well-known for solid conducting objects:

- i) any electric current flowing in the conductor creates its own magnetic field
- ii) motion of a conductor in the magnetic field generates electric current inside the conductor

The former effect allows one to create magnetic fields in space using arrangement of coils (also noted hereafter “inductors”) of various geometry to which the electric potential $\Delta\Phi$, static or oscillating, can be applied¹. With the *static* potential difference, the direct current, DC, circulates in the coil and creates the continuous (DC) magnetic field. Oscillating potential difference generates the alternated current (AC) in the coil and creates around it magnetic field, oscillating with the same frequency. According to the second effect mentioned above, if an electrically conductive load is placed near the coil, then the generation of the eddy current, heating, and the resulting effect of the electromagnetic force in the load depend on the character of the magnetic field, whether it is DC, monophasic AC or polyphasic AC.

Complete formulation of electromagnetic problem consists of four Maxwell equations – Faraday’s law, Ampere’s law, Gauss law for electric and magnetic field – completed with constitutive laws that relates electric charges, electric current with electric and magnetic fields and polarization, etc. For non-magnetic and non-polarizable materials this system of equation is simplified. Furthermore, modeling of electromagnetic field in application to material processing generally satisfies so-called “steady-state” or “electromagnetic” approximation. The latter assumes that the period of time required for electric charges to be redistributed within the media is significantly shorter than the characteristic time for variation of electromagnetic fields, i.e. no free (non-compensate) electric charges exist in conductors. Then, equations to be solved are:

$$\text{Maxwell-Thomson law: } \nabla \cdot \mathbf{B} = 0 \quad (1.1) \quad \text{Ampere law: } \nabla \times \frac{\mathbf{B}}{\mu_m} = \mathbf{j} \quad (1.3)$$

$$\text{Faraday law: } \nabla \times \mathbf{E} = -\frac{\partial \mathbf{B}}{\partial t} \quad (1.2) \quad \text{Ohm law: } \mathbf{j} = \sigma \mathbf{E} + \sigma \mathbf{u} \times \mathbf{B} \quad (1.4)$$

¹Alternatively, traveling (AC) magnetic field and continuous (DC) magnetic fields can be created with system of permanent magnets, which, in case of traveling field should be put in motion whereas for DC field they should be kept stationary. Yet, this does not change general ideas presented below

The volume density of the Lorentz force acting in the conductor is given as

$$\mathbf{F}_{emf} = \mathbf{j} \times \mathbf{B}, \quad N/m^3 \quad (1.5)$$

and volume density of the heat released due to the resistance heating – Joule effect – is given as

$$q_{emf} = \frac{\mathbf{j}^2}{\sigma}, \quad \frac{W}{m^3} \quad (1.6)$$

The set of equations (1.1)-(1.6) can be combined and presented in different manner to highlight various phenomena related to electromagnetic field depending on their “nature”. In particular, it can be demonstrated that Laplace force given by eq.(1.5) can be split into two parts, corresponding to electromagnetic pressure and to driving force, also known as irrotational and rotational parts of electromagnetic force:

$$\mathbf{F}_{emf} = \mathbf{F}_{emf,IR} + \mathbf{F}_{emf,R} = -\underbrace{\nabla \left(\frac{\mathbf{B}^2}{2\mu_m} \right)}_{\text{magnetic pressure}} + \underbrace{\frac{1}{\mu_m} (\mathbf{B} \cdot \nabla) \mathbf{B}}_{\text{driving force}} \quad (1.7)$$

Generally, the system of equations (1.1)-(1.4) is to be coupled with the hydrodynamic equations which, if required, should provide the velocity field \mathbf{u} to Ohm’s eq. (1.4) and take the Lorentz force (eq. (1.5)) as an input parameter. If the heating effects are of interest, the energy transport equation should be added with the Joule power given by the eq. (1.6) set as a source term and to provide temperature distribution in the conductor since the latter can have crucial effect on the electrical conductivity (and magnetic permeability) of the materials. Furthermore, as it can be seen in the chapter 4, for some processes the calculation of the shape of the load is essential, i.e. numerical methods allowing such calculations, like Volume-of-Fluids (VOF), Level Set, Phase Field, etc should be added to the system.

1.2 Expected effects of DC and AC magnetic fields

Let us describe briefly effects that the electromagnetic fields of different character are expected to produce on the load. Hereafter the load is considered to be electrically conductive and paramagnetic with the constant relative permeability $\mu_r = \mu_m/\mu_0 = 1$ ($\mu_0 = 4\pi \cdot 10^{-7}$ H/m, magnetic permeability of the vacuum). The latter is true for the liquid metals since their melting temperature is above the Curie point.

Effect of DC magnetic field: damping of the flow

The decay of the DC magnetic field \mathbf{B} depends only on the distance to the coil (or the permanent magnet) due to which the field is generated, i.e. at which extent the DC magnetic field penetrates the load depends only on this distance. Since the magnetic field does not vary in time, the eddy current may appear only if motion exists in the load.

Effect expected with the application of the DC magnetic field is illustrated in fig.1.1. Here the eddy current

$$j_{DC} \approx \sigma U_0 B_0$$

is generated and the Laplace force

$$F_{DC} \approx \sigma U_0 B_0^2$$

appears in a direction opposite to the flow.

Note that the Laplace force tries to diminish the component of the fluid flow which tends to cross the lines of the magnetic field (fig.1.1) that may also alter configuration of the flow.

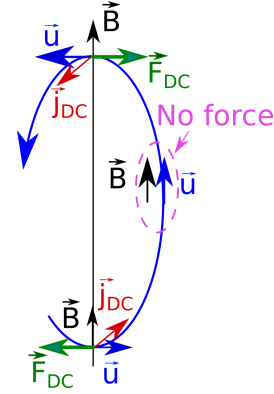


Figure 1.1: Damping effect expected with use of the DC magnetic field: the induced electromagnetic force is directed opposite to the velocity of the liquid

Yet, such effect of the DC magnetic field not always attained. For example, if the direction of DC magnetic field is parallel to the vorticity of the flow $\nabla \times \mathbf{u}$, the non-uniform electric potential Φ appears in the liquid according to the eqs.(1.8)-(1.10) and prevents circulation of the eddy current.

One can interpret that the eddy current due to the liquid motion $j_U \approx \sigma u B$ is canceled by the current due to the potential gradient $j_\Phi \approx \sigma \nabla \Phi$. Consequently, no Lorentz force appears in the liquid.

$$\mathbf{E} = -\nabla \Phi \quad (1.8)$$

$$\nabla \cdot \mathbf{j} = \sigma \nabla \cdot (-\nabla \Phi + \mathbf{u} \times \mathbf{B}) = 0 \quad (1.9)$$

$$\Delta \Phi = \nabla \cdot (\mathbf{u} \times \mathbf{B})$$

$$\Delta \Phi = \mathbf{B} \cdot (\nabla \times \mathbf{u}) \quad (1.10)$$

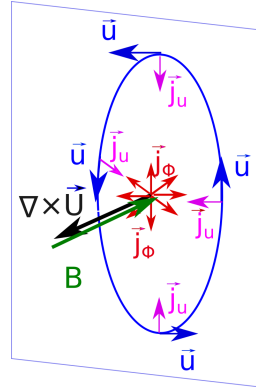


Figure 1.2: Cancelling of the eddy current when DC magnetic field is directed parallel to the vorticity of the flow: $j_{Phi} \approx \sigma \nabla \Phi$ cancels $j_u \approx \sigma u B$

The role of the continuous magnetic field in solidification of alloys is discussed in the chapter 3 with respect to the thermoelectric current which might appear during solidification and interact with the superposed magnetic field. Interestingly, in this situation the DC magnetic field is actually a reason which cause convective flow in the liquid. Yet, at the same time it modifies and damps this convection as it is demonstrated in the section 3.3, chapter 3.

Use of monophasic AC magnetic field: magnetic pressure and heating

Let the electric current which circulates in the coil oscillate with the angular frequency $\omega = 2\pi f$, in other words it changes periodically its direction in the coil. Magnetic field around each coil oscillates with the same frequency and its intensity decreases with the

distance to the coil, resulting magnetic field in space is a superposition of standing waves. Oscillating magnetic field seen by the electrically conductive load generates in the latter oscillating eddy current that also creates magnetic field. Superposition of the phase-shifted oscillating fields may result in “zeroing” of the magnetic field inside the load. A characteristic thickness inside the load within which the intensity of the magnetic field rapidly decreases is known as skin depth, and is defined with eq.(1.11).

$$\delta_m = \sqrt{\frac{2}{\mu_m \sigma \omega}} \quad (1.11)$$

Interaction of the eddy current and the magnetic field inside the load leads to the appearance of the Lorentz force composed of the constant mean value and the oscillating part, the mean value is oriented inside the load and tends to “squeeze” the load. It can be shown that for the cylindrical inductor and the load, with both of infinite lengths, the mean component of the Lorentz force is perpendicular to the load surface (fig. 1.3).

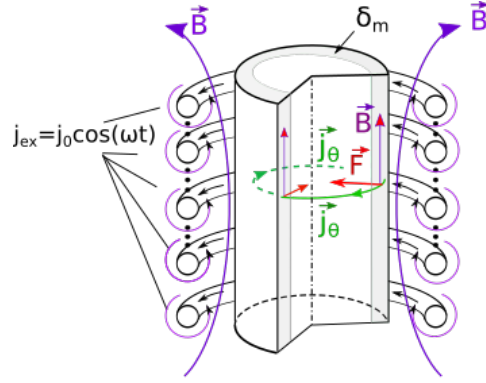


Figure 1.3: With use of the monophas AC current in the coil: magnetic fields penetrates in the load over the distance δ_m (eq.(1.11)), the eddy current is mainly generated there. The averaged in time Lorentz force is directed perpendicularly to the surface of the load and plays the role of a magnetic pressure.

In reality, finite dimensions of the load (or inductor) leads to the non-uniform intensity of magnetic field along the surface of the load that make the irrotational part of the electromagnetic force, $(\mathbf{B} \cdot \nabla)\mathbf{B}$, non-zero, i.e. driving force appears in the load as well and affect fluid motion.

Magnetic pressure can compete with gravity and may serve for making the levitation. However, the primary desired effect in industry is the heating which is produced in the load, according to the eq.(1.6), mainly within the skin depth.

Application of the polyphase AC magnetic field: electromagnetic stirring

The system with AC magnetic field can be realized with use of n electric currents, the l^{th} current has a phase $\varphi_l = (l-1) \cdot 2\pi/n$, then the l^{th} current is presented as $I_l = I_0 \cos(\omega t + \varphi_l)$ where I_0 is the amplitude of the AC current taken similar for all currents. Example of realization of a linear **three-phase** motor is shown in fig.1.4, where $\varphi_2 = 120^\circ = 2\pi/3$ and $\varphi_3 = 240^\circ = 2 \cdot 2\pi/3$. Let us consider the time moment $t = 0$, then, according to the adopted scheme, the instant values for the currents which enter corresponding coils (conductors) are $I_{1,in} = I_0$, $I_{2,in} = I_0 \cos(2\pi/3) = -I_0/2$ and $I_{3,in} = I_0 \cos(4\pi/3) = -I_0/2$, while at the exit from the coil these currents are expressed as $I_{1,out} = -I_0$, $I_{2,out} = I_0 \cos(2\pi/3 + \pi) = I_0/2$ and $I_{3,out} = I_0 \cos(4\pi/3 + \pi) = I_0/2$. This is taken into account, and the “entrance” and “exit” for each current are arranged in space in such a way to get a wave of the AC current travelling in space, as shown in fig.1.4. Consequently, in

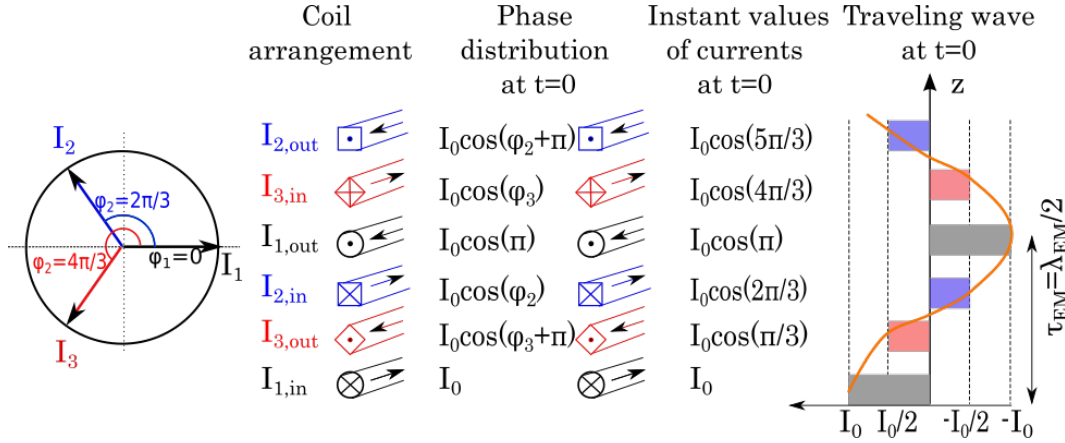


Figure 1.4: Illustration to the current supply in a three-phase linear motor: the 3 AC currents circulate in the system with phase difference of $2\pi/3 = 120^\circ$, but due to the coils' arrangement the phase shift between neighboring coils is $\pi/3$. Attention should be given to the actual current direction: the “out” direction with the phase $(\varphi_3 + \pi)$ corresponds finally to the direction “in”.

the surrounding space one gets a superposition of electromagnetic waves traveling along the inductor, i.e. of the type $B \cos(\omega t - kz)$, where z is the coordinate taken along the “generatrix” of the inductor and k is a wave number. The latter is related to the so-called “pole pitch” τ_{EM} (which is a distance between the coils where the current phase is reversed by π) and to the associated wavelength λ_{EM} (which presents the distance between the coils with the phase difference 2π), see eq.(1.12) and fig.1.4, fig.1.5 for the notations, the index EM is introduced to avoid confusion with similar notations in other chapters.

The amplitude of the traveling magnetic waves (intensity of the magnetic field B) is related to the amplitude of the AC current I_0 and decreases with the distance to the coil, yet, it also depends on the coil arrangement, in particular, on the pole pitch. Consequently, the skin depth over which the magnetic field penetrates in the load also depends on the pole pitch and can be expressed, for example, as in eq.(1.13)[3].

$$k = \frac{2\pi}{\lambda_{EM}} = \frac{\pi}{\tau_{EM}} \quad (1.12)$$

$$\frac{1}{\delta_p} = \frac{\pi}{\sqrt{2}\tau_{EM}} \left(1 + \sqrt{1 + 4 \left(\frac{\tau_{EM}}{\pi\delta_m} \right)^4} \right)^{1/2} \quad (1.13)$$

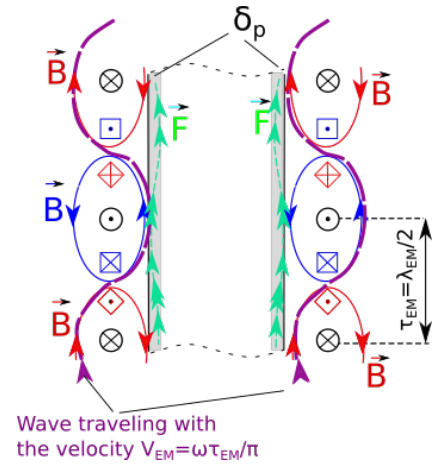


Figure 1.5: Illustration to the polyphase AC system: the driving force is directed mainly along the surface of the load, the skin depth δ_p depends both on the pole pitch τ_{EM} , the frequency and the electrical conductivity of the load

where δ_m is the skin depth as it is defined for the case of the application of the monophasic AC magnetic field, i.e. given by the eq.(1.11). Consequently, if the pole pitch τ is compa-

rable with or less than the “monophase” skin depth δ_m , then the value of $(\tau/(\pi \cdot \delta_m))^4$ may be significantly less than unity and the skin depth δ_p will be defined only by τ according to the eq.(1.13). This can happen, for example, if the frequency of the AC current used for the coil alimentation is not very high, about tens of Herz.

It should be mentioned also that, contrary to the monophase AC system the heating of the load is not expected if the polyphase configuration is used. Indeed, with similar electric current circulating in the coils polyphase system generates less total energy because of superposition of waves with different directions: the waves generated by coils are compensated by the waves generated by coils where the current has the opposite phase.

1.3 Summary

The following table summarizes the information given above with respect to the effect of the electromagnetic fields of different origin: DC, monophase AC and polyphase AC.

	DC m.f.	monophase AC m.f.	polyphase AC m.f.
applied potential external current	$\Delta\Phi_{ext} = const$ $j_{ext} = const$	$\Delta\Phi_{ext} = u_0 \cos(\omega t)$ $j_{ext} = j_0 \cos(\omega t)$	$\Delta\Phi_{ext,p} = u_0 \cos(\omega t + \varphi_p)$ $j_{ext,p} = j_0 \cos(\omega t + \varphi_p)$
magnetic field outside load	$\mathbf{B} = \mathbf{B}(\mathbf{r})$	Standing wave $\mathbf{B} = \mathbf{B}_0(\mathbf{r}) \cos(\omega t)$	Traveling wave $\mathbf{B} = \mathbf{B}_0(\mathbf{r}) \cos(\omega t + \mathbf{k}\mathbf{r})$ Wavenumber $k = \frac{2\pi}{\lambda_{EM}} = \frac{\pi}{\tau_{EM}}$ Wave velocity $V_{EM} = \omega \tau_{EM} / \pi$
penetration depth into load	–	$\delta_m = \sqrt{\frac{2}{\mu_m \sigma \omega}}$	$\frac{1}{\delta_m} = \Re\{\sqrt{k^2 + i\mu_m \sigma \omega G}\}$, \Re -real part, $i = \sqrt{-1}$
expected effect	Damping of the motion (flow)	Magnetic pressure heating	Driving force: stirring

Table 1.1: Summary of parameters characterized DC, monophase AC and polyphase AC magnetic fields

Remarks to the notations used in the table 1.1:

In the expression for the potential difference $\Delta\Phi_{ext,p}$ and density of the electric current $j_{ext,p}$, p is the “index of a loop” which constitute the coil and φ_p is the phase associated with that loop. It should be noted that this representation is extremely simplified for the sake of brevity.

Chapter 2

Solidification of alloys under the polyphase AC magnetic fields

In casting processes performed under terrestrial conditions, the melt flow always appears because of gravity and local thermal and concentration gradients (denoted hereafter \mathbf{G}_T and \mathbf{G}_C , respectively) inherent to solidification of multi-component materials. Convection is responsible for various kinds of defects, most important of which are macro and meso-segregations¹, the latter may form even if solidification conditions seem to be stabilizing, i.e. the flow does not spread over large distance and decay with time. Yet, more often combination of \mathbf{G}_T , \mathbf{G}_C happens to have destabilizing effect and intensifies natural convection that creates also macro-segregation while meso-segregation may be aggravated. On the other hand, some experimental observations report that proportion of small equiaxed grains (which are supposed to promote better mechanical properties) increases in solidified samples if strong convection exists during solidification. Consequently, in many applications, it seems interesting to have intense yet well-controlled fluid flow and this can be realized, for example, with *polyphase AC magnetic fields*. Then, a problem which arises is related to the choice of parameters of AC magnetic field. Nowadays this is solved mostly with trial and error methods, yet many experimental results remain puzzling because during solidification multiple phenomena come into play one after another and leave their imprints on the final segregation patterns and microstructure. Possibility of in-situ observations would facilitate interpretation but it is not always realizable (in fact, impossible in industrial processes) first, while the second reason is that even the direct observation provides limited information about the process. Therefore, *numerical modeling is of ultimate importance* for comprehension of the effect of application of AC magnetic fields. Yet, at this point – necessity of use of numerical modeling – another problem comes out related to the fact that numerical models used for the study of solidification at macroscale are complex and most of them use (multiple) closure relations either adopted from other scientific fields or based on experimental observation. Thus a

¹Segregation is a non-uniform distribution of the components of the alloy; notions “macro” and “meso-” are related to the linear size of areas affected by segregation and actually depend on the scale at which the process is considered. Hereafter “meso-” corresponds to the scale comparable with the size of a dendrite grain while “macro-” is comparable with the characteristic size of the process

vicious circle is formed and here we come to the necessity of having so-called benchmark experiments and to the verification and validation of the models using these benchmarks. Yet, although multiple experimental results are reported on solidification of alloys, very few of them provide detailed analysis of samples along with information about solidification conditions which would be sufficient for numerical simulations of the process and for comparison with numerical results as discussed below.

Because of rather accurate analysis of concentration distribution at different stages of solidification along with presentation of solidified macrostructure, experiments performed by Hebditch and Hunt several decades ago [4] have been modeled repeatedly and still attracts attention of modelers. Proposed size and configuration of experimental set-up with vertical position of the crucible and lateral cooling allows studying of effect of natural convection on solidification process at various scales, including macro-scale, while size of the volume (100 mm×60mm×10 mm) remained reasonable from the point of view of phenomena which occur at the scale of dendrite grains. Based on Hebditch & Hunt experiment, construction of solidification benchmark, referred hereafter as AFRODITE, was initiated in early 2000s in SIMAP with the idea to study the effect of electromagnetic stirring on solidification. Since then the AFRODITE set-up has been continuously optimized and a complete series of experiments on solidification of binary alloy Sn-Pb was realized between 2005-2013 with and without use of polyphase AC magnetic fields in a form of traveling magnetic field, TMF (cf. section 1.2).

Although on-ground laboratory environment allows one to create sophisticated and well equipped set-up, uncontrolled gravity and natural convection still impede study of fluid flow on solidifying microstructure. Indeed, natural convection prevails if intensity of electromagnetic stirring is weak, and contributes to the flow if stirring is moderate. Moreover, at the very small scale the forced convection is ineffective, hence, gravity flow prevails between dendrites, in the so-called *mushy zone*. To avoid effects related to gravity, MICAST² project under coordination of European Space Agency [5] was launched at the end of last century aimed to use the Material Space Laboratory onboard the International Space Station (MSL-ISS). Since then experiments on solidification of different Al-based alloys without and with the action of rotating magnetic field (RMF) were performed at MSL-ISS. These microgravity experiments were accompanied with on-ground experimental activity assured by a research group headed by Prof. A. Roósz at the University of Miskolc in Hungary. On-ground experiments were performed with RMF and TMF which created forced convection significantly more intense than that in AFRODITE experiment and configuration of solidification zone was also different.

Obviously, to study the effect of the electromagnetic stirring on solidification processes one should be able, first of all, to model solidification processes of alloys. My activity between 2007-2010 was devoted to the study of solidification theory, application of already developed codes and development of my own code, based on the lever rule. All these models dealt with the *columnar* dendrite growth in solidification of *binary alloys*. A

²Abbreviation MICAST stands for “Microstructure Formation in Casting of Technical Alloys under Diffusive and Magnetically Controlled Convective Conditions”, see https://www.esa.int/Science_Exploration/Human_and_Robotic_Exploration/Blue_dot/Materials

summary of my activity in this field is presented below in a table.

In the next sections the numerical simulations of more complicated processes are considered and include:

- columnar growth in *ternary alloys* under effect of RMF within the frame of MICAST project, cf. section [2.1.1](#)
- columnar growth in *ternary alloys* under effect of TMF within the frame of MICAST project, cf. section [2.1.2](#)
- *equiaxed growth* in binary alloys under effect of TMF in application to the AFRODITE experiment, cf. section [2.2](#)

Following the strategy already adopted in the group EPM, the codes were based on the use of ANSYS® Fluent®, numerical description of solidification phenomena was realized by introduction additional equations via User-Defined Scalars (UDS) and User-Defined Functions (UDF).

Publications referred in the table

- a. O. Budenkova, A. Noepfel, J. Kovács, A. Rónaföldi, et al, **Materials Science Forum**, **2010**, 649, 269-274
- b. A. Noepfel, A. Ciobanas, X. D. Wang, K. Zaidat, N. Mangelinck, O. Budenkova, et al, **Met. Mat. Trans. B**, **2010**, 41 (1), 193-208
- c. M. Bellet, H. Combeau, Y. Fautrelle, D. Gobin, M. Rady, E. Arquis, O. Budenkova, et al., **Int. J. Thermal Sci.**, **2009**, 48(11), 2013-2016
- d. S. Ganina, V. Ginkin, O. Budenkova, B. Saadi, et al, **Defect and Diffusion Forum**, **2012**, 326-328,599-604, [doi:10.4028/www.scientific.net/DDF.326-328.599](https://doi.org/10.4028/www.scientific.net/DDF.326-328.599)
- e. H. Combeau, M. Bellet, Y. Fautrelle, D. Gobin, E. Arquis, O. Budenkova, et al., **IOP Conf. Series: Mater. Sci. and Eng.**, **2012**, 33, 012086 [doi:10.1088/1757-899X/33/1/012086](https://doi.org/10.1088/1757-899X/33/1/012086)
- f. O. Budenkova, C. Nagy, Y. Du Terrail Couvat et al., Proc.6th Decennial Conf. on Solidif. Procesing, 25-28 July 2017, Old Windsor, UK
- g. R. Boussaa, O. Budenkova, L. Hachani, X-D. Wang, et al, **Proc. 141st TMS Annual Meeting and Exhibition, Symp. CFD Modeling and Simulation in Materials Processing, 11-15 March, Orlando, Florida, USA, 2012**, ISBN:978-1-11829-615-8,163-170
- h. R. Boussaa, L. Hachani, O. Budenkova, V. Botton, et al., **Int. J. Heat and Mass Transfer**, **2016**, 100, 680-690, [10.1016/j.ijheatmasstransfer.2016.04.120](https://doi.org/10.1016/j.ijheatmasstransfer.2016.04.120)

Columnar growth

segregation patterns from different simulations are presented

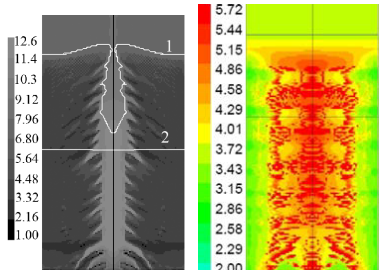
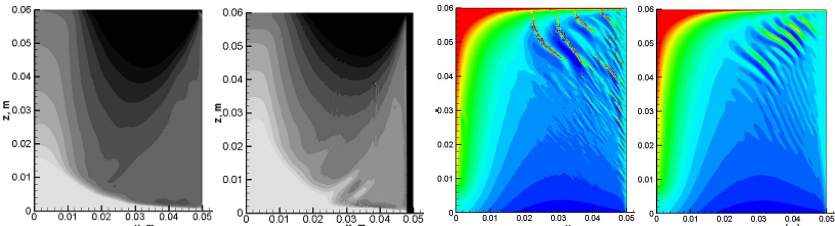
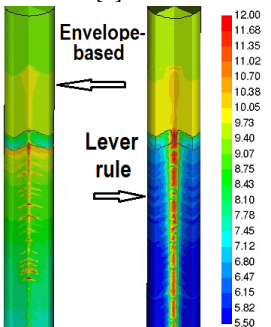
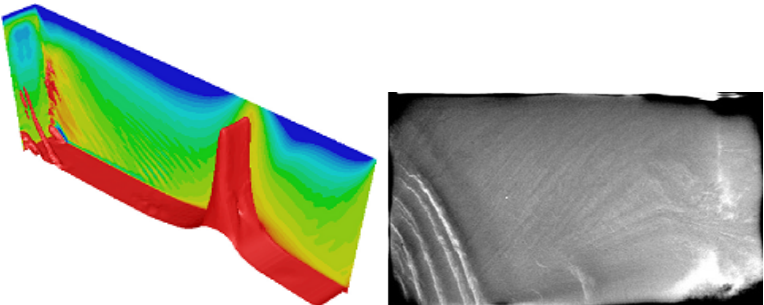
Existing envelope-based models	Development of a columnar model based on the lever rule for binary alloys, LRBM
<p>Binary Al-7wt%Si under RMF in microgravity, ref.[a] and Al-3.5wt%Ni under TMF and gravity, ref.[b], simulations.</p> 	<p>Comparison of LRBM with other realizations: Sn-Pb, and Pb-Sn alloys, calculations are made in response to the call for a numerical benchmark, cf. refs.[c,d,e] below. <u>All figures are obtained numerically</u></p> 
<p>Comparison with LRBM: Al-7wt%Si under RMF, in 3D, ref.[f] below</p> 	<p>Application to AFRODITE, Sn-3wt%Pb alloy, natural convection, cf. refs.[g,h] below. In the left (color) – simulations, in the right (gray scale) – experimental results</p> 

Table 2.1: Summary of activity with binary columnar solidification

2.1 Effect of rotating and traveling electromagnetic fields on columnar solidification of Al-based ternary alloys studied in MICAST project

To date the set of several samples of Al-7wt%Si, Al-7wt%Si-1wt%Fe and Al-7wt%Si-1wt%Mn were directionally solidified in microgravity in the frame of MICAST project. Several samples of two former alloys were solidified with different cooling rates under diffuse growth and forced convection created by RMF with studying of microstructure, that were primary dendrite arm spacing (PDAS, λ_1) and secondary dendrite arm spacing (SDAS, λ_2). Analysis of Al-Si and Al-Si-Fe samples revealed that while dependence of PDAS on local solidification rate were similar for the two alloys ($\lambda_1 \sim v_{sol}^{-0.25}$), coarsening process of secondary dendrite arms for the ternary alloy did not correspond to the expected one. In particular, it was found that SDAS of Al-7wt%Si-1wt%Fe were insensitive to the forced fluid flow since with activated RMF the coarsening of secondary dendrite arms occurred as it would happen in diffuse conditions, fig.2.1. This was assigned to the effect of intermetallics which is formed during solidification of this alloy in form of platelets and therefore can block fluid flow within the mushy zone, fig.2.2.

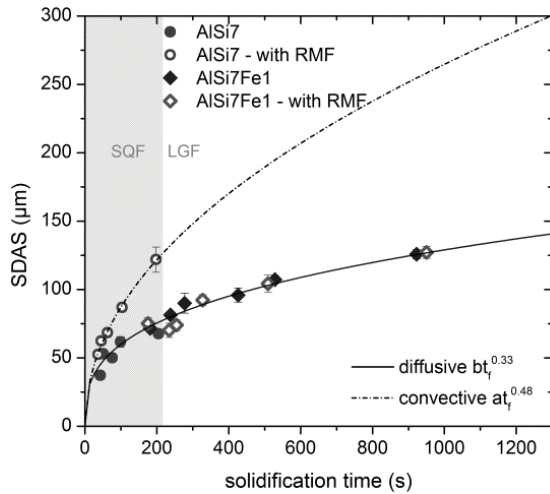


Figure 2.1: Secondary dendrite arm spacing (SDAS) on solidification time for Al-7wt%Si and Al-7wt%Si-1wt%Fe alloys processed under diffusive conditions (filled symbols) and forced fluid flow (RMF; open symbols) with Solidification and Quench Furnace (circles, grey shaded region) and Low Gradient Furnace (diamonds)[6]

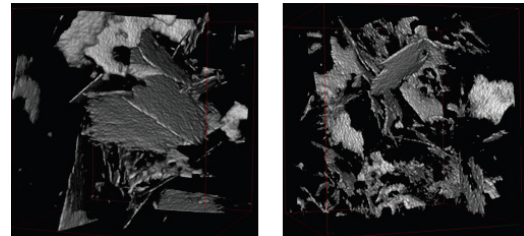


Figure 2.2: The Al-7wt%Si-1wt%Fe sample solidified with the RMF, pulling velocity $v=0.6\text{mm/s}$, then cut and studied using tomography with Al-based dendrites etched out, i.e. only *intermetallics* remains. The left images is from the outer parts of the sample and the right image is from the center, size $650 \times 650 \times 650\mu\text{m}$ [7]

Solidification path for Al-7wt%Si-1wt%Fe alloy in Al-rich corner is traced over the liquidus surface in fig.2.3, the starting point corresponds to the nominal concentration of the alloy. According to this path, the solidification of hypo-eutectic Al-7wt%Si-1wt%Fe occurs in three stages: during the first stage the Al-rich dendrites are formed, during

the second stage the growth of Al-rich dendrites is accompanied with the formation of β -intermetallics, and finally the alloy solidifies at the "eutectic point". During solidification at the eutectic point, to the already mentioned two solid phases, the formation of Si-rich phase is added. In the analysis of the samples of Al-7wt%Si-1wt%Fe solidified under the action of RMF the accumulation of the intermetallic at the samples' center was observed along with segregation there of Si (fig.2.3b). Given above images issued from tomography analysis (fig.2.2) showed, that, in fact, the size of intermetallic platelets at the center of the sample was larger than at its periphery if solidification was performed with RMF stirring.

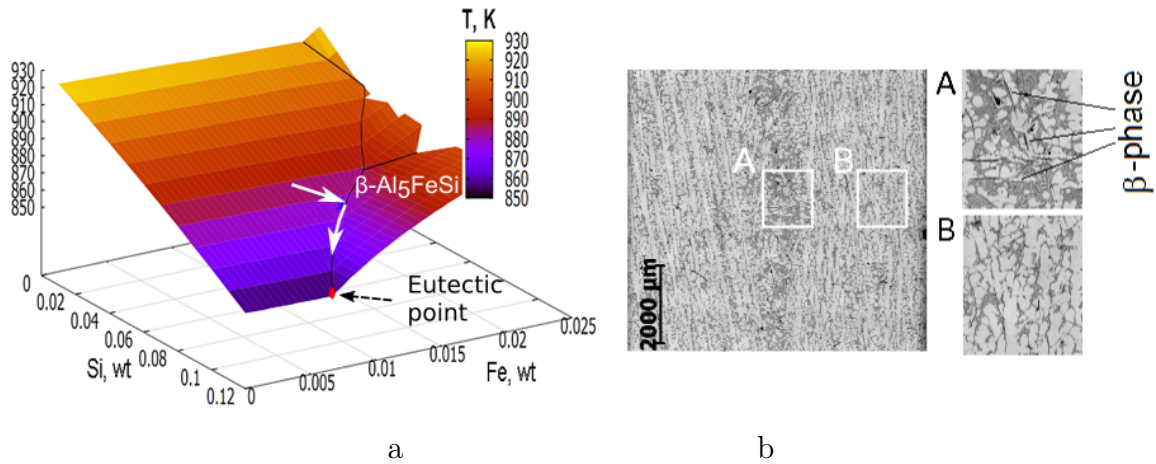


Figure 2.3: a) Liquidus plane for AlSiFe alloy in Al-rich corner, interpolated with data obtained from CIRIMAT (J.Lacaze, private communication); b) Image of the sample showing segregation of Si and accumulation of β -phase in the sample center

There are two remarks to be made. First, from the point of view of simulation at macroscale, both, accumulation of the intermetallics, and larger size of the intermetallic platelets, are interpreted via the increase of volume fraction which corresponds to that intermetallic phase. Secondly, to our knowledge, nucleation and growth process of intermetallic plates has never been observed experimentally with good enough resolution despite some attempts, therefore, there is no data about their growth kinetics, required undercooling, etc. In other words there are no grounds to prefer one or another solidification model which relates growth kinetics, solute and temperature fields. According to our experience related to simulations of other processes and comparison discussed above, it can be assumed that classical models based on lever rule or Scheil rule should provide results sufficiently good at first approximations. Consequently, I extended the lever-rule based model for the simulations of the ternary alloys with accounting for the simultaneous formation of two solid phases, one of which is intermetallics.

In the presentation below the following notations were introduced:

- Indices S, L are for the solid and liquid phase, respectively, and indices α and β are for the Al-rich solid phase (corresponding to the dendrites) and for the intermetallics, respectively
- f_i - is the volume fractions for the phase $i=S, L, \alpha, \beta$. For instance, f_α, f_β are volume fractions for the Al-rich dendrite phase and for the intermetallics, respectively

-
- $C_{Si,i}, C_{Fe,i}$ - concentration of the Si and Fe, respectively, in the phase $i=S,L,\alpha, \beta$
 - k_j - equilibrium partition coefficient between the solid and the liquid phase for the corresponding component $j = \{Si, Fe\}$ when Al-rich dendrite is formed
 - q_1, q_2, r_1, r_2 - auxiliary coefficients determined from the phase diagram.

The lever-rule based model extended for ternary alloy relies on the following assumptions:

- linearized liquidus plane in Al-rich corner, which is approximated with “partial” slope coefficients m_{Si} and m_{Fe} via eq.(2.1)
- eutectic line is approximated as a straight line that gives a set of linear relations between $C_{Si,L}$ and $C_{Fe,L}$, $C_{Si,L}$ and T_L , and $C_{Fe,L}$ and T_L , eqs.(2.2) and (2.3).

Consequently, obtain

For liquidus plane:

$$T_L = T_m + m_{Si}C_{Si,L} + m_{Fe}C_{Fe,L} \quad (2.1)$$

with

$$m_{Si} = \frac{\partial T_L}{\partial C_{Si,L}} \quad \text{and} \quad m_{Fe} = \frac{\partial T_L}{\partial C_{Fe,L}}$$

For eutectic line:

$$C_{Si,L} = q_1 T_L + r_1 = q_{Fe} C_{Fe,L} + r_{Fe} \quad (2.2)$$

or

$$C_{Fe,L} = q_2 T_L + r_2 = q_{Si} C_{Si,L} + r_{Si} \quad (2.3)$$

- according to the lever rule, chemical diffusion in the solid and the liquid is infinitely fast³
- for solidification of aluminium-rich dendrites the concentrations of the solute i in the solid $C_{i,\alpha}$ and the liquid $C_{i,L}$ are related via the corresponding equilibrium partition coefficients:

$$C_{Si,\alpha} = k_{Si} C_{Si,L} \quad \text{and} \quad C_{Fe,\alpha} = k_{Fe} C_{Fe,L} \quad (2.4)$$

- the concentration of each component in the intermetallic phase is known by composition of the latter, taken as Al_5SiFe

These conditions gives following relations for the conservation of solute concentration:

For liquidus plane:

$$f_\alpha + f_L = 1 \quad (2.5)$$

$$C_{Si} = f_L C_{Si,L} + f_\alpha k_{Si} C_{Si,L} \quad (2.6)$$

$$C_{Fe} = f_L C_{Fe,L} + f_\alpha k_{Fe} C_{Fe,L} \quad (2.7)$$

For eutectic line:

$$f_\alpha + f_\beta + f_L = 1 \quad (2.8)$$

$$C_{Si} = f_L C_{Si,L} + f_\alpha k_{Si} C_{Si,L} + f_\beta C_{Si,\beta} \quad (2.9)$$

$$C_{Fe} = f_L C_{Fe,L} + f_\alpha k_{Fe} C_{Fe,L} + f_\beta C_{Si,\beta} \quad (2.10)$$

Further, the combination of eqs.(2.1) – (2.7) leads to the quadratic equation from which the volume fraction of Al-rich dendrites can be calculated during the first stage of solidification (eq.(2.12)). With this fraction known, variation of concentrations in the liquid $C_{Si,L}$ and $C_{Fe,L}$ can be also calculated (eqs.(2.13) and (2.14)). For the second stage of solidification corresponding to the eutectic line, another system of equations is obtained and provides information about

³This definition, introduced in the solidification theory for a small volume subjected to the solidification, is somehow in contradiction with the modeling at macroscale. In the latter, this statement for the infinitely fast diffusion is actually supported for those computational cells where solidification takes place, i.e. $f_s \neq 0$ and $f_L \neq 0$ but not in the pure liquid ($f_s = 0$), where diffusion, in fact, is often neglected and only convective transport is taken into account

evolution of the volume fractions f_α and f_β .

For liquidus plane:

$$f_s = f_\alpha \quad (2.11)$$

$$f_\alpha = \frac{-B + \sqrt{B^2 - 4AE}}{2A} \quad (2.12)$$

where

$$A = (k_{Si} - 1)(k_{Fe} - 1)(T_L - T_m)$$

$$B = (k_{Si} + k_{Fe} - 2)(T_L - T_m)$$

$$- (k_{Fe} - 1)m_{Si}C_{Si,L}$$

$$- (k_{Si} - 1)m_{Fe}C_{Fe,L}$$

$$E = T_L - T_m - m_{Si}C_{Si,L} - m_{Fe}C_{Fe,L}$$

$$C_{Si,L} = \frac{C_{Si}}{1 + f_\alpha(k_{Si} - 1)} \quad (2.13)$$

$$C_{Fe,L} = \frac{C_{Fe}}{1 + f_\alpha(k_{Fe} - 1)} \quad (2.14)$$

For eutectic line:

$$f_s = f_\alpha + f_\beta \quad (2.15)$$

$$f_\alpha = \frac{\frac{C_{Si} - C_{Si,L}}{C_{Si,L} - C_{Si,\beta}} - \frac{C_{Fe} - C_{Fe,L}}{C_{Fe,L} - C_{Fe,\beta}}}{\frac{C_{Fe,L} - C_{Fe,\beta}}{C_{Fe,L} - C_{Fe,\beta}} - \frac{C_{Si,L} - C_{Si,\beta}}{C_{Si,L} - C_{Si,\beta}}} \quad (2.16)$$

$$f_\beta = \frac{\frac{C_{Si} - C_{Si,L}}{C_{Si,L}(1 - k_{Si})} - \frac{C_{Fe} - C_{Fe,L}}{C_{Fe,L}(1 - k_{Fe})}}{\frac{C_{Fe,L} - C_{Fe,\beta}}{C_{Fe,L}(1 - k_{Fe})} - \frac{C_{Si,L} - C_{Si,\beta}}{C_{Si,L}(1 - k_{Si})}} \quad (2.17)$$

$C_{Si,L}$ and $C_{Fe,L}$ can be found from the equations for eutectic line, eqs.(2.2) (2.3).

The system of governing equations for solidification with convection in the liquid phase and stationary solid phase with intrinsic velocity $\mathbf{u} = f_L \mathbf{u}_f$ is written as follows:

$$\rho_0 \frac{\partial \mathbf{u}}{\partial t} + \frac{\rho_0}{f_L} (\mathbf{u} \cdot \nabla) \mathbf{u} = \nabla(\mu_l \nabla \mathbf{u}) - f_L \nabla p - \frac{\mu_l f_L}{K_p} \mathbf{u} + f_L \tilde{\rho} \mathbf{g} + f_L \mathbf{F} \quad (2.18)$$

$$\rho_0 c_p \frac{\partial T}{\partial t} + \rho_0 c_p \mathbf{u} \nabla T = \varkappa \nabla^2 T + \rho_0 L \frac{\partial f_s}{\partial t} \quad (2.19)$$

$$\rho_0 \frac{\partial C_{Si}}{\partial t} + \rho_0 \mathbf{u} \nabla C_{Si,L} = 0 \quad \rho_0 \frac{\partial C_{Fe}}{\partial t} + \rho_0 \mathbf{u} \nabla C_{Fe,L} = 0 \quad (2.20)$$

$$\tilde{\rho} = \rho_0(1 - \beta_T(T - T_{ref}) - \beta_{C,Si}(C_{Si,L} - C_{Si,ref}) - \beta_{C,Fe}(C_{Fe,L} - C_{Fe,ref})) \quad (2.21)$$

$$K_p = K(1 - f_\beta)K \quad (2.22)$$

$$K = \frac{\lambda_2^2}{180} \frac{f_L^3}{(1 - f_L)^2} \quad (2.23)$$

The effect of the **electromagnetic force**, which in the case of the polyphase AC field should be a driving force (cf. section 1.2) is taken into account in the momentum equation (2.18) via the term $f_L \mathbf{F}$, it is supposed that \mathbf{F} is calculated elsewhere or estimated analytically.

Other terms in the eq.(2.18) correspond to :

- the volume force which accounts for the Boussinesq approximation for the thermal and concentration volume expansion of the liquid $f_L \tilde{\rho} \mathbf{g}$ with $\tilde{\rho}$ calculated with eq.(2.21)
- and to the pressure drop $\mu_l f_L \mathbf{u} / K_p$ due to the flow through the solid dendrites, the latter considered as a porous media and Darcy approximation is used with the permeability K_p , which depends on fraction of intermetallics according to the eq.(2.22)-(2.23).

The system of equations (2.18)-(2.23) is closed with equations allowing calculations of solid fraction and concentration of components in the liquid which should be calculated with eqs.(2.12)-(2.14) if solidification occurs with aluminium-rich dendrites only or with eqs.(2.2)-(2.3) and (2.16), (2.17) if aluminium-rich dendrites grow together with intermetallics, respectively.

This model was applied to simulation of several experiments performed in the frame of MICAST under microgravity and in on-ground facility at Miskolc University. Only some of these simulations are presented below.

2.1.1 Effect of Rotating Magnetic Field on directional solidification of a ternary Al-Si-Fe alloy in microgravity

Experiments in microgravity were performed in low-gradient furnace (MSL-LGF) initially and solidification - quenching (MSL-SQF) furnace afterwards, the latter one is still in use. Both furnaces are aimed at directional solidification of cylindrical sample with radius of $R_0 \approx 4\text{mm}$ placed with its crucible inside the electromagnetic coil which generates rotating magnetic field, the scheme is shown in fig.2.4. Electromagnetic coil can move along the sample, its displacement is coordinated with the pulling mechanism of the sample such that the position of the coil center corresponds (approximately) to that of the solidification front, i.e. to the position of dendrites' tips defined prior to the experiment. The thermocouples placed in grooves at the external side of the crucible allows one to follow temperature evolution along the sample during the experiment and their measurements can be used as boundary conditions for energy equation.

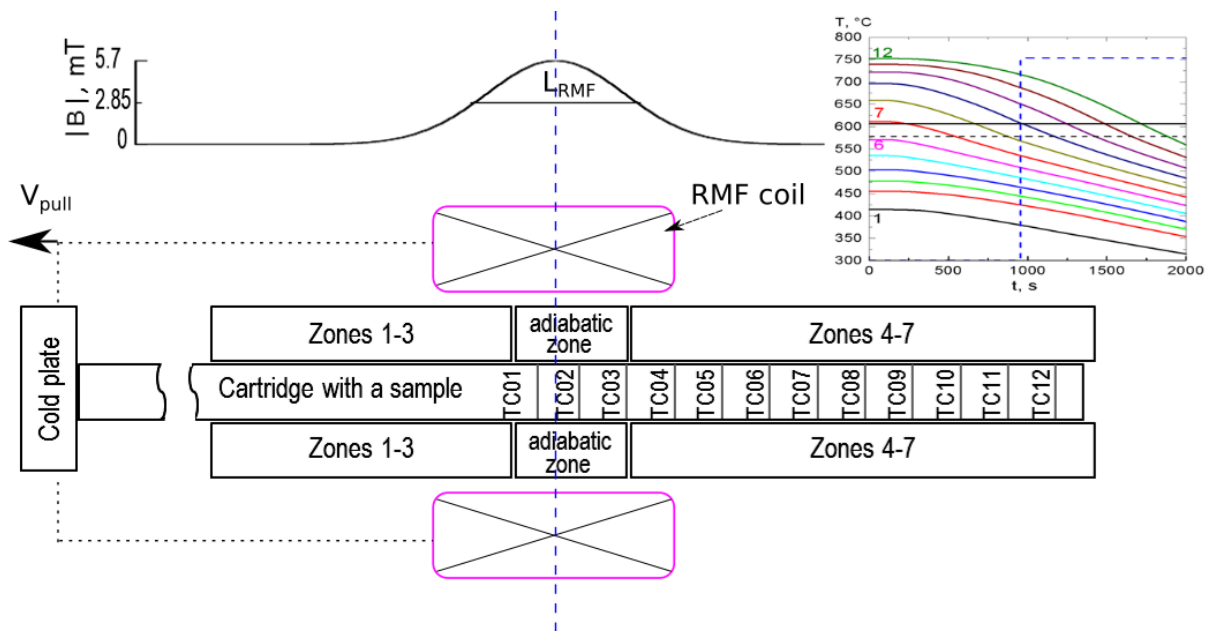


Figure 2.4: Scheme for the experimental set-up used in solidification experiment in microgravity with indication of the positions of thermocouples and example of obtained temperature curves, the intensity of the effective value of magnetic field along the growth direction is shown at the top part of the drawing [8]

Analytic solution known for rotating magnetic field in case of cylindrical load and coil of infinite height gives the Lorenz force directed azimuthally inside the load. In the present case, since the height of the coil is smaller than the sample, other components of the force should appear in the liquid because of end effects. Yet, detailed information about the construction of the electromagnetic coil could not be provided by its producer that makes detailed simulation of electromagnetic field impossible. Consequently, to diminish the number of uncertain parameters, the Lorenz force acting in the liquid was approximated with only one azimuthal component

which decreased along the sample with the distance from the center of the coil according to the provided measurement as described with eq.(2.24). The maximal value of the magnetic field measured within the furnace if $B_{max} = 5.7\text{mT}$ and the frequency of the AC current is $f = 57\text{Hz}$, the value of the coefficient Z_B was determined to satisfy measurements of the magnetic field.

$$\mathbf{F} = \mathbf{e}_\varphi F_\phi(r, z)$$

$$F_\phi(r, z) = \pi f \sigma B_{max}^2 R_0 \times$$

$$\times \Phi\left(\frac{r}{R_0}\right) \times \Psi(z) \quad (2.24)$$

$$\text{with } \Phi\left(\frac{r}{R_0}\right) = \frac{r}{R_0}$$

$$\text{and } \Psi(z) = \exp[-Z_B(z - z_c)^2]$$

where the coefficient

$$Z_B \approx 297\text{m}^{-2}$$

and z_c correspond to the axial coordinate of the center of the coil

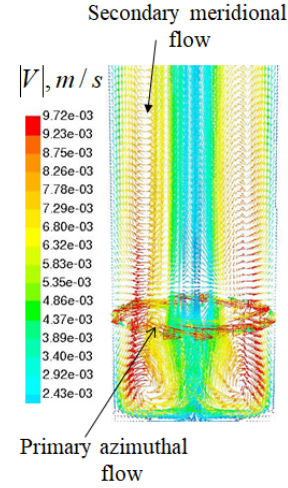


Figure 2.5: Scheme of the flow under the effect of RMF in microgravity experiments, from presentation at SP17 conference

In microgravity the buoyancy effects are absent, so, in the system of equations (2.18)-(2.23), the density variation given by (2.21) may be omitted and electromagnetic force given with eq.(2.24) generates well-known structure of vortices in the liquid [9, 10] which consist of the primary azimuthal and secondary meridional flow, mainly ahead of the solidification front fig.2.5. Intensity of the flow decreases drastically when it enters the mushy zone, i.e. when it starts to interact with the growing solid phase, fig.2.6a.

According to the experimental data, with the activation of the RMF, the solidification continued with growth of columnar dendrites, therefore penetration of the flow in the mushy zone for a binary alloy would depend on primary and secondary arm spacing. Based on consideration accepted in [2] as well as our results in [11], the permeability of the mushy zone was calculated with use of secondary dendrite arm spacing λ_2 (eq.(2.23)), yet, a question arises if intermetallics can impede flow to pass through the mushy zone. The latter assumption was proposed by Steinbach & Ratke [12] to explain insensitivity of SDAS of the ternary alloy to the forced convection (fig.2.1). It seems that this question cannot be answered yet with the macroscopic model and requires further studies, preferably with in-situ observation of microstructure development. Indeed, according to the phase diagram (fig.2.3a), the solidification starts with the appearance and growth of Al-rich dendrites while β -intermetallics appears in the liquid whose composition should be more rich in aluminium and iron compared to the nominal composition of the alloy and, what is important, at *lower temperature*. Due to the solute transport by convective vortices generated by electromagnetic force, the enriched liquid exists ahead of the tips of Al-rich dendrites, yet, the second condition for lower temperature and configuration of the thermal field during *directional* crystallization impose that nucleation of intermetallics happens *behind* solidification front. If one remains in the frame of the equilibrium model without accounting for any kinematic effects,

the structure of the mushy zone and fluid flow would correspond to the one given in fig.2.6 [8]. There the mushy zone may be considered being of two parts, the first (“primary” mushy zone) of them consists of Al-rich dendrites whose fraction is higher near crucible walls and lower at the centerline 2.6b. This part is followed by the secondary (“eutectic”) mushy zone composed of dendrites and intermetallic plates 2.6c. According to the simulations, the fraction of intermetallics is higher closer to the axis of the sample, that explain experimental observation described above with larger intermetallic plates at the center of the sample.

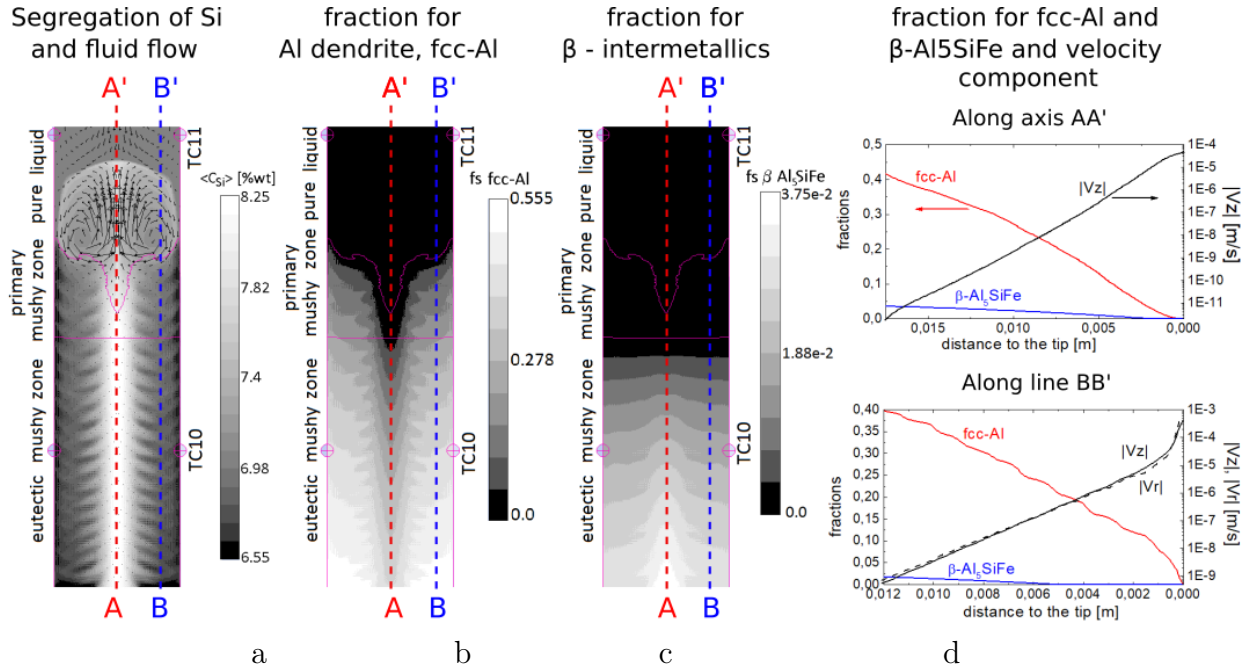


Figure 2.6: Results of simulations: a) Segregation pattern for Si and superposed flow field; b) Distribution of the volume fraction of Al-rich dendrites; c) Distribution of the volume fraction of β -intermetallics; d) Distribution of volume fractions of the two solid phases and module of the axial and radial velocities along the lines indicated in figs.a-c, from [8]

In the graph constructed over the axis of the sample and over a line at the distance of 3mm from the axis (1 mm from the crucible wall) variation of the fractions of dendrites and intermetallic plates is given together with variation of axial and radial velocities along these lines fig.2.6d. It is seen that when intermetallic phase appears, velocity value is already very small, i.e. if intermetallic plates block the flow, they make it zero instead of $\approx 2 \cdot 10^{-6}$ m/s according to the equilibrium solidification model.

It should be underlined, however, that we have no information about growth process of intermetallics! For example, the latter may really nucleates at the deep mushy zone but it has anisotropic form (platelets) which may grow rapidly toward dendrite tip instead of lateral development in the mushy zone. At this point, the lack of experimental observation makes physical and mathematical description of the process impossible and let researchers to guess or to make assumptions regarding it.

Also, presented simulations were performed in two-dimensional axisymmetric form with swirl flow that takes into account azimuthal velocity v_ϕ but assumes that all variables are independent on azimuthal coordinates. Although this assumption is rather strong, it seems to be reasonable

for weak flow which is realized in the present studies. Yet, according to the assumption of axial symmetry, the azimuthal flow cannot affect solidification. Three-dimensional simulations were realized later but confirmed the hypothesis that the flow created by such Lorentz force was generally rather weak and use of 3D approach did not bring new information. One can conclude that more detailed simulations can be made once the growth kinetics of the intermetallics is known.

2.1.2 Effect of Traveling Magnetic Field in directional solidification of a ternary Al-Si-Fe alloy in terrestrial conditions

Experimental facility that can be installed at ISS should meet various restrictions related to their size, weight and power consumption. In on-ground laboratories these restrictions usually do not exist that allows one to construct a large facility even if solidification of small, laboratory-scale samples is foreseen. A unique electromagnetic inductor was produced at Miskolc University (Hungary) allowing realization of vast variety of configurations of traveling magnetic field. In fact, the inductor is composed of two linear motors with flat coils whose connection can be done in different ways. In particular, such configuration allows one to create electromagnetic waves which can travel in the same direction along both motors (either upward or downward) or in different directions, that is, upward on one side and downward on another. Such motion of traveling waves can be done with some phase shift between left and right sides that should lead to inclination of vectors of Lorentz force with respect to the central vertical plane parallel to that of the motors. Experiments on directional solidification of the samples of the ternary Al-7wt%Si-1wt%Fe alloy were performed with use of this inductor to support the experimental solidification campaign in space. Numerical modeling was provided in the frame of the PhD Thesis Csaba Nagy which was co-supervised by Dr. Y. Du Terrail (Grenoble, France), Prof. A. Roosz (Miskolc, Hungary), and me.

To obtain the resulting electromagnetic force acting in the liquid for such construction of the coil, 3D simulation was performed with COMSOL[®] Multiphysics[®] software using the scheme presented in 3D and 2D sketch in fig.2.7. According to the information, provided by the manufacturer of the coil, University of Miskolc, for the experiment presented below, six-phase alimentation was used that means the phase shift of $\phi = \pi/6$ between the neighboring coils, as schematically shown in fig.2.7, the AC frequency was $f = 50Hz$. Details regarding geometry of the coil are given elsewhere [13]. The electromagnetic simulations provided distribution of the effective Lorentz force inside the crucible filled with the melt with corresponding electric conductivity σ_l . Since these studies were realized in the frame of MICAST project, the radius of the crucible was kept equal to that in microgravity: $R \approx 4mm$. Due to a procedure of comparison between simulations of convective heat transfer inside the crucible filled with the melt and measurements which are described elsewhere [14, 13] the Lorentz force calculated with COMSOL[®] Multiphysics[®] software was corrected with a factor 0.1 and used in further simulations of solidification of ternary alloy with system of equations eq.(2.18) given above.

As expected, under the Lorentz force acting downward onto a half of the liquid and upward for another half, the flow presents a single vortex which occupies the whole crucible (fig.2.7). Note that the top of the crucible is closer to the upper end of the inductor that leads to a weaker Lorentz force and the flow also slows down. Such configuration of the flow means that during the directional solidification, in a half of the crucible the rejected solute is brought through the mushy zone toward pure liquid making the next portion of the solidifying sample more enriched.

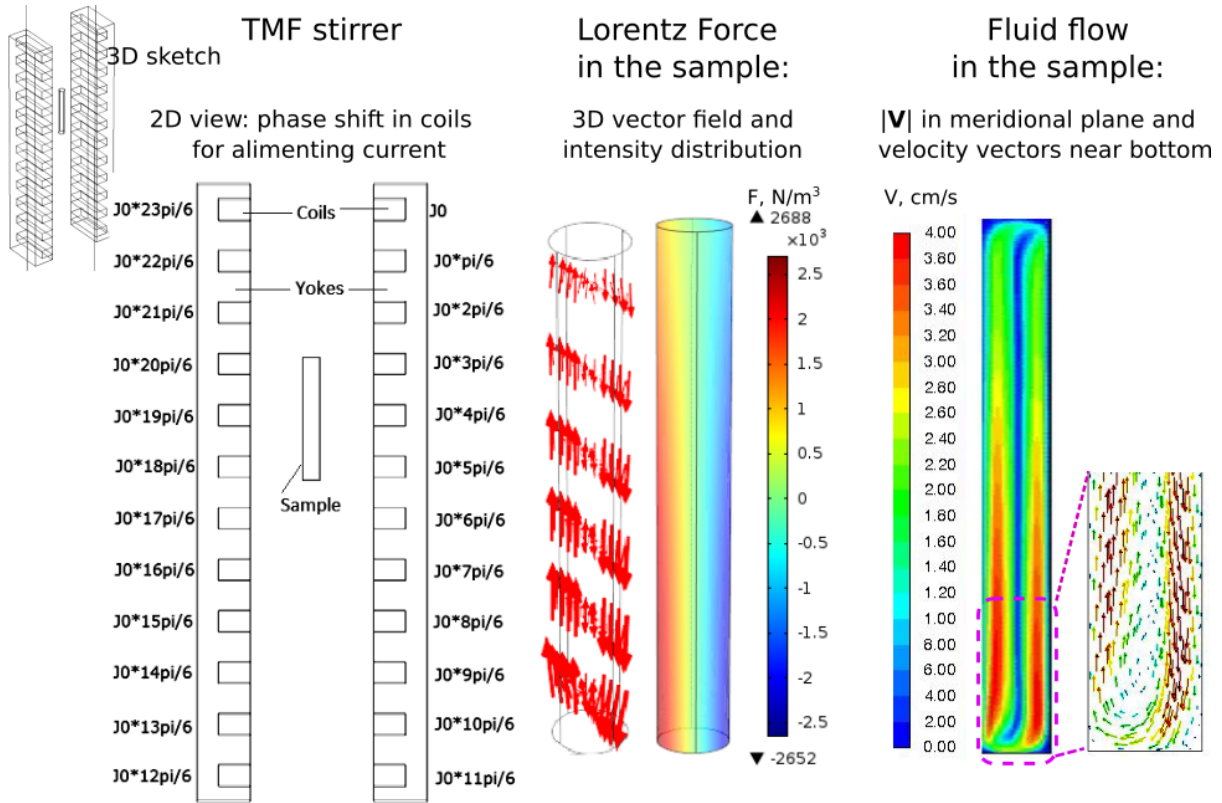


Figure 2.7: Scheme of TMF stirrer developed in the Materials Science Research group of University of Miskolc, Lorentz force in the sample calculated with COMSOL® Multiphysics® software and fluid flow obtained in crucible filled with the melt under the action of calculated force taken with the factor 0.1 and gravity, the figures are taken from the ref. [13]

For another half of the crucible, the flow tends to push the rejected solute back to the mushy zone. It should be reminded that *under normal gravity the buoyancy solute and thermal forces are also active*. It can be expected that under assumption of columnar growth, i.e. stationary solid phase, stirring of the liquid by Lorentz force becomes less efficient in the mushy zone and the buoyancy flow may prevail over it, that may lead to formation of channels, as was observed in the ref [15]. The instantaneous results of simulation are presented along the solidification direction at fig.2.8a and comparison of concentration distribution taken at a cross section of the sample after its solidification with results obtained in simulations are given in fig.2.8b.

Based on the comparison between the results observed in the experiments and obtained in simulations, we can conclude that the developed model for columnar solidification of the ternary alloy allowed us to explain qualitatively the effect of the electromagnetic stirring on segregation in the solidified samples. It would be interesting to make deeper studies related to characteristics of microstructure, i.e. PDAS and SDAS and to look for distribution of intermetallics. Yet, this work remains at discretion of the team of University of Miskolc as owners of samples.

Furthermore, it would be interesting to apply equiaxed model similar to the one presented below which was developed and applied for simulation of AFRODITE experiment, yet, difficulties to be foreseen are related to the appearance and growth of intermetallics whose kinetics is not actually known.

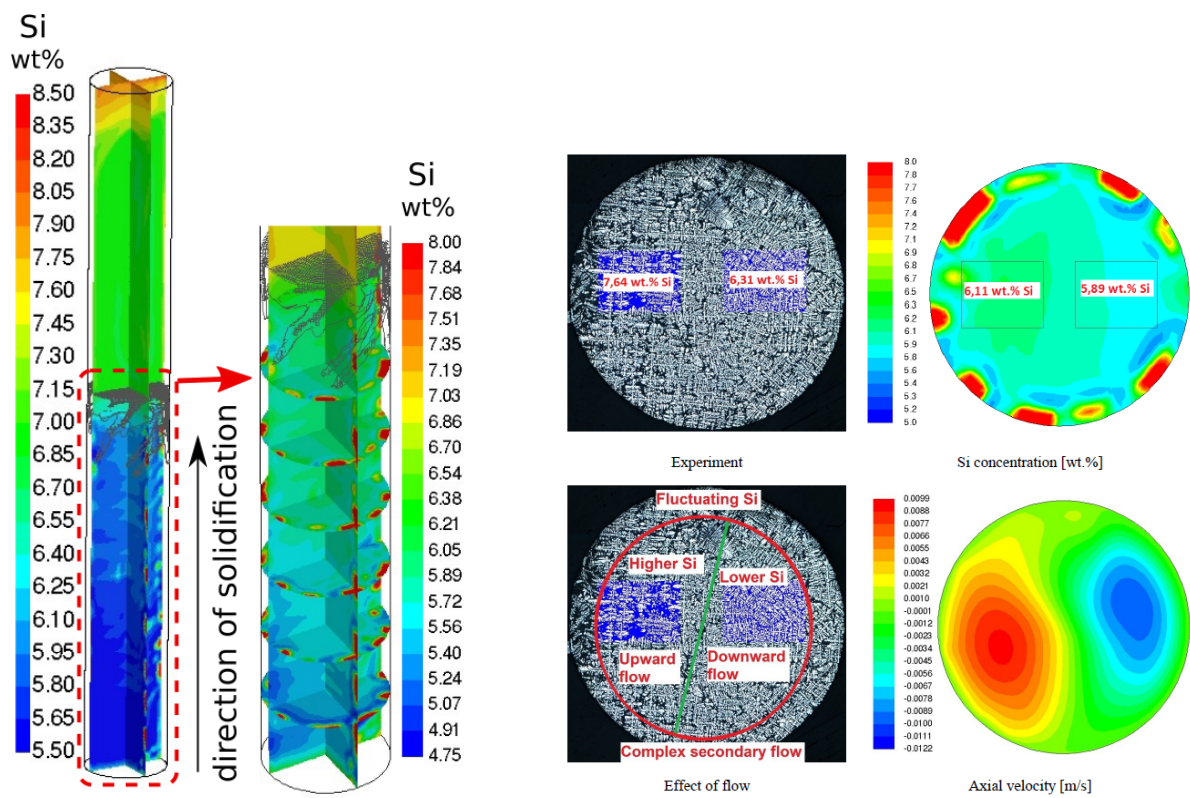


Figure 2.8: Comparison between results obtained in experiment and in calculations in solidification of a ternary AlSiFe-alloy with TMF stirring [13]

2.2 Application of the Traveling Magnetic Field and Equiaxed Growth and in the AFRODITE benchmark

During the columnar regime of solidification the emerging solid phase remains attached to the walls, consequently, convective transport phenomena occur only in the liquid phase. Otherwise, the growing solid grains can be in motion inside the bulk liquid and generally they have a more symmetrical shape, therefore they are called “equiaxed grains” (fig.2.9a). It is known that the appearance and further formation of the columnar or equiaxed grains depend on the thermal and concentration gradient in the liquid, on the density of nucleation centers and on their size which defines the undercooling required for the formation of the stable nuclei. This is summarized via a so-called Hunt-LGK diagram, fig.2.9b).

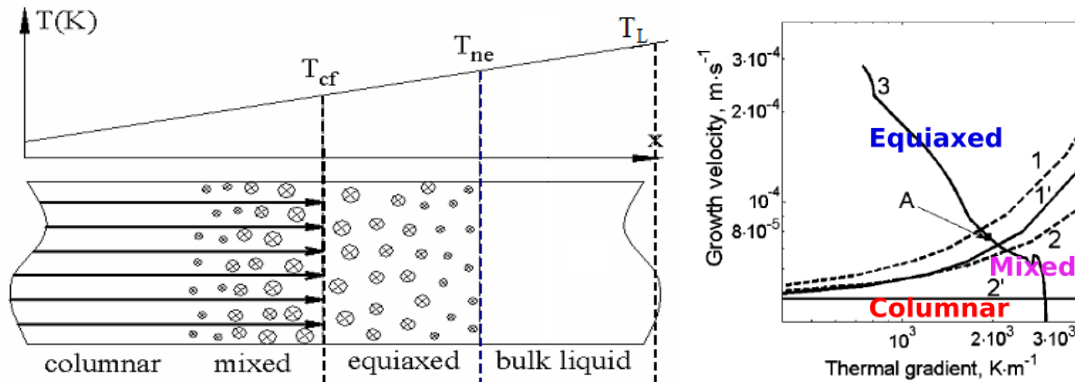


Figure 2.9: a) Presentation of the columnar and equiaxed zone: T_L - liquidus temperature of the alloy, $T_{ne} < T_l$ - temperature of nuclei formation, $T_{CF} < T_{ne}$ - temperature at the tip of columnar dendrites, which can be below the T_{ne} because of kinetics effect, from ref. [16], b) Hunt diagram calculated for the refined Al-7wt%Si alloy, zones of different growth are indicated, from ref. [17]

In industrial casting production, a large equiaxed grain region is often expected because it is supposed to provide better homogeneity than the structure consisting of columnar grains. For instance, in a production of the large steel ingots, the equiaxed grains play the crucial role in the ingot quality. ***For this reason, the numerical models capable to treat equiaxed growth are of vital importance.*** Yet, realization of the latter is much more challenging compared to the columnar growth model because the convective transport phenomena are related to both phases, and even more phenomena should be considered, as indicated in the Table 2.2 below.

Hitherto several equiaxed models for macroscale simulations were presented by various teams, aimed for simulations of the casting of large steel ingots [18, 19, 20, 21], yet, to our knowledge, none of them was validated with a suitable benchmark experiment prior our work devoted to AFRODITE which is described below.

As it was mentioned above, the design of the AFRODITE is based on that of the Hebdith & Hunt experiment [4] with the crucible $5cm \times 10cm \times 1cm$ and water-cooled resisting heaters placed on the lateral sides of the crucible, as shown in fig.2.10. Configuration of the set-up allows one to realize solidification in horizontal direction and to study the effect of the buoyancy flow. Moreover, a flat coil placed below the cavity creates traveling magnetic field (acts as linear

Phenomenon	Columnar growth	Equiaxed growth
Grain growth	Yes, <i>for stationary grains</i>	Yes
Solute mesoscale diffusion	Yes, <i>for stationary grains</i>	Yes
Drag force	Yes, <i>for stationary grains</i>	Yes
Nucleation	No	Yes
Grain motion	No	Yes
Grain packing	No	Yes
Fragmentation of dendrites	No	<i>Probably</i>

Table 2.2: Accounting for phenomena in columnar and equiaxed model

motor) and allows one to study the effect of the forced convection on the solidification process as well. To remind, a distinct feature of the AFRODITE setup is the equipment of the crucible with the array of thermocouples placed over the large wall that allows following of the evolution of the two-dimensional temperature map during the solidification process. The set of thermocouples placed on each lateral heater should allow one to evaluate heat fluxes or/and temperature at the boundaries of solidifying volume.

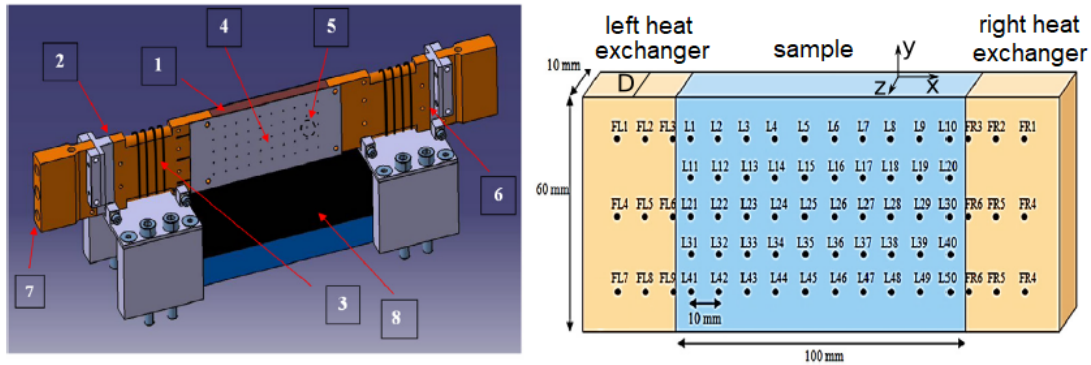


Figure 2.10: Scheme of the AFRODITE facility and sketch showing the positions of the thermocouples on the side wall of the crucible. Indicated components of shown AFRODITE setup : (1) sample, (2) left heat exchanger, (3) resistance, (4) stainless steel crucible, (5) thermocouples positions, (6) right heat exchanger, (7) water cooling system, (8) flat electromagnetic inductor, the figures are taken from the ref. [22]

A list of experiments performed with the AFRODITE set-up can be found elsewhere [23]. In particular, it was found that the electromagnetic stirring in the direction opposite to the flow driven by the thermal buoyancy leads to formation of mostly equiaxed structure in the solidified sample. Accounting for the fact that very probably it was the first experiments with mostly equiaxed structure obtained in a benchmark experiment⁴, its numerical modeling is almost a must for verification and validation of (any) developed equiaxed code.

It must be underlined however that despite the great efforts made to achieve a good control of boundary conditions and to extract maximum information from the experiment, *the uncertainties regarding the electromagnetic driving force and the actual temperature evolution inside the volume near cooling walls still exist* that affect numerical results. Regarding the thermal

⁴the experiment which provides information sufficient for performing its numerical simulation

boundary conditions the uncertainty problem was recognized already in simulations of columnar solidification [22]. Indeed, from the point of view of temperature measurements, a “blind zone” exists near these boundaries because the temperature in the liquid is not known there, but only at the distance of 0.5cm from the wall. Yet, convective flow exists within this liquid zone and its intensity depends both of the supplied heat flux and on the applied stirring force which is not well known either. At the first approximation in simulations, it is supposed that the conductive heat flux prevails over convective one and the temperature at the boundary is recalculated according this assumption.

Further, as discussed in details in subsection below, the electromagnetic field generated within the cavity is not actually known and some of parameters which characterize it are extrapolated from indirect measurements.

Below the results of the numerical simulations of the **experiment on solidification of a binary Sn-10wt%Pb alloy with electromagnetic stirring** is presented.

2.2.1 Estimation of the Lorentz force in the AFRODITE benchmark

Electromagnetic field inside the solidifying volume was generated by the flat inductor placed below the crucible (fig.2.11a). This inductor consisted of set of coils and was alimeted with three-phase AC current with the frequency $f = 50\text{Hz}$. Geometrical size and placement of coils define the pole pitch $\tau = 32\text{mm}$ (distance between coils at which phase difference of alimenting current is 2π), the length of the traveling wave $l = 2\tau = 64\text{mm}$ and the corresponding wave vector $k = 2\pi/l = 98.2\text{m}^{-1}$. For the case of infinite two-dimensional coil and semi-infinite adjacent volume characterized with electrical conductivity σ_l this set of parameters defines analytical solution which was taken as a basis for further analysis of such inductor performed in [24]. In particularly, it was assumed that the finite thickness of the crucible D affects the circulation of the eddy current in the melt and a correction to the wave vector, which became equal to k^* was proposed in the form of eq.(2.25) below. Analytical solution provided three components for electromagnetic force F_x , F_y and F_z (axis shown in right-hand fig.2.10), yet, only x -component of the force drives fluid flow.

$$k^* = \sqrt{k^2 + \left(\frac{\pi}{2D}\right)^2} \quad (2.25)$$

$$F_x = C_{em} A_{em,0}^2 \times \frac{2\pi f \sigma_l k^*}{2} e^{-2k^* y} \quad (2.26)$$

with $k = 65.45\text{m}^{-1}$ and $k^* \approx 321\text{m}^{-1}$.

It is seen that the final expression for the force given by eq.(2.26) contains three parameters. First, C_{em} is a reduction factor to account for a finite size of the inductor, second, $A_{em,0}$ corresponds to the amplitude of the potential vector \mathbf{A} at the inner surface of the bottom side of the cavity and the third is the modified wave vector k^* . Among these three parameters only the last one can be actually known since it is based on geometry of the inductor. Two others, C_{em} and $A_{em,0}$, should be extracted from some measurements. Two studies were devoted to the definition of these parameters via the measurements of characteristics of the flow of low-temperature GaInSn alloy in identical configuration [24, 25]. These studies provided different recommendations already for the value of the wave number: $k^* = 65\text{m}^{-1}$ in [25] contrary to the value $k^* = 314\text{m}^{-1}$ derived in

[24] and recommendation for the values of $A_{em,0}$ and C_{em} were also different.

To clarify the situation, Tao Wang during his work on PhD Thesis performed simulations and reproduced numerically the measurements which made for GaInSn alloy with Doppler technique, cf. ref. [26]. Calculations were performed with ANSYS[®] Fluent[®] software with properties of GaInSn melt given elsewhere. These simulations revealed that the electromagnetic force defined by $k^* = 314\text{m}^{-1}$ decreased very fast near the bottom of the cavity and the velocity profiles measured in experiment could not be reproduced. Yet, with the value of wave vector $k^* = 65\text{m}^{-1}$ the calculation and measurements for velocity of GaInSn had much better agreement. Then, to evaluate the amplitude of the electromagnetic force we presented the latter in the form

$$F_x = A_{emf,GaInSn} e^{-2k^*y} \text{ with } k^* = 65\text{m}^{-1} \quad (2.27)$$

and we were looking for a coefficient $A_{emf,GaInSn}$ which depends on the electric conductivity of the media, for GaInSn alloy $\sigma_l = 3.4 \cdot 10^4 (\Omega \cdot \text{m})^{-1}$. The values $A_{emf,GaInSn} = 160\text{N}/\text{m}^3$ and $A_{emf,GaInSn} = 320\text{N}/\text{m}^3$ provided satisfactory results although we found that a good comparison cannot be actually made for multiple reasons, which are described in details in the PhD Thesis of Tao Wang [26]. Then, accounting for a nearly 2 times difference in the values of electric conductivity between the GaInSn and PbSn alloys, one can expect that the value for the coefficient A_{emf} for the latter alloy should be between 80-160 N/m^3 . Further adjustment of the coefficient preceding the exponent in case of SnPb alloy was made based on the comparison of the two-dimensional temperature distribution obtained numerically and with the thermocouple measurements in the AFRODITE experiment. We found that the range 110-180 N/m^3 for the coefficient A_{emf} was more suitable.

Consequently, in further calculations for AFRODITE experiments with PbSn alloy we used the following expression for the electromagnetic force:

$$F_x = A_{emf} e^{-2ky} \text{ with } k^* = 65\text{m}^{-1} \text{ and } A_{emf} = 180\text{N}/\text{m}^3 \quad (2.28)$$

with the adjustable parameters A_{emf} supposed to be in the range 110 – 180 N/m^3 .

Results of simulations of the flow and temperature field in the Sn-10wt%Pb alloy prior solidification and at the very beginning of the solidification process are shown in fig.2.11. Although the thermal boundary conditions (at the left and right wall) were corrected based on the measurements realized in the experiment, it should be recognized that there exist some difference between the temperature fields observed in the experiment and those from calculations (fig.2.11). Based on the shape of the temperature isolines, one can suppose that the thermal buoyancy convection near the hotter (left) wall is underestimated while intensity of the Lorentz force is probably overestimated. These are uncertainties related to the lack of information about boundary conditions and electromagnetic force. Yet, numerical results reproduce important characteristics of the temperature fields that are higher thermal gradient near the cold wall than near the warm one and nearly constant temperature in the central part of the liquid volume.

2.2.2 Equiaxed model for the AFRODITE benchmark

Apart of the problems presented above that are related to uncertainties in thermal boundary conditions and in electromagnetic force driving liquid flow, the following phenomena got special attention in numerical model.

1. Grain packing phenomena

Experimental observation show that the equiaxed grains may attach to the wall of the cavity

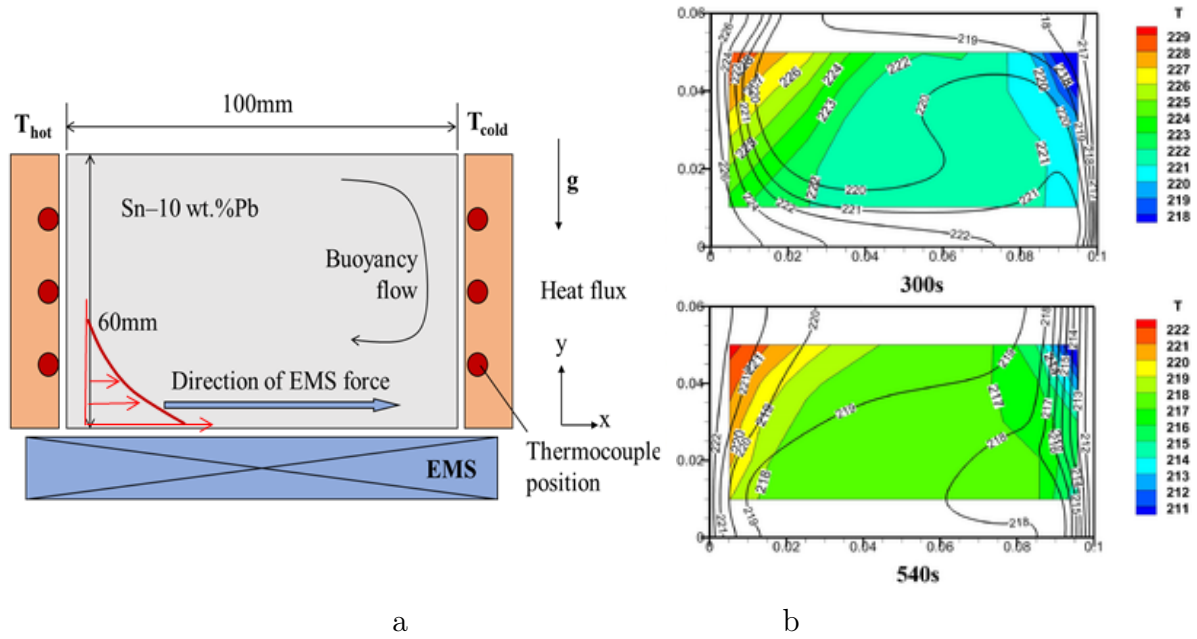


Figure 2.11: a) Scheme presenting flow directions in the experiment and b) Comparison of temperature obtained in simulations with $A_{emf} = 180 N/m^3$ and measured during the experiment: two-dimensional temperature field in the beginning (upper figure, $t=300s$) and in the middle ($t=540s$, lower figure) of solidification process, from [27]

and coalesce with other grains. In numerical models, it is supposed that coalescence of grains happens at some critical fraction whose value is predefined and depends on adopted model chosen for equiaxed simulation (globular or dendritic), no other criteria were recommended. However, this approach seems to be relevant for the case of weak and “regular” convective flow which does not affect monotone distribution of temperature in the cavity and layer-by-layer character of solidification. Yet, due to electromagnetic stirring a system of vortices can be created in the liquid and because of them a region with lower temperature may happen somewhere in the bulk liquid. Following these vortices, some grains may be taken from the walls of cavity and brought to bulk liquid without been melted, on the contrary, they may grow because of temperature perturbation! In this situation grains may coalesce but travel together, i.e. their “packing” in sense of blockage does not look logical. Consequently, it was proposed to block only those grains whose grain fraction was large or equal the critical one and which were near cavity walls or had already packed grains as neighbors as described elsewhere [27].

2. Solidification in turbulent flow and interaction of turbulent flow with porous solid

It could be expected and it was confirmed by our simulations that the flow of the melt under the action of electromagnetic stirring in the AFRODITE experiment is weakly turbulent. Yet, if models for growth kinetics of grains which accounts for convective flow exist, they were not extended to turbulent flow. In simulations performed for AFRODITE experiment the problem of turbulence was solved “ad-hoc”⁵: we used a widely adopted realizable $k-\varepsilon$ model with extended treatment of the wall.

3. Evolution of electromagnetic field in time during solidification

This question may arise if we suppose that electrical conductivity inside solidifying volume evolves

⁵fashioned from whatever is immediately available, <https://www.merriam-webster.com/dictionary/ad%20hoc>

in time either due to variation of electrical conductivity with temperature or because of phase transition. The former situation is simpler since it assumes changing at macroscale and can be treated with formal variation of σ_l in the expression for the force given by eq.(2.26). In this case only the lack of data on $\sigma(T)$ prevents realization of such simulations. Yet, the change of electrical conductivity due to the phase transition is more difficult to treat because it is related to the nucleation and growth of solid grains and it can be expected that at small solid fraction the variation of the electrical conductivity is negligible. However, at certain grain size or due to accumulation of grains (both are interpreted with solid fraction), the effect of phase transition should become remarkable and it would be non-uniform. In this case we face both with lack of the experimental data on $\sigma(fs)$ and on the absence of the corresponding electromagnetic model. On the other hand, it should be noted that at first approximation similar “mixture” model presenting effective conductivity proportional to fraction of phases would be probably appropriate.

Other problems related to the drag force acting on the liquid and grains and effect of convective flow on the growth kinetics of dendrites were considered at the stage of the development of the equiaxed model and are presented in details in the publications of Tao Wang et al. [28].

2.2.3 Application of the equiaxed model to the AFRODITE benchmark experiment performed with the use of the Traveling Magnetic field

Effect of the forced and buoyancy convection during solidification is illustrated with fig.2.12. Initially (2.12a) the forced convection occupies most of the liquid volume and transport the appearing solid grains upward and to the centre of the cavity. It should be noted also that the density of the solid phase is smaller than the density of the liquid enriched with the rejected Pb, the grains can float upward. However, with grains packing the effect of the forced convection decreases because the packed grains damp the forced flow giving possibility to the thermal buoyancy to occupy the upper part of the liquid volume (2.12b). According to the model, the *extradendritic* liquid(which is the liquid outside of the grains), can still move and since it is heavily enriched, it flows downwards and brings the rejected Pb toward the bottom of the cavity. Note that such configuration of the flow affects also temperature distribution: at the time corresponding to the situation illustrated with the fig.2.12a the temperature at the upper part is defined by the forced convection which brings there colder melt, but at the moment corresponding to the fig.2.12b the buoyancy convection brings to the central upper part the warmer liquid from the hotter wall. Detailed analysis of the interaction of the forced and buoyancy convection affected by the growth of the dendrite grains, their transport and packing was performed in our publication [27]. Below the final patterns for the distribution of the Pb in the solidified sample and calculated density of the grain number is presented and compared with those obtained in the experiment, cf. fig.2.13. As it was mentioned in the beginning regarding the experimental results, although the most of part of the solidified volume is occupied by the equiaxed grains, columnar growth is observed in right bottom part. The presence of columnar grains can affect the forced convection, and this is not taken into account in the numerical model. Because of this, the channels enriched with the Pb in the region of the columnar growth obtained in the experiment are not observed in the simulations. However, the distribution of the density of the grain number n , obtained numerically, correspond to the variation of grains’ size visible in the sample: higher value of n near closer to the left (warmer) wall of the sample correspond to

smaller grains in the experiment. Qualitative comparison regarding concentration of the Pb in the solidified sample based on the X-Ray image is not possible, but it is seen that the location of the region enriched with Pb corresponds to the porous region in the sample. The latter could be the indication that this volume was solidified at the latest, similar to calculations. Overall, character of segregation – negative at the top and positive near the lateral and bottom walls – correspond to the experimental observations.

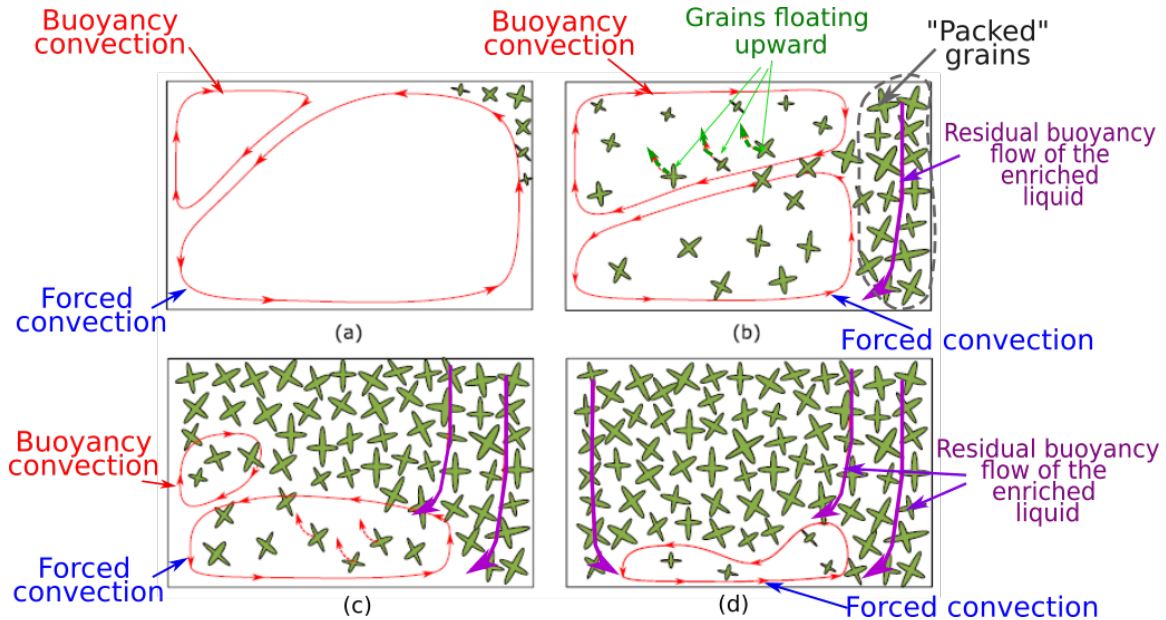


Figure 2.12: Illustration to the effect of the buoyancy and forced convection during the solidification process, from the PhD Thesis of Tao Wang [26]

2.3 Conclusion

In this chapter the work performed for solidification processes under polyphase AC electromagnetic fields obtained with various configurations of coils is presented. In particular, we considered the solidification with application of rotating magnetic field (section 2.1.1) and with two types of traveling magnetic fields (section 2.1.2 and 2.2). Regarding simulations performed for the project MICAST, it is interesting to see how the mesoscale modeling has difficulty with providing deeper insight in the process because of lack of the information regarding the microstructure development. Indeed, as it was discussed above, the absence of information on the growth of intermetallic solid phase in solidification of Al-Si-Fe alloy impedes satisfactory description of mushy zone. Consequently, the fluid flow cannot be treated properly that makes the analysis regarding the coarsening of dendrites impossible at the this stage. On the contrary, advanced comprehension on growth kinetics in binary dendrites growth allows one to understand quite well the transport processes in the AFRODITE benchmark experiment.

It is found that the polyphase AC magnetic field serves for creating a driving force which may transport the liquid and the solid phase, the concentration of the components of the alloy in the volume is affected by the convective transport. The latter can have negative effect, i.e. aggravates the segregation, as it was observed in the experiments performed within the MICAST project or makes it smoother, as shown in the AFRODITE experiment. Note that in both

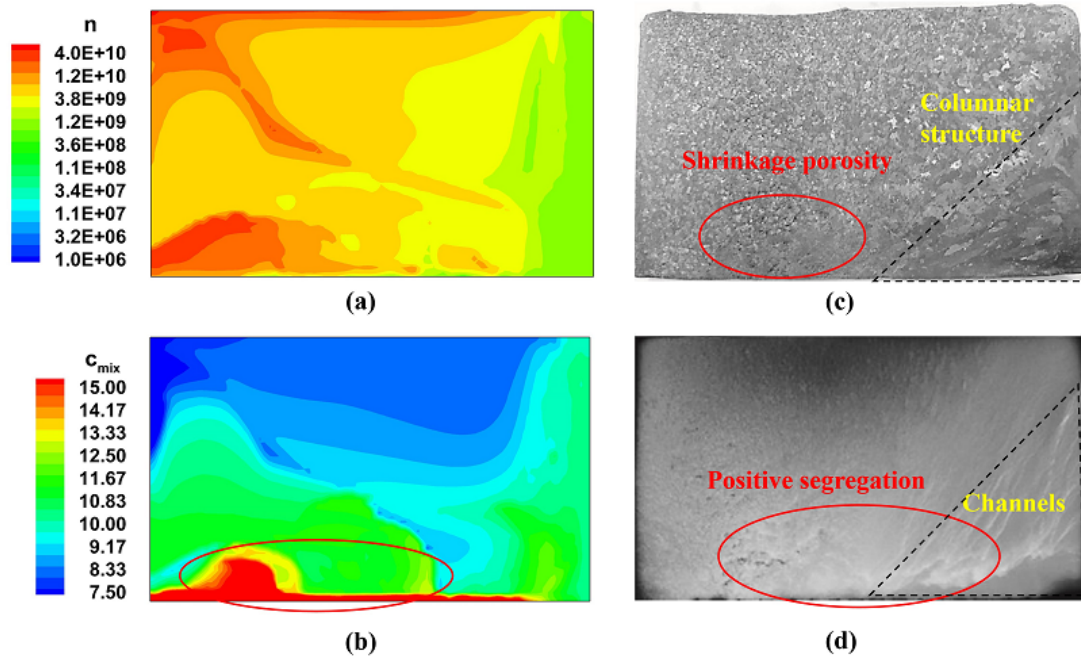


Figure 2.13: Comparison of numerical simulations and experimental observations: calculated grain number density distribution (a), calculated macrosegregation map at center plane of the sample (b), grain structure of ingot(c) and X-radiography of the ingot (d), the figure is taken from the ref. [27]

cases the structure of the solid phase – columnar or equiaxed – was imposed in solidification. Although some models which can treat simultaneous columnar and equiaxed growth exist, such simulations remain challenging and rely on quite a large number of parameters unknown a priori. Yet, development of such model is foreseen by the author in the future.

Finally, it should be stated that at the current stage the numerical models developed for solidification of alloys really help to reveal the sequence of physical phenomena which prevail at the different stage of solidification. However, the question remains about the ability of such models to predict correctly the results for novel processes.

2.3.1 The author contribution

Regarding solidification of alloys under the action of the polyphase AC magnetic field, the author of the present work contributed to the following actions:

- Implementation of the system of equations for a binary columnar solidification model into ANSYS® Fluent® - realized by the author
- Performing simulations for the numerical benchmark of the columnar solidification of the binary alloys, comparison with the calculations of other laboratories
- Development of the system of equations for the ternary alloy and implementation of them into ANSYS® Fluent® in the frame of the MICAST project - realized by the author
- Coordination of the numerical simulations for the AFRODITE benchmark with the columnar growth under the natural convection
- Coordination of the numerical simulations for the on-ground experiments for the ternary alloy in the frame of the MICAST project (co-supervisor of PhD Thesis of C. Nagy)

- Coordination of development of the numerical model for the solidification of binary alloys in the equiaxed regime and of the simulation of the AFRODITE experiment with electromagnetic stirring (co-supervisor of PhDThesis of T. Wang and supervisor of PostDoc S. Semenov)

Chapter 3

Application of Continuous Magnetic Field in solidification of alloys: Magneto - Thermo - Electric Force

As it was indicated in the introduction, the main effect expected from the application of continuous magnetic field over a solidifying volume is the damping of the convective flow. Yet, in 1980s several experiments on solidification of alloys performed in laboratory conditions with use of the DC magnetic field demonstrated some modifications of structure that could not be explained by diminishing of intensity of fluid flow [29, 30, 31]. On the contrary, these experiments indicated appearance of new force(s) which apparently was active both in liquid and solid phases. Now it seems complicated (if not impossible) to cite the very first work where a guess was made regarding the possible emergence of the thermo-electric current in such systems and further interaction of this current with DC magnetic field which could lead to appearance of Lorentz force in the system. Among early works one can cite the work of Mikelson and Karklin [29]. Below a brief explanation of the phenomenon in application to solidification of alloys is given.

In a form reduced to the thermoelectric (Seebeck) effect only, the system of the governing equations includes a differential equation for the static temperature distribution T and for the continuity of the electric current \mathbf{j} , as well as a relation between the density of electric current and the temperature gradient through Seebeck coefficient:

$$\nabla(\varkappa\nabla T) = 0 \quad (3.1)$$

$$\nabla \cdot \mathbf{j} = 0 \quad (3.2)$$

$$\mathbf{j} = -\sigma\nabla\Phi - \sigma S\nabla T \quad (3.3)$$

with Φ in eq.(3.3) for the electric potential which appears in a media due to the temperature gradient, \varkappa and σ for the thermal and electrical conductivity, respectively, and S for a thermoelectric power (Seebeck coefficient). These equations should be updated with the boundary conditions, this will be discussed in the sections below as well as coupling of these equation with convective flow.

Thus if the Seebeck coefficient varies in the domain subjected to the thermal gradient, for example, due to the phase transition from solid to liquid, the thermoelectric current \mathbf{j} given by eq.(3.3) may appear in the system. Furthermore, if a magnetic field \mathbf{B} is superposed over the system, the interaction of the thermoelectric current and the magnetic field may lead to the appearance

of the magneto-thermo-electric force $\mathbf{F} = \mathbf{j} \times \mathbf{B}$. Finally, this force can affect the motion of the liquid and of the solid particles.

3.1 Experiments and theory of Magneto-Thermoelectric Force in application to solidification of alloys: state of art

Study of the effect of continuous magnetic fields on macrostructure of alloys was initiated in the group EPM (at that time laboratory MADYLAM) by Dr. R. Moreau at the end of the last century. Systematic fundamental experiments realized in the frame of thesis of O. Laskar [32], T. Alboussiere [33] and P. Lehman [34] clearly demonstrated that the effect of a continuous magnetic field, applied during solidification of alloys, on the microstructure of the latter cannot be explained by the damping of the natural convection. Hence, the hypothesis regarding the thermoelectric effect at the origin of the observed modifications was supported. In the former work,

an analytical solution was proposed for a planar 2D interface, as well as qualitative expressions for the thermoelectric current in the liquid and in the solid phase near the dendrite front:

$$\mathbf{j}_s = -\frac{\sigma_s \sigma_l f_L}{\sigma_l f_L + \sigma_s f_s} (S_s - S_l) \mathbf{G}_T \quad (3.4)$$

$$\mathbf{j}_l = \frac{\sigma_s \sigma_l f_s}{\sigma_l f_L + \sigma_s f_s} (S_s - S_l) \mathbf{G}_T \quad (3.5)$$

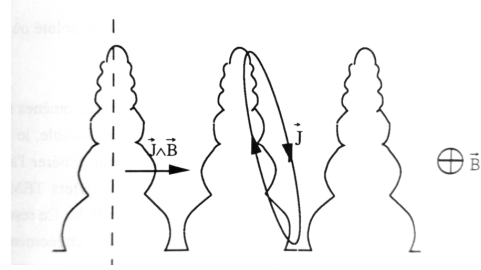


Figure 3.1: Thermoelectric current in the dendrite and surrounding liquid [32]

In eqs.(3.4)-(3.5) f_s, f_l correspond to the solid and the liquid volume fractions, respectively, and the thermal gradient \mathbf{G}_T is supposed to be aligned with the growth direction of dendrites, both are considered to be along z -axis.

Also, qualitative diagrams showing thermoelectric current in dendrites and surrounding liquid were demonstrated for the case of DC magnetic field directed perpendicular to growth direction and parallel to it (Fig.3.2).

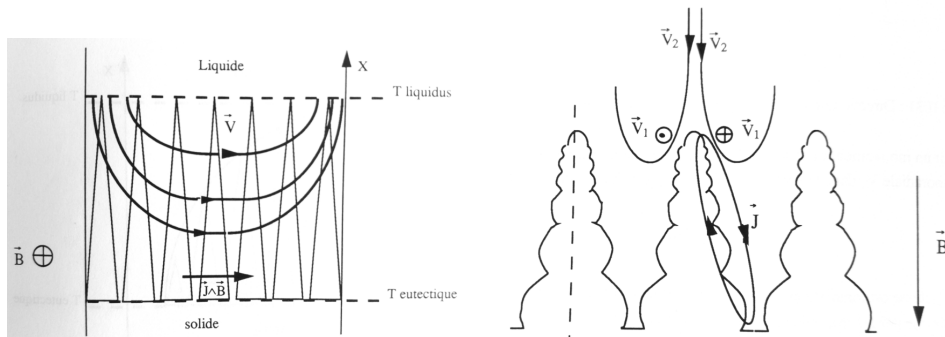


Figure 3.2: Thermoelectric current and convective flow in the mushy zone dependent on direction of applied DC magnetic field defined with the vector \mathbf{B} [32]

These works made possible next series of experiments in more complex configuration that were

3.2 Effect of the size and orientation of a solid particle on the intensity of the thermoelectric current

Consideration of a solid particle of a spherical shape does not allow us to understand if anisotropic thermoelectric effects may exist in the solid-liquid system. To verify if the shape of the particle may have an effect on the thermo-electric phenomena, we considered a particle in the form of prolate spheroid (ellipsoid) which can be oriented differently with respect to the imposed external thermal gradient $\mathbf{G}_{T,\infty}$ (Fig.3.4).

Similar to the case of the spherical particle, the solid and liquid phases are characterized with the electrical and thermal conductivities σ_s, σ_l and \varkappa_s, \varkappa_l , respectively, which could be equal for the solid and the liquid, but the Seebeck coefficients S_s, S_l should be different for the two phases.

The ellipsoid is characterized with the semi-major and semi-minor axis a and b and the eccentricity of the ellipsoid e :

$$e = \sqrt{1 - b^2/a^2} \quad (3.9)$$

Note, that for a sphere $a = b$ and $e = 0$.

It is convenient to obtain the solution for the thermo-electric problem with two particular orientations of the thermal gradient: parallel to the major axis of the ellipsoid $G_{T,\infty}^{\parallel}$ and parallel to the minor axis of the ellipsoid $G_{T,\infty}^{\perp}$. Then linear combinations of obtained solutions allows description for a general case with arbitrary orientation of the ellipsoid with respect to the thermal gradient.

A detailed solution of the problem is given in [47], here only results are briefly presented. The remarkable finding is that the density of the current in the solid particle depends on the *eccentricity* of the ellipsoid but not on the size of the latter. This dependence is presented with the help of a function $\mathcal{F}(e)$ written as:

$$\mathcal{F}(e) = \left(\frac{1}{e^2} - 1 \right) \left(\frac{1}{2e} \ln \frac{1+e}{1-e} - 1 \right) \quad (3.10)$$

with two limits: $\mathcal{F}(e)|_{e \rightarrow 0} \rightarrow \frac{1}{3}$ and $\mathcal{F}(e)|_{e \rightarrow 1} \rightarrow 0$.

Assume that the orientation of the imposed thermal gradient parallel to the major axis of the ellipsoid means that $\mathbf{G}_{T,\infty} = \mathbf{e}_x G_{T,\infty}^{\parallel}$ is directed along x -axis. For the perpendicular orientation it can be supposed that $\mathbf{G}_{T,\infty} = \mathbf{e}_y G_{T,\infty}^{\perp}$, i.e. directed along y -axis. Then, obtain for the current in the solid particle:

$$\mathbf{j}_s^{\parallel}(e) = -\mathbf{e}_x G_{T,\infty}^{\parallel} \frac{\sigma_s(S_S - S_L) [1 - \mathcal{F}(e)]}{[1 - (1 - k_{\sigma})\mathcal{F}(e)] [1 - (1 - k_{\varkappa})\mathcal{F}(e)]} \quad (3.11)$$

$$\mathbf{j}_s^{\perp}(e) = -\mathbf{e}_y G_{T,\infty}^{\perp} \frac{2\sigma_s(S_S - S_L) [1 + \mathcal{F}(e)]}{[2 - (1 - k_{\sigma})(1 - \mathcal{F}(e))] [2 - (1 - k_{\varkappa})(1 - \mathcal{F}(e))]} \quad (3.12)$$

with $k_{\sigma} = \sigma_s/\sigma_l$ and $k_{\varkappa} = \varkappa_s/\varkappa_l$.

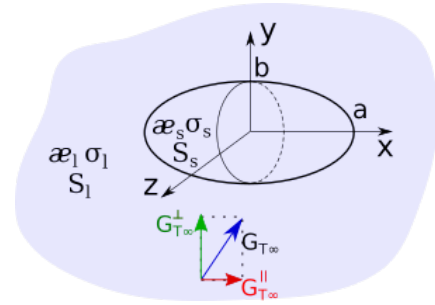


Figure 3.4: Particle in the form of prolate spheroid (ellipsoid) in the infinite liquid pool under the external thermal gradient $\mathbf{G}_{T,\infty} = \mathbf{e}_x G_{T,\infty}^{\parallel} + \mathbf{e}_y G_{T,\infty}^{\perp}$

It can be shown that at the limit $e \rightarrow 0$, i.e. in a case of the spherical particle, both solutions given by eqs.(3.11) and (3.12) tend to the expression obtained for a sphere given by the eq.(3.6). However, it is interesting to compare the case of a sphere $e \rightarrow 0$ and of a highly elongated ellipsoid, $e \rightarrow 1$ when $\mathcal{F}(e)|_{e \rightarrow 1} \rightarrow 0$. This comparison is summarized in the Table 3.1 below, and is easier if all properties for liquid and solid, except the Seebeck coefficients, are supposed equal.

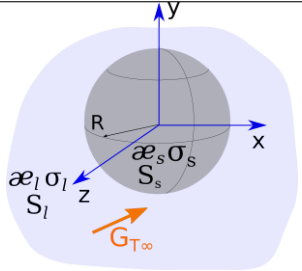
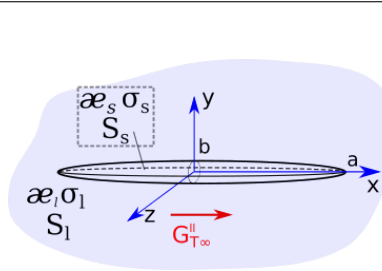
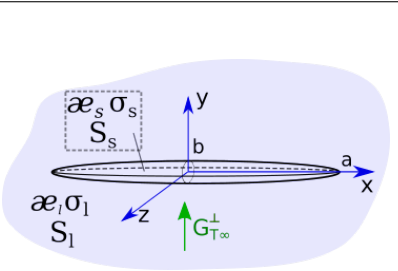
Sphere $e = 0$	Elongated ellipsoid $e \rightarrow 1$, main axis $\parallel G_T$	Elongated ellipsoid, $e \rightarrow 1$, main axis $\perp G_T$
		
$\mathbf{j}_s^{sp} = -\mathbf{G}_{T,\infty} \frac{2\sigma_s\sigma_l}{\sigma_s + 2\sigma_l} \times \left(\frac{3\kappa_l}{\kappa_s + 2\kappa_l} \right) (S_s - S_l)$	$\mathbf{j}_s^{\parallel} _{e \rightarrow 1} = -\mathbf{G}_{T,\infty} \times \sigma_s (S_S - S_L) \quad (3.13)$	$\mathbf{j}_s^{\perp}(e) _{e \rightarrow 1} = -\mathbf{G}_{T,\infty} \frac{2\sigma_s\sigma_l}{[\sigma_l + \sigma_s]} \times \frac{\kappa_l}{[\kappa_l + \kappa_s]} (S_S - S_L) \quad (3.14)$
if $\sigma_s = \sigma_l$ and $\kappa_s = \kappa_l$		
$\mathbf{j}_s^{sp} = -\mathbf{G}_{T,\infty} \frac{2\sigma_s}{3} \times (S_s - S_l)$	$\mathbf{j}_s^{\parallel} _{e \rightarrow 1} = -\mathbf{G}_{T,\infty} \times \sigma_s (S_S - S_L) \quad (3.15)$	$\mathbf{j}_s^{\perp}(e) _{e \rightarrow 1} = -\mathbf{G}_{T,\infty} \frac{\sigma_s}{2} \times (S_S - S_L) \quad (3.16)$

Table 3.1: Comparison of the thermoelectric current originated in a spherical particle and in a highly elongated ellipsoid for two different orientation of the latter with respect to the thermal gradient

In particular, it can be observed, that if elongated particle is oriented perpendicularly to the thermal gradient, the density of thermoelectric current inside the particle will be 4/3 times smaller than in the spherical particle, if all properties for liquid and solid (except S_S, S_L) are considered equal, compare eq.(3.16) and eq.(3.15). One can observe that eqs.(3.16),(3.15) have the same structure as equations obtained by Leenov & Kolin [48] for the problem of the electromagnetophoresis.

Note that the direction of the thermoelectric current inside the particle is parallel to the direction of the thermal gradient if the latter is oriented along one of its axis. To obtain the intensity of the thermoelectric current for the arbitrary orientation of the ellipsoid under external thermal gradient one can use the linear combinations of \mathbf{j}_s^{\parallel} and \mathbf{j}_s^{\perp} . In particular, the thermoelectric current will flow at the angle of $\arctan(|\mathbf{j}_s^{\perp}|/|\mathbf{j}_s^{\parallel}|)$ with respect to the major axis of the ellipsoid with its density equal to $\sqrt{(\mathbf{j}_s^{\perp})^2 + (\mathbf{j}_s^{\parallel})^2}$ while $|\mathbf{j}_s^{\perp}|$ and $|\mathbf{j}_s^{\parallel}|$ will be defined by the modules $G_{T,\infty}^{\parallel}$ and $G_{T,\infty}^{\perp}$.

The analytic solutions given above allowed us to explain the results obtained numerically in the simulation of a thermoelectric problem for a 2D dendrite particle (fig.3.5) [47]. Indeed, in the dendrite particle one can distinguish two primary arms directed almost along the thermal external gradient $\mathbf{G}_{T,\infty} = 3000 \text{ K/m}$, and the third primary arm which is strongly inclined with respect to the $\mathbf{G}_{T,\infty}$. Numerical simulations showed that the density of the thermoelectric current was different in these primary arms.

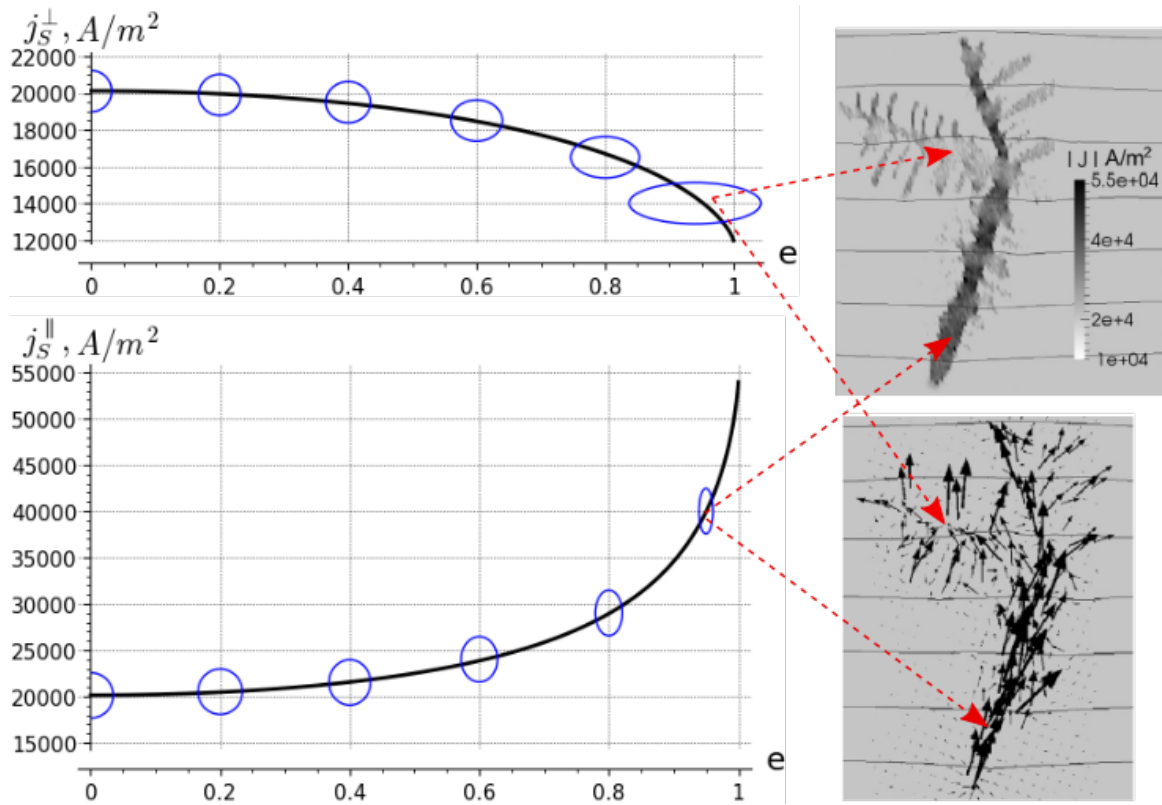


Figure 3.5: Thermoelectric current through a dendrite particle and the explanations with use of the analytical solutions, properties are given in the table 3.2. Nearly horizontal lines in the figure corresponds to the temperature isolines with $\Delta T = 0.05K$ [47]

Moreover, the density of the thermoelectric current in the small secondary dendrite arms, which are parallel to the $\mathbf{G}_{T,\infty}$, is larger than in a large primary arms. This correspond to our solutions obtained with the ellipsoid particle, which demonstrated dependence on the particle orientation in the thermal field and on the ratio of its geometrical characteristics, but not on the size of the particle. Moreover, since the dendrite arms resemble the elongated ellipsoid with $e \rightarrow 1$, the density of the thermoelectric current can be estimated theoretically based on the properties given in the table 3.2 and the imposed thermal gradient $\mathbf{G}_{T,\infty} = 3000 \text{ K/m}$.

Physical properties	value		unit
	liquid	solid	
Thermo-electric constant S	-3.8×10^{-6}	-5.4×10^{-6}	V m^{-1}
Electrical conductivity σ	4×10^6	1×10^7	$\Omega^{-1} \text{m}^{-1}$
Thermal conductivity \varkappa	95	150	$\text{W m}^{-1} \text{K}^{-1}$

Table 3.2: Numerical values of physical properties used in calculations with a dendrite particle

3.3 Intensity and configuration of the liquid flow around a spherical particle due to Magneto-ThermoElectric force

In the section above the main attention was given to the thermoelectric current which circulates in the solid particle. Actually, the analytical solution was obtained for a generalized thermoelectric potential $W = \Phi - ST$ both, for solid and liquid phases. Therefore, the thermoelectric current in the liquid phase can be also found and one can try to estimate the effect of the DC magnetic field superposed over this system.

The role of the DC magnetic field \mathbf{B} in the appearance of the magneto-thermoelectric force $\mathbf{F}_{MTE} = \mathbf{j} \times \mathbf{B}$ is twofold. Indeed, without the magnetic field a thermoelectric current circulates in the system, but no driving force exists. The latter appears once a magnetic field is superposed over the system and seems to be linearly proportional to the intensity of magnetic field $|\mathbf{B}|$, i.e. one might expect that convection in the liquid intensifies with the increase of $|\mathbf{B}|$. Yet, as it was discussed in the section 1.2, the interaction of the velocity of fluid \mathbf{u} with the magnetic field \mathbf{B} generally leads to the generation of the eddy current $\sigma_l \mathbf{u} \times \mathbf{B}$ and to the modification of the electric potential Φ according to the source $\sigma_l \mathbf{B} \cdot (\nabla \times \mathbf{u})$. Hence, the magnetic field \mathbf{B} is at the origin of the convective flow but at the same time it may tend to damp the flow and to alter the thermoelectric current. The dominant effect depends on the configuration of the flow, in particular, on the direction of $\nabla \times \mathbf{u}$ with respect to the direction of the vector \mathbf{B} . This interesting problem was studied by J. Shercliff in application to the stirring of the liquid metals in nuclear reactors or to metallurgy [49]. In particular, he studied a case of spherical impurity which could be considered similar to spherical particle. Yet, in his consideration the impurity was not bounded with a surface at which liquid flow would become zero, and the thermoelectric properties of the media varied in smooth manner. These factors allowed him to avoid certain problems with boundary conditions, as we shall see below.

To consider the thermoelectric problem coupled with the hydrodynamic problem, the system of equations (3.1),(3.2) and (3.3) formulated initially for immovable media should be updated with the Navier-Stokes equation, and an additional term should appear in the eq.(3.3) due to the effect of electromagnetic induction. That gives the following system of equations in the steady state:

$$\mathbf{j} = -\sigma \nabla \Phi - \sigma S \nabla T + \sigma (\mathbf{u} \times \mathbf{B}) \quad (3.17) \quad \nabla \cdot \mathbf{j} = 0 \quad (3.20)$$

$$\rho (\mathbf{u}, \nabla) \mathbf{u} - \nabla \cdot (2\mu D(\mathbf{u})) + \nabla p = \rho \mathbf{g} + \mathbf{j} \times \mathbf{B} \quad (3.18) \quad \nabla \cdot \mathbf{u} = 0 \quad (3.21)$$

$$\rho C_p \mathbf{u} \nabla T - \nabla (\varkappa \nabla T) = 0 \quad (3.19)$$

In eq.(3.18) D represents the symmetric part of the velocity gradient. This system of equations is updated with the boundary conditions that include no-slip velocity at the surface of the solid particle, continuous temperature and electric potential for the solid and the liquid there, as well as continuity of the heat flux and the normal component of the electric current through the solid-liquid interface:

$$(\mathbf{j} \cdot \mathbf{n})_{r=R,s} = (\mathbf{j} \cdot \mathbf{n})_{r=R,l} \quad (3.22)$$

$$(\varkappa_s \nabla T \cdot \mathbf{n})_{r=R,s} = (\varkappa_l \nabla T \cdot \mathbf{n})_{r=R,l} \quad (3.23)$$

$$\mathbf{u}|_{r=R} = \mathbf{0} \quad (3.24)$$

$$\Phi_{r=R,s} = \Phi_{r=R,l} \quad (3.25)$$

$$T_{r=R,s} = T_{r=R,l} \quad (3.26)$$

Below an analytical solution is presented for a simplified case and compared with the numerical solution of the complete problem. The theoretical analysis assumes the *infinite liquid media* with the external temperature gradient $\mathbf{G}_{T,\infty}$ imposed over the system. Yet, numerical solution is performed in a bounded domain (fig.3.6), consequently, the boundary conditions are also required at the walls of calculation domain. They are usually formulated as no velocity at the external walls and no current through them:

$$\mathbf{u}|_{\text{box wall}} = \mathbf{0} \text{ and } \mathbf{j} \cdot \mathbf{n}|_{\text{box wall}} = 0 \quad (3.27)$$

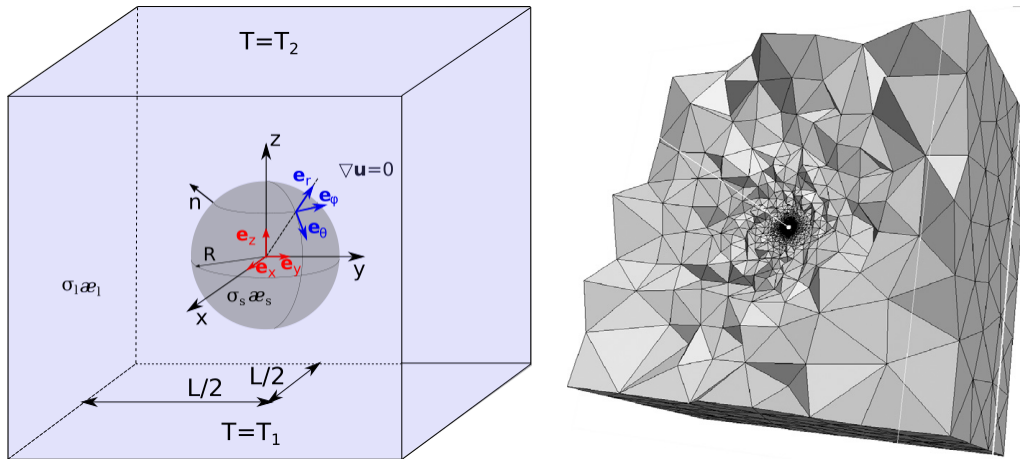


Figure 3.6: Configuration of a calculation domain for the numerical simulations (a) and illustration of the mesh used for calculations to capture the strong variations of the physical variables near the surface of the particle, from the ref. [50]

Conditions for the temperatures T_1 and T_2 (fig.3.6) are chosen such that they provide the required thermal gradient $\mathbf{G}_{T,\infty}$ at the large distance from the particle.

Let us first discuss the analytical solution and then compare it with the numerical one.

3.3.1 Analytical solution of an uncoupled convective magneto-thermo-electric problem for a spherical particle

In the section 3.2 above, the thermoelectric current which circulates in the solid particle was discussed in details. It was found that the density of the electric current in the solid phase is constant and its direction is related to the orientation of the thermal gradient in the particle.

However, the electric current is supposed to conserve in the system, consequently, the lines of the thermoelectric current should be closed in the liquid which surrounds the particle as illustrated in fig.3.7. Moreover, as it was indicated above, the density of the electric current strongly diminishes with the distance from the particle according to the equation already given above and repeated here, eqs.(3.28)-(3.29)

$$\mathbf{j}_l^{sp} = -\frac{2\sigma_s\sigma_l}{\sigma_s + 2\sigma_l} (S_s - S_l) |\overline{\mathbf{G}_{T,\infty}}| \times \frac{R_0^3}{r^3} (\cos\theta\mathbf{e}_r + \sin\theta\mathbf{e}_\theta) \quad (3.28)$$

with

$$\overline{\mathbf{G}_{T,\infty}} = \left(\frac{3\kappa_l}{\kappa_s + 2\kappa_l} \right) \mathbf{G}_{T,\infty} \quad (3.29)$$

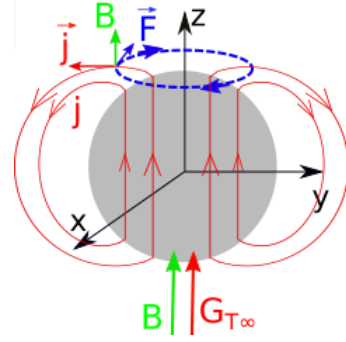


Figure 3.7: Illustration for the thermoelectric current in the liquid and appearance of the azimuthal magneto-thermoelectric force, case of a spherical particle and vectors \mathbf{B} and \mathbf{G}_T co-directed along the z -axis

In the situation illustrated in the fig.3.7, the external thermal gradient $\mathbf{G}_{T,\infty}$ and the imposed DC magnetic field \mathbf{B} have the same direction, along which the z -axis was chosen as well. The magneto-thermoelectric force (Lorentz force) does not exist in the particle since the vector of the thermoelectric current \mathbf{j}_s and the vector \mathbf{B} are parallel. Then the magneto-thermo-electric force associated with the thermoelectric current given by eq.(3.28) and the magnetic field \mathbf{B} has only the azimuthal coordinate which is expressed as

$$\mathbf{F}_l = \mathbf{e}_\varphi F_{l,\varphi} = \mathbf{e}_\varphi \frac{9}{2} \frac{\sigma_s\sigma_l}{\sigma_s + 2\sigma_l} \frac{\kappa_l}{\kappa_s + 2\kappa_l} (S_s - S_l) GB \frac{R^3}{r^3} \sin(2\theta) \quad (3.30)$$

This force should drive the azimuthal flow, while secondary flow in the meridian plane should appear because of viscous effect. It can be expected, however, that for a weak flow:

- the meridional flow is negligible
- effects related to the interaction of the magnetic field and velocity are negligible as well¹

Thus *the thermoelectric problem is decoupled from the hydrodynamic one*, i.e. the thermoelectric part is solved independently on the fluid flow. Then, only the azimuthal component of the velocity is affected by the force given by the eq.(3.30). The corresponding equation is:

$$\frac{\partial}{\partial r} \left(r^2 \frac{\partial U_\varphi}{\partial r} \right) + \frac{\partial}{\partial \theta} \left(\frac{1}{\sin\theta} \frac{\partial (U_\varphi \sin\theta)}{\partial \theta} \right) + \frac{r^2}{\mu} F_{l,\varphi} = 0 \quad (3.31)$$

and the boundary conditions

$$U_\varphi(r,\theta)|_{r=R} = 0, \quad U_\varphi(r,\theta)|_{r \rightarrow \infty} = 0 \quad (3.32)$$

$$U_\varphi(r,\theta)|_{\theta=0} = 0, \quad U_\varphi(r,\theta)|_{\theta=\pi} = 0 \quad (3.33)$$

Then the analytical solution for the problem given by eqs.(3.30)-(3.33) is found in the form [50]:

$$U_\varphi(r,\theta) = 4\sqrt{12}U_{\varphi,max} \left(\frac{R}{r} - \frac{R^3}{r^3} \right) \sin\theta \cos\theta \quad (3.34)$$

with

$$U_{\varphi,max} = \frac{\sqrt{12}}{8\mu} \frac{\sigma_s\sigma_l}{\sigma_s + 2\sigma_l} \frac{\kappa_l}{\kappa_s + 2\kappa_l} (S_s - S_l) |\mathbf{G}_{T,\infty} B| R^2 \quad (3.35)$$

¹both, modification of the electric potential because of the source $\sigma_l \mathbf{B} \cdot (\nabla \times \mathbf{u})$ and the eddy current $\sigma_l \mathbf{u} \times \mathbf{B}$ are neglected

where $U_{\varphi,max}$ is an absolute maximal value of the velocity located at $r = \sqrt{3}R \approx 1.732R$ and angles $\theta = 45^0$ and $\theta = 135^0$.

3.3.2 Numerical solution for a coupled convective magneto - thermoelectric problem for a spherical particle and co-directed vectors \mathbf{B} and $\mathbf{G}_{T,\infty}$

The main difficulty for the numerical solution of coupled system of equations (3.17)-(3.21) is typical for MHD problems and is related to the term $\mathbf{u} \times \mathbf{B}$ which should be taken into account when the continuity equation for the electric current (3.20) is solved. That implies a good knowledge of the velocity profile which varies rapidly within a boundary layer, known as Hartmann layer, whose characteristic size is defined as

$$\delta_{Ha} = \frac{R}{Ha} = \sqrt{\frac{\mu}{\sigma_l}} \frac{1}{|B|} \quad (3.36)$$

From the point of view of numerical solution, this means that several mesh cells should be placed within the layer of thickness δ_{Ha} . Using typical values for dynamic viscosity $\sim 10^{-3}$ Pa·s and electric conductivity $\sim 10^6$ S/m, estimation is that $\delta_{Ha} \sim 10^{-4}/|B|$ m. Thus, the (linear) size of the calculation elements decreases down to $10^{-5} - 10^{-6}$ m if magnetic field higher than 1T is used whereas the linear size of the calculation domain is several centimeters. The number of such small elements adjacent to the sample surface increases with the size of the sample. Therefore, the accurate calculation of the thermoelectric current requires considerable computational resources, especially if the problem is solved in three dimensions. Because of this, one might be tempted to decouple the thermoelectric and hydrodynamic problem and to consider the term $\sigma(\mathbf{u} \times \mathbf{B})$ as an “extra” current added to the thermoelectric one, even if numerical approach is used. Yet, it should be noted that such consideration does not satisfy the law of the current conservation $\nabla \cdot \mathbf{j} = 0$.

The coupled problem was solved numerically with software **Rheolef** [51] which is based on the Finite Element Method and optimized for the use of adapting meshes. It is the latter feature of the code that allowed us to refine the mesh near the spherical particle and to consider the problem in a domain whose linear size was 50 times larger than the radius of the sphere to diminish the effect of the walls on convection fig.3.6. The latter condition is essential for comparison of the numerical results with the analytical solution obtained for a particle in the infinite pool of liquid.

3.3.3 Comparison of the analytical and numerical solution for a coupled magneto-thermoelectric problem

Illustration to the fluid flow and the distribution of velocity magnitude $|\mathbf{u}|$ in the meridional plane (x, z) around of particle with $R = 50\mu\text{m}$ obtained numerically for the two values of magnetic field $B = 0.1T$ ($Ha \approx 0.3$) and $B = 0.5T$ ($Ha \approx 1.4$) are presented in fig. 3.8. For a weak magnetic field the velocity distribution in meridional plane is quadruple with the maximal value of the velocity at $\theta = 45^0 + n\pi/2$, as predicted by the analytic solution given above by eq.(3.34). For a higher intensity of the magnetic field, the vortex of the azimuthal flow is squeezed toward the z -axis while intensity of the flow increases.

A more detailed comparison of the analytic and numerical solutions regarding the velocity profile,

which is taken along the line at 45° to the z -axis (fig 3.9) indicates that both solutions provide similar results for magnetic field up to $0.1T$ that, for the chosen size of the particle $R = 50\mu m$ corresponds to $Ha \approx 0.3$. The difference between the numerical and the analytic results for $B = 0.01T$ and $B = 0.1T$ at the large distance from the particle, i.e. for $r/R > 6$, can be assigned to the effect of external walls which exist in the numerical solution. Then, note, that in fact, if configuration of the flow remains azimuthal, this resembles the situation with the $\nabla \times \mathbf{u}$ parallel to the vector \mathbf{B} , therefore, one can expect the absence of the damping effect! Consequently, with increase of B the flow intensifies because the magneto-thermoelectric force (Lorentz force) increases proportionally to B . On the other hand, for $B = 0.5T$ the numerical solution clearly differs from the analytical one, and two factors are responsible for this. First, the term $\mathbf{B} \cdot (\nabla \times \mathbf{u})$ alters the distribution of the electric potential Φ , consequently, the thermoelectric current is also affected, as well as the “primary” driving force, and velocity field is modified. Second, the meridional (secondary) flow becomes more intense, consequently, the local vectors of $\nabla \times \mathbf{u}$ may be not aligned with the z -axis and a damping effect might be finally manifested.

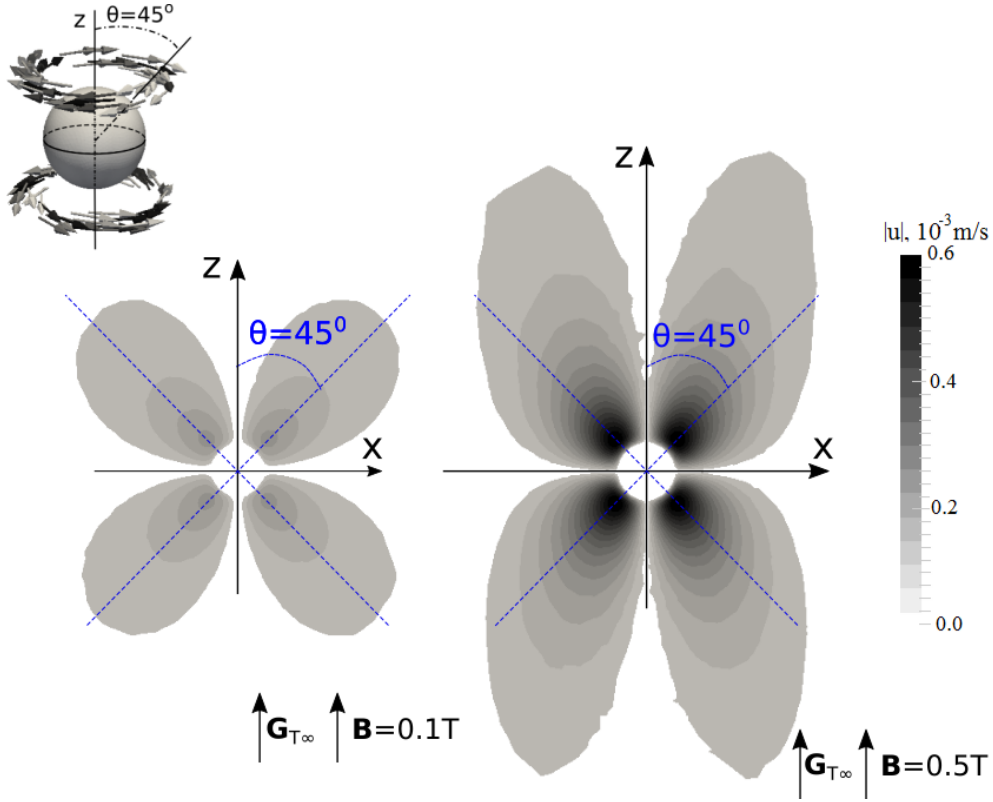


Figure 3.8: Effect of the intensity of the magnetic field \mathbf{B} on the flow around the spherical particle, the case of the vector \mathbf{B} parallel to the imposed thermal gradient $\mathbf{G}_{T,\infty}$ is considered, from the ref. [50]

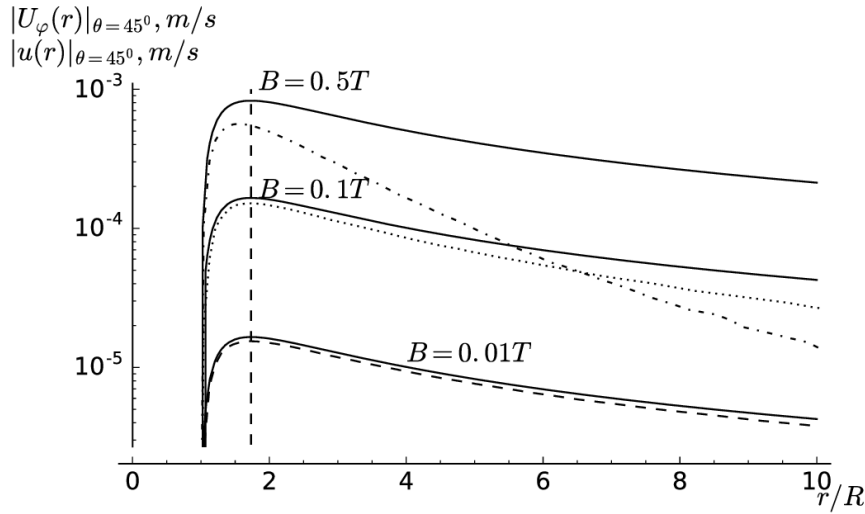


Figure 3.9: velocity profiles along the line $\theta = 45^0$ passing through the sphere center for $B = 0.01T$ ($Ha \approx 0.03$), $B = 0.1T$ ($Ha \approx 0.3$) and $B = 0.5T$ ($Ha \approx 1.4$): solid lines are for $|U_\varphi(r)|$ given by eq.(3.34)-(3.35) and dashed, dotted and dashed-dotted lines are for numerical solution of coupled problem stated with eqs.(3.17)–(3.26) for the indicated values of B . The vertical dashed line at $r/R = \sqrt{3}$ shows the location of maximum velocities defined in analytical solution, from the ref. [50]

One can expect that if the magnetic field \mathbf{B} is directed perpendicular to the vector of the thermal gradient $\mathbf{G}_{T,\infty}$, then the damping effect might be observed more clearly. This is really the case, as demonstrated in our publication [50], to which the reader is referred. Note however that the velocity field in the latter case is essentially three-dimensional that makes the presentation of the results rather complicated.

3.4 Conclusion

Analytical solutions presented in the section allowed us to reveal some interesting features related to the appearance of the thermoelectric current in the systems in which the Seebeck coefficient of the material changes abruptly when passing from one phase to another. These solutions can serve for the first estimation of the effect of the thermoelectric force in real systems provided that the thermoelectric properties of the latter are known, that, unfortunately, is rarely the case. It should be noted however that for the better estimation of the thermoelectric effects in the real system it would be interesting to consider more complicated systems which comprise at least two particles with the idea to study analytically the effect of the interaction between the particles. Also, analytic study of semi-parabolic particles attached to the boundary of the domain that would mimic the columnar dendrites would be of high interest.

Otherwise, obtained solutions can be used for the verification of numerical models since the numerical results are extremely sensitive to the size of the calculation mesh and precautions should be taken in order to obtain reasonable numerical results.

Furthermore, on the one hand, it would be interesting to try to account for the thermoelectric effects over the larger scale using the volume averaging or ensemble averaging technique. On

the other hand, one can assume that with the symmetry inherent to the system (the lines of the thermoelectric current are always closed) the averaging procedure can lead to the annulment of the effects at the macroscale. Currently the level-set method which treats the physical phenomena at the scale of individual dendrites is used for the numerical simulations at the scale of the laboratory experiments and gives satisfactory results [42, 43].

3.4.1 The author's contribution

Analytic solutions presented in the current section for the thermoelectric current in the ellipsoid particle and for the azimuthal flow around the spherical particle were obtained by the author of the present work.

The author coordinated development of the numerical code and numerical simulations for the thermoelectric current in the dendrite particle, realized during the PostDoc of R. Tarpagkou, which was financially supported by the LABEX Tec21.

The author coordinated numerical simulations of the magneto-thermoelectric flow performed with the **Reolef** software during the PostDoc of N. Bernabeu.

Chapter 4

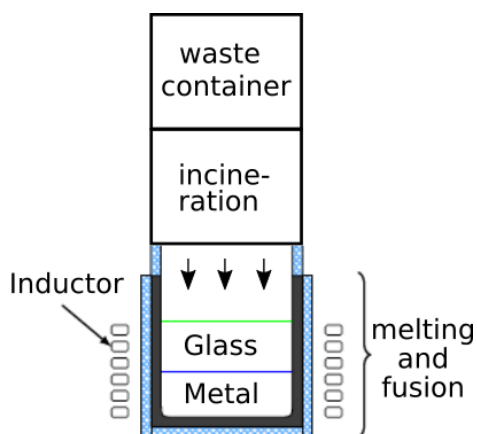
Application of single-phase AC magnetic fields in processing of metallic alloys and measurements of their properties

In this chapter two examples of utilization of monophasic AC magnetic fields are given. As it was discussed in the section 1.2, if monophasic AC magnetic fields are used, then, the interaction of the eddy current circulating in the object with a resulting magnetic field inside the latter leads to the appearance of the magnetic pressure $p \sim B_0^2/(2\mu)$ which – in ideal case – acts perpendicular to the surface of the object (see also [52]). Due to this pressure, the object may be deformed, but also this pressure can counteract gravity. Examples given below are remarkable because they demonstrate how the effect of the AC magnetic field is adapted to the specific needs via the frequency chosen for the AC current. In the first process, related to the treatment of the nuclear waste, the aim for the use of the electromagnetic fields is the heating and the stirring of the load. Consequently, the optimal frequency of the AC current is low $f \sim 30\text{Hz}$ to allow the EMF penetrate through the crucible and act inside the metallic load. Interestingly, it appears that the magnetic pressure plays an important role in the process since formation of the metal's dome is the necessary condition for the sufficient heating and stirring of the glass which is also present in the system. In the second process, the aim for the use of the EMF is twofold: to keep a metallic sample in levitation and to melt the sample. The key parameter is the electromagnetic pressure which is more efficient if the penetration depth into the load is small. Therefore, a high frequency AC current is used in the process, $f \sim 10^5\text{Hz}$.

4.1 Application of monophasic AC magnetic fields for nuclear waste treatment

In the nuclear industry, wastes of different degree of radioactive contamination can be produced during various stages of technological or research processes. Some of such wastes require long-time storage during which the environment contamination should be avoided. This is done with producing compact hermetic packages for metallic and organic wastes, which are generally

treated separately. Metallic parts are compacted via remelting with further casting and “sealing” in concrete or cans [53],[54]. Organic materials are usually incinerated and their ash is incorporated in the melted glass, which is solidified afterwards – this process is called vitrification, and in France it is performed with the inductive heating of the glass. To optimize the procedure of nuclear waste treatment, Orano group¹, ANDRA² and CEA³ develop a PIVIC process which combines incinerating stage of organic material and vitrification of the produced ash along with the remelting of the metals with further “in-can” solidification in a compact package [55], [56]. A scheme of the process is presented in fig. 4.1.



The “lower” part of the process is a *melter* which is fed with metallic and incinerated organic wastes as well as with glass frit. Low-frequency inductive heating is used to heat and melt the metal, then, the glass, which is lighter, overlays the metal and is heated and melted due to its contact with the hot metal. As it is demonstrated below, the surface of the metal becomes deformed because of the action of the magnetic pressure and the metal is also stirred intensively.

Figure 4.1: Scheme of the PIVIC process

Yet, the crucial question for the process is if the glass is stirred and heated enough to remain in the liquid state since if it solidifies, the process should be interrupted. This is defined by the parameters of the AC current used in the system: frequency and intensity of the AC current⁴ but also depends on the amount of the metal and the glass in the melter. In this process the electromagnetic pressure acts on the lateral and the upper side of the metal volume, but intensity of the AC magnetic field strongly decreases with the distance to the electromagnetic coil, i.e. toward the central axis. Because of this, the pressure on the lateral side of the metal is stronger than over its upper surface and, if amount of glass permits, the metal takes the shape of the dome emerging out of the glass (fig.4.2). Exchange of the heat and momentum between the metal and the glass takes place along the metal surface covered with the glass.

One of the key results of the work performed in the frame of the thesis of R. Bourrou [57] was the explanation of the role of the metals’ dome for the heat transfer in the system and estimation of the critical mass of the glass which could be charged in the melter. The estimation of the height of the dome of the metal accounting for the amount of the charged glass was performed analytically and compared with numerical results [58]. Analytic solution of the problem was based on the equation of the static pressure equilibrium (eq.(4.1)) and on the assumption that the dome shape is parabolic, i.e. the axial coordinate of its surface is related to the radial as

¹ex. Areva, a nuclear fuel cycle company

²Agence nationale pour la gestion des déchets radioactifs – French national agency for radioactive waste management

³Commissariat à l’énergie atomique et aux énergies alternatives – French Alternative Energies and Atomic Energy Commission

⁴Actually, the control parameters passed to the generator is the electric potential while intensity of the AC current which circulates in the coil depends on construction features of the generator and the coil

$z_m(r) = h_m(1 - r^2/R^2)$ that allows one to obtain the height of the glass h_g for a given mass of the glass M_g (eq.(4.2)). Vice versa, the critical mass of the glass $M_{g,crit}$ can be obtained under condition that the height of the glass is equal to that of the metal's dome h_m . The solution of the quadratic equation for the height of the metal dome h_m is expressed as eq.(4.3) and the critical mass of the glass which would cover the metal is given with eq.(4.4).

$$h_m \rho_m g = \frac{B_0^2}{2\mu_0} + h_g \rho_g g \quad (4.1)$$

$$h_g = \frac{1}{R} \sqrt{\frac{2M_g h_m}{\pi \rho_g}} \quad (4.2)$$

$$h_m = h_1 + h_2 + \sqrt{h_2} \sqrt{2h_1 + h_2} \quad (4.3)$$

$$\text{with } h_1 = \frac{B_0^2}{4\mu_0 \rho_m g}$$

$$\text{and } h_2 = \frac{M_g \rho_g}{\pi R^2 \rho_m^2}$$

$$M_{g,crit} = \frac{\pi R^2 \rho_g B_0^2}{8\mu_0 g (\rho_m - \rho_g)} \quad (4.4)$$

ρ_m and ρ_g is the density of the metal and the glass, respectively.

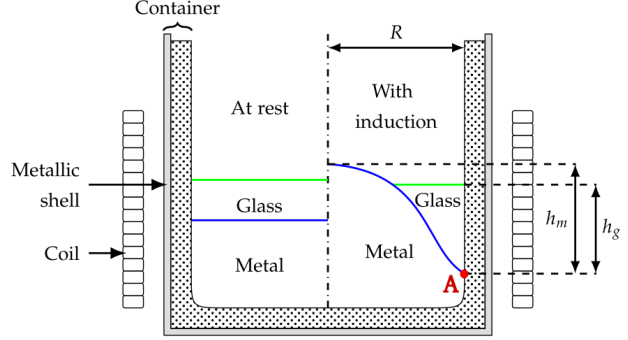


Figure 4.2: A meridional section of the melter, the metal is covered with the glass: the deformation of the surface of the metal due to the electromagnetic pressure, and the formation of a dome emerging from the glass is shown on the right, this figure corresponds to the Fig.2 from the ref.[58]

In the expressions above, B_0 is the effective value of the magnetic induction near the *point A* indicated in fig. 4.2. The value of B_0 is a function of operational parameters, and should be either measured or calculated. In the referred works [58] and [57], the value of B_0 was taken equal to 0.13 Tesla that is produced with the AC current of the frequency of 40Hz and under condition that $Q_{th}^* = 35\text{kW}$ is released in the charge.

We demonstrated that both analytic and numerical solutions gave similar results if the height of the glass does not exceed that of the metallic dome, as illustrated in the left part of the fig. 4.3a. Yet, contrary to the assumption made in the analytic solution, once the height of the glass exceeds that of the dome of the metal, the glass does not cover the metal because of the hydrodynamic effect (right part of the fig. 4.3a). Namely, instead of moving toward the axis, the glass is pulled downward due to the viscous interaction with the metal's surface, which is driven by the electromagnetic force, as discussed below. Consequently, a part of the dome near its apex remain uncovered even if the amount of glass is larger than the critical one is charged in the system. For instance for a given configuration of the melter and operational parameters ([58] and [57]), the critical mass of the glass was nearly about 35 kg yet, actually 50 kg of glass could be charged.

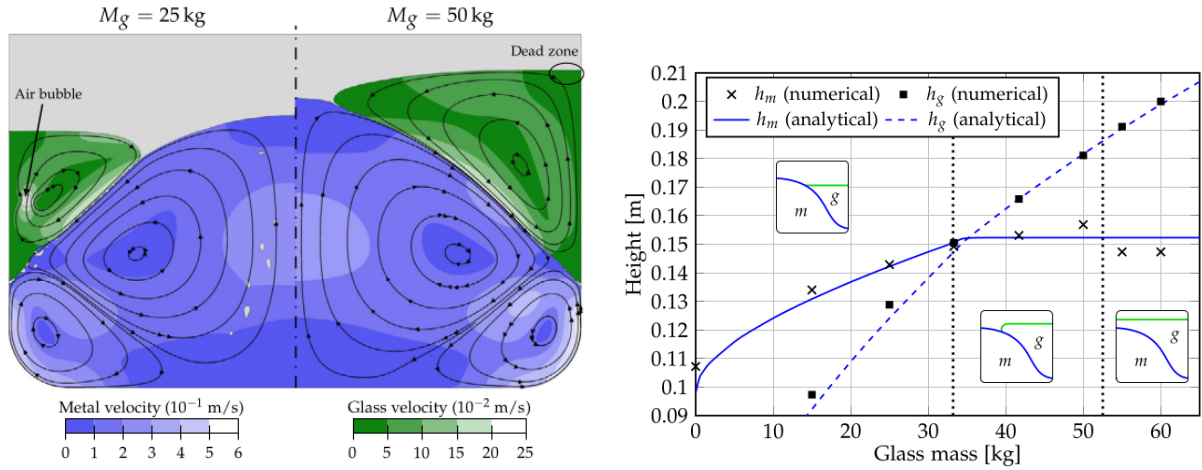


Figure 4.3: a) Illustration to the effect of the amount of glass charged in the crucible on the height of the dome of the metal and of the glass; b) Comparison of the results of solution of eqs.(4.1)-(4.4) and results obtained numerically for the height of the metal and the glass for different amount of the latter, $B_0 = 0.13 \text{ T}$, the vertical lines indicate the transition between different surface geometry as shown in inserts, from ref. [58]

Let us recall some theoretical notions presented in the section 1.2.

The electromagnetic force acting on the load can be presented as a summation of the *irrotational part* \mathbf{F}_{IR} given by eq.(4.5) and *rotational part* \mathbf{F}_R , expressed with eq.(4.6). The former, F_R , is supposed to be responsible for the magnetic pressure while the latter, F_{IR} , is a driving force acting inside the liquid.

$$F_{IR} = -\nabla \left(\frac{\mathbf{B}^2}{2\mu_m} \right) \quad (4.5)$$

$$F_R = \frac{1}{\mu_m} (\mathbf{B} \cdot \nabla) \mathbf{B} \quad (4.6)$$

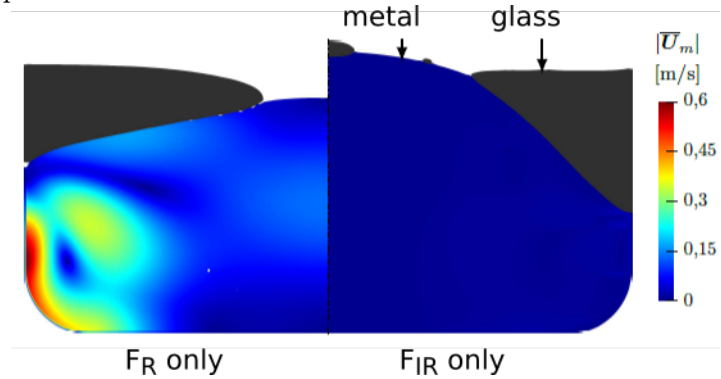


Figure 4.4: Illustration to the effect of the rotational (left) and irrotational (right) part of the electromagnetic force, F_R and F_{IR} , respectively, on the shape of the surface of the metal and velocity field

However, as can be seen in fig.4.4(left part), apart of the stirring of the metal, the rotational part of the force F_R affects the shape of the metal surface, although at the significantly less extent than the irrotational part F_{IR} , whose effect is shown in the right part of the fig.4.4. Similarly, F_{IR} produce some stirring of the metal but variation of the velocity is hardly seen in the figure. During the study of the PIVIC process, a phenomenon of the air trapping along the triple line was observed regularly in numerical simulations (fig. 4.3). Various attempts aimed to get rid of the appearance of air bubbles during simulations were not successful. In particular, with making the calculation mesh finer, a smaller bubbles were observed. This could be assign to an inherent defect of the surface reconstruction in Volume-of-Fluid model, used for presented numerical studies, when three different liquids are involved in simulations as explained in [57, p. 72–74]. On the other hand, it should be noted that the air trapping by a liquid jet falling into

a pool is a well-known hydraulic phenomenon which exists in nature (waterfalls) and can be also observed at a small scale in the laboratory experiment [59]. According to the indicated ref.[59], if the velocity of the pool surface is smaller than that of the jet, it cannot easily “assimilate” irregularities of the jet surface and captures air at the inception point. Therefore, it seems that *the only way to confirm or refute the numerically observed air entrainment would be a realization of a laboratory-scale experiment for a given configuration*, i.e. with a surface between the two liquids of significantly different viscosity and a force acting onto this surface.

To this question joins another one which concerns behavior of turbulence near such surface. Indeed, the vortices that originate in the liquid metal due to the shear stress produced by the electromagnetic force, should not be blocked at the interface between the two liquids, but penetrate, to a limited depth, into the viscous glass. It could be expected that a proper boundary condition at the interface, if the latter is treated as a real surface (not with the help of VOF model), should not be limited to the continuity of velocity and shear stress across the interface, but also take into account “continuity” of the turbulent energy.

Conclusions and open questions

Detailed numerical modeling performed for the prototype PIVIC allowed us to describe the most important effects related to the variations of different operational parameters of the setup, that are, intensity and frequency of the AC current and the mass of the glass charged in the crucible. It would be interesting to relate further studies to the physical phenomena arising between the two liquids with different viscosity when one of the liquid is subjected to the shear stresses acting near its surface.

4.2 Electromagnetic levitation: an environment and a measurement tool

With use of the electromagnetic pressure created by the monophasic AC magnetic field, $p \sim B_0^2/(2\mu)$, a metallic sample, both in solid and liquid state, can be held in space thus avoiding contamination that might occur via the contact with a support. Since the surrounding atmosphere can also be perfectly controlled, such configuration is attractive for studying of physical processes at the sample surface as well as in the bulk. The latter is, however, more complicated and either requires the use of X-rays or implies indirect measurements via (non-trivial) processing of experimental data. The simplest example is the measurement of the thermophysical properties of the liquid metals usually performed in microgravity conditions but also feasible on the Earth, the properties that assessed are surface tension, viscosity of the liquid, specific heat, thermal conductivity, total hemispherical emissivity, density and electrical resistivity [60],[61], [62], [63], [64]. Coupling of microgravity with electromagnetic levitation may seem surprising, yet, there are multiple advantages. First, the absence of gravity allows one to use the electromagnetic coils (also denoted hereafter as levitator) whose shape is adjusted to produce nearly symmetrical magnetic fields (fig.4.5). Second, the sample has only to be kept near its equilibrium position, that allows decreasing of the electromagnetic force acting on the sample and, consequently, the forced convective flow inside the sample is less intense compared to the levitation in Terrestrial conditions. Finally, since the liquid sample is only weakly perturbed with EMF, it keeps the spherical shape.

Nearly spherical shape, virtual absence of convection and only potential flow once the sample is perturbed, facilitate significantly processing of the experimental data obtained in the micrograv-

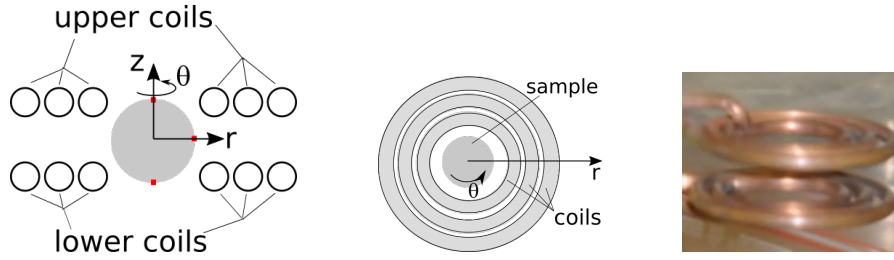


Figure 4.5: Scheme of the inductor used in microgravity conditions, lateral and top view and the photo of the actual levitation coil used in Material Space Laboratory at the International Space Station. To retain the sample, positioning current is supplied with phase difference $\Delta\varphi_p = \pi$ between the upper and the lower coils that creates quadruple magnetic field, to heat the sample and bipolar magnetic field is created with the second current which is supplied to coils without phase shift

ity [65], [66]. Questions arise however when values for thermophysical properties issued from the processed experimental data show some deviation from the data measured earlier and/or with other procedures. One may think that numerical modeling could be helpful, yet, such numerical problem remains challenging as discussed below in the section 4.2.1.

On the other hand, experiments in microgravity require long period of preparation, use of such facilities is expensive, and is restricted to certain materials because of safety reasons. Furthermore, it is hard to implement modifications in the experimental set-up and in the measurement procedure to verify rapidly new ideas. Consequently, similar measurements on Earth, would be of ultimate interest. Also, new measurement protocols could be first verified in the on-Earth set-up. The latter becomes even more interesting with application of Deep Learning algorithms. However, the gravity does pose the problem for such measurements in the Terrestrial conditions because the stronger electromagnetic forces that are required to held the sample, create also the stronger forced convection in the droplet. The latter makes the data treatment for surface tensions more complicated and hardly feasible for viscosity. Furthermore, since the convective heat transport prevails over conduction, calorimetry measurements could neither be realized. Yet, it is supposed that the damping effect of the DC magnetic field can be used to decrease the intensity of the fluid flow in the droplet. This idea was indeed realized in a set-up where AC magnetic field was used for levitation, DC magnetic field, directed vertically (parallel to the gravity vector) for the velocity damping, and periodic laser heating for calorimetry [67].

The study of the use of the electromagnetic levitation as an environment for the measurements of thermophysical properties was initiated in SIMAP/EPM by Dr. J. Etay, who participated in the ESA-MAP ThermoLab⁵. In particular, the development of the set-up was motivated by a new measurement protocol for the calorimetry proposed by Schetelat & Etay [68] that had to be verified. Continuation of this development is presented in the section 4.2.2.

4.2.1 Modeling of electromagnetic levitation in μg

The measurement procedure implemented in microgravity is based on specially constructed electric circuits which allows one to supply to the inductor two AC currents with different characteristics.

⁵See for details <https://thermolab.net/>

One of these AC currents, with the frequency $f_p \approx 150$ kHz, supplied to the inductor with a constant phase shift $\Delta\varphi_p = \pi$ between the upper and lower coils, produces a so-called “quadruple” magnetic field aimed to retain the sample near the equilibrium position which corresponds to the geometric center of the levitator (fig.4.6a).

The second AC current is supplied to the coil with the frequency of $f_h \approx 300$ kHz and has the same phase in the upper and lower coils that produce a bipolar field and a force which “squeezes” the droplet and generates significantly higher heating (fig.4.6b).

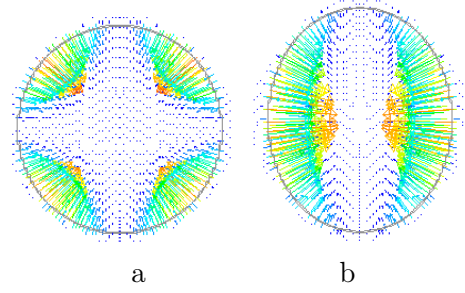


Figure 4.6: Electromagnetic force acting on the droplet with the AC current having: opposite phases in the top and bottom coil, quadruple field (a) and the same phase on the coil, bipolar field (b)

At the beginning of the experiment a solid metallic sample is placed at the center of an electromagnetic inductor and the first AC current is supplied to the coil that positioned the sample and makes it slightly heated. With supply of the second AC current during some (short) period of time the sample can be melted and over-heated up to required temperature. Then the second AC current is stopped and re-activated later in different modes for short periods of time during the cooling phase of the liquid sample that leads to deformation of the droplet and allows collecting various sets of data. In particular, two high-speed video cameras film the sample from its lateral side and from the top and temperature of the sample is measured at different areas with pyrometers. According to the Lamb’s theory [65], once the shape of the liquid sphere is slightly perturbed and released, the droplet returns to its initial spherical form with gradually attenuating oscillations of various modes n . Then, the surface tension at the interface between liquid and surrounding media γ can be measured through the frequency of these oscillation f_γ , eq.(4.7), and the dynamic viscosity η can be found via the time of decay of oscillations’ amplitude τ , eq.(4.8), as illustrated in fig.4.7. Viscosity affects also the frequency of the surface oscillations according to the eq.(4.9), yet, for the values typical for liquid metals, i.e. $\eta = O(10^{-6})\text{Pa}\cdot\text{s}$, this effect is negligible.

For a weak and (presumably) axially symmetric perturbation of the droplet, the surface oscillation of the second mode only, $n = 2$ is expected, yet, in a real experiment in microgravity, the translational oscillation can exist as well as rotation of the droplet.

$$f_{\gamma,n}^2 = \frac{n(n-1)(n+2)\gamma}{4\pi^2\rho R_0^3} \quad (4.7)$$

$$\tau_n = \frac{\rho R_0^2}{\eta(n-1)(2n+1)} \quad (4.8)$$

$$f_{\gamma,n}^* = f_{\gamma,n} \left[1 - \frac{1}{(2\pi f_{\gamma,n} \tau_n)^2} \right]^{1/2} \quad (4.9)$$

Eq.(4.9) is taken from [69]

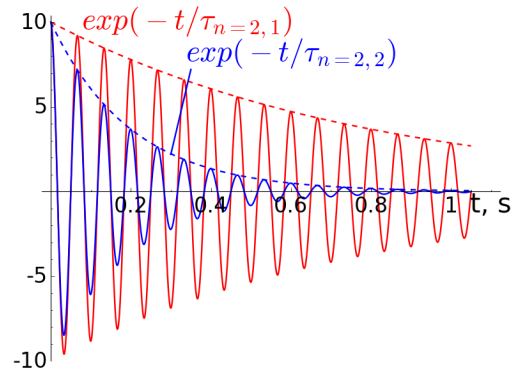


Figure 4.7: Illustration to the damping effect of the viscosity on the amplitude of the oscillation of the droplet surface for the case of the second mode $n = 2$, with the two values for time decay $\tau_{n=2,1} = 0.8\text{s}^{-1}$ and $\tau_{n=2,2} = 0.2\text{s}^{-1}$

Numerical modeling of such process is challenging because it requires that calculations of fluid flow, shape and position of the droplet and electromagnetic fields were coupled. Moreover, since the frequency of the oscillation of the droplet surface is nearly 30Hz that implies that calculation of electromagnetic field should be updated at least every 0.02s to properly account for the effect of the latter. Consequently, often accepted approach with coupling of two software, one for electromagnetic simulations (based on Finite Element Methods) and another one for calculations of the fluid flow (based on Finite Volume Methods) would hardly be possible.

Yet, the group SIMAP/EPM disposed the numerical code for the solution of the EM problem with use of the AC magnetic field, based on the Finite Volume Method ⁶ and integrated into the commercial software ANSYS[®] Fluent[®] which allows one to solve efficiently fluid flow problems including those with turbulent flow. Furthermore, use of Volume-of-Fluid (VOF) approach allows one to account for the variation of the droplet shape. Consequently, the only constraint that remains for such coupled calculations is the two-dimensional axisymmetric approach. Moreover, this constraint is related to the resources required by three-dimensional simulations, and not by the physics of the problem.

The need for resources – memory and calculation time – comes actually from two requirements issued from the boundary conditions. On the one hand, it is assumed that the intensity of the electromagnetic field decreases with the distance from the coil, consequently, the boundary conditions for the electromagnetic problem are assumed to be set “at the infinity”, i.e. the size of the calculation domain should be sufficiently large to treat these conditions properly. On the other hand, the better treatment of the droplet’s surface requires the finer spatial discretization, i.e. the larger number of computational cells that implies further the smaller time step in non-stationary computations. The advantage of the VOF method is that the calculation mesh is fixed and should not be rebuild with variation of the shape of the droplet.

Simulations were performed for the droplet of nickel, the properties can be found in the table 4.1. The first run of the numerical simulations demonstrated that with the use of the laminar model for the hydrodynamic flow the droplet could never be stabilized near the equilibrium position whereas use of (any) turbulent model provided such stabilization that corresponded to the earlier observations [70]. This can be surprising since the maximal velocity associated with the stirring of the liquid inside the droplet is nearly $V \approx 2.5$ cm/s, that with the radius of the undisturbed (spherical) droplet $R = 3.25$ mm and chosen viscosity (table 4.1) gives the value for the Reynolds number $Re \approx 81$, i.e. far below the values associated with the turbulent flow. However, there exist also oscillations of the droplet in the first mode (translation of the droplet) and of the higher modes. For example, the frequency of the oscillation of the second mode is about $f_{\gamma,2} = 35.7$ Hz and if this is associated the wavelength $\lambda_{\gamma,2} = 2\pi R_0/2$, then the corresponding velocity for the displacement of the droplet’s surface is of order $V = f_{\gamma,2}\lambda_{\gamma,2} \approx 0.35$ m/s with the corresponding value $Re_{\gamma,2} = 1137.5$. Therefore, the flow associated with the motion of the droplet surface can have the characteristics of the low-turbulent flow.

For further simulations various types of turbulent models were tested: $k - \varepsilon$ and SST $k - \omega$, both based on Boussinesque approximation of isotropic turbulent viscosity, and two versions of the Reynolds Stress models. The $k - \varepsilon$ model failed at the first stage of simulation, when only positioning AC current was considered and the position of the droplet was supposed to be stabilized that never happened in simulations. With other models the stabilization of the droplet

⁶Created by the Prof. Yves Delannoy, who is currently in the laboratory LEGI <http://www.legi.grenoble-inp.fr/web/>

Physical properties	value		unit
	Ni	Ar	
Density ρ	$8 \cdot 10^3$	1.62	$\text{kg}\cdot\text{m}^{-3}$
Dynamic viscosity η	$8 \cdot 10^{-3}$	$2 \cdot 10^{-5}$	$\text{Pa}\cdot\text{s}$
Electrical conductivity σ	$1 \cdot 10^6$	0	$\Omega^{-1} \text{m}^{-1}$
Surface tension γ	1.7		$\text{N}\cdot\text{m}^{-1}$

Table 4.1: Properties of Ni and Ar taken in the numerical simulations

was obtained and similar pattern for the fluid flow inside the droplet was observed. However, it was found that the interface between the liquid droplet and the surrounding gas was more diffuse in simulations made with the SST $k - \omega$ model than those made with the models based on calculations of Reynolds Stress. That could lead to the detachment of small amount of liquid from the droplet during the next stage of simulation with excitation of the droplet by the second AC current. For this reason in further numerical studies only the Reynolds Stress models for the turbulent flow were adopted. These two models, referred hereafter as RSM- ε and RSM- ω models have different approach to the treatment of the pressure-strain term, the reader is referred to the publication [71] and to the documentation of the ANSYS[®] Fluent[®] for further details.

The second stage of simulations consisted in activation of another AC current, with the same phase in the upper and lower loops of the inductor. As it was discussed above, the corresponding electromagnetic force squeezed the droplet. During 0.1s, the duration of the activation of the second current, the droplet experienced the squeezing (i.e. its diameter in vertical direction increased), accompanied with the oscillations, as it is seen in variation of the droplet diameter in vertical direction during the period t_1 shown in fig.4.8. Once the second current was stopped, the periodic variations of the droplet diameter decreased, period t_2 in fig.4.8. Both turbulent models produced nearly similar variations of the vertical diameter of the droplet during the both stages of simulations, however, it is seen that period of oscillations were slightly different.

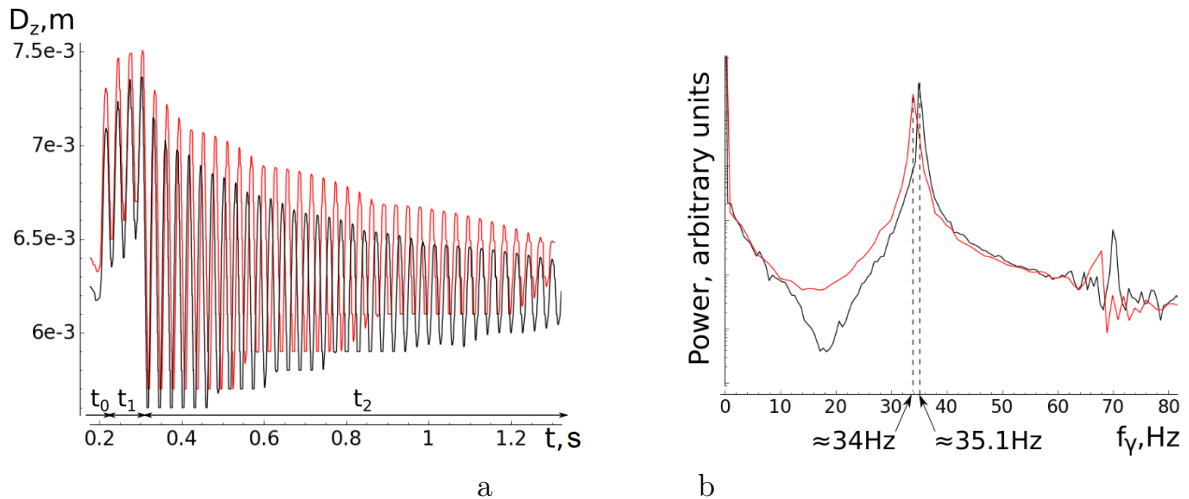


Figure 4.8: a: Variation of the vertical diameter of the droplet in simulations obtained with the two turbulent models, black line is for RSM- ω model and red line for RSM- ε model. Indicated periods of time correspond to the action of the positioning current only ($t < t_0$ and $t > t_1$) and to the activation of both currents during the period t_1 ; b: Fourier spectrum of the oscillations presented in the part a of the figure. Both figures were presented in the ref.[71]

The Fourier transformation of the periodical signals (fig.4.8b) indicated that the maximal power corresponded to the frequency $\approx 34\text{Hz}$ for the simulations with use of the RSM- ω model and $\approx 35.1\text{ Hz}$ for the simulations with the RSM- ε model, while the expected value was 35.7Hz . It should be noted that:

(a) The spectrum clearly indicates oscillations with higher frequency, nearly doubled compared to the $f_{\gamma,n=2}$. This corresponds to the oscillation in the third mode since, according to the eq.(4.7): $f_{\gamma,n=3}/f_{\gamma,n=2} = \sqrt{30}/\sqrt{8} \approx 1.93$. Since the third mode was generated that could be the indication that perturbation of the droplet surface was too strong.

(b) A very low frequency exist in the spectrum that corresponds to the droplet oscillation near its equilibrium position. This translation oscillation is not related to the presence of gravity (as it was found in [72]) but occurred because neither initial position of the droplet, nor its shape described with VOF function correspond to the stationary conditions.

The difference between the values estimated from the simulations and the expected one could be explained with the appearance of the turbulent flow which lead to the increase of the effective viscosity of the melt. According to the eq.(4.8), increase of the viscosity of the liquid diminish the decay time for the oscillations that, according to the eq.(4.9) should decrease the actual frequency of the oscillations $f_{\gamma,n}^*$. However, using the value $0.3\text{Pa}\cdot\text{s}$ for the viscosity and the theoretical value $f_{\gamma,n} = 35.7\text{Hz}$, one obtains the time decay for the second oscillations mode $\tau_{n=2} = 0.056\text{s}^{-1}$, the correction factor equal to 0.996 and the corrected frequency $f_{\gamma,n=2}^* = 35.58\text{Hz}$. The obtained value is still higher than the value of 35.1Hz estimated from the frequency of the oscillations. Consequently, various assumptions can be made, for example:

- i) As it was indicated above, probably the perturbation of the droplet was too strong, consequently, the theory is not completely applicable;
- ii) Since the flow inside the droplet is not potential because of the Lorentz force, the theory is not completely applicable;
- iii) The difference in the calculated and theoretical frequency is related to the chosen method of solution (VOF) with diffuse presentation of the droplet surface, i.e. this is a numerical artifact.
- iv) Turbulence affects the dissipation of the energy in the droplet, but this effect cannot be transposed straightforwardly via the turbulent viscosity.

All these assumptions should be verified in further research, as well as the effects related to the decay of the oscillations which was not study in details in the present work. It would be appropriate to mention that the bibliography regarding oscillation of a droplet in electromagnetic levitation is vast, yet, comparison between numerical simulation and experimental results is still rare, apart of experiments performed in microgravity.

4.2.2 Experimental set-up for the measurements of the thermo-physical properties of the liquid metals in Terrestrial conditions

As it was mentioned above, the reports about the measurements of the thermophysical properties of the liquid metals with use of electromagnetic levitation under Terrestrial conditions can be found in literature. According to these publications, the surface tension can be measured rather well either for a small droplet [73], or if some correction related to the droplet deformations because of the presence of *both, electromagnetic and gravity force*, is taken into account [72], [60], [74]. Yet, it should be noted that, to the knowledge of the author, nowadays this type of measurements is made only in the set-up constructed in Tohoku University, Sendai, Japan,

referred hereafter PROSPECT[74]. In particular, it is supposed and it has been demonstrated that the procedure of the modulated calorimetry can still be applied in terrestrial conditions if an external magnetic field of order of 4 Tesla is used to damp the convective flow in the droplet. Such coupling of the AC and DC magnetic field is realized in the aforementioned experimental set-up and modulation of the heating of the sample is made with use of the laser [74], [75], [76]. Development of the experimental set-up for the measurements of the thermophysical properties of the liquid metals in Terrestrial conditions with use of the electromagnetic levitation, referred hereafter AEXAM, was initiated in the group EPM of the SIMAP laboratory for several reasons issued from Material's Science, Magnetohydrodynamics, Electromagnetic theory, etc. Indeed, even for metals that are already in use, the thermophysical properties at high temperature are often badly known and effect of various surrounding atmosphere has never been studied. From the point of view of the Magnetohydrodynamics, effect of two external magnetic fields, AC and DC, has rarely been considered. In particular, few numerical simulations were realized for the case of AC electromagnetic levitation with superposed DC magnetic field directed vertically [77] since this configuration allows two-dimensional axisymmetric consideration and this configuration is adopted in the PROSPECT set-up. In the case of a DC field directed horizontally, as done in AEXAM set-up, a three-dimensional approach is necessary and interesting effect on the flow in the droplet can be expected. Moreover, development of the set-up in EPM was motivated, as it is already mentioned above, by a new measurement procedure proposed by Schetelat & Etay [68], which was verified numerically while experiments were done mostly with solid samples and not in levitation.

The first version of the set-up was put in use during the Thesis of A. Diarra supervised by J. Etay and A. Gagnoud [78] and measured data were reported elsewhere [79]. The scheme of the set-up is presented in fig.4.9.

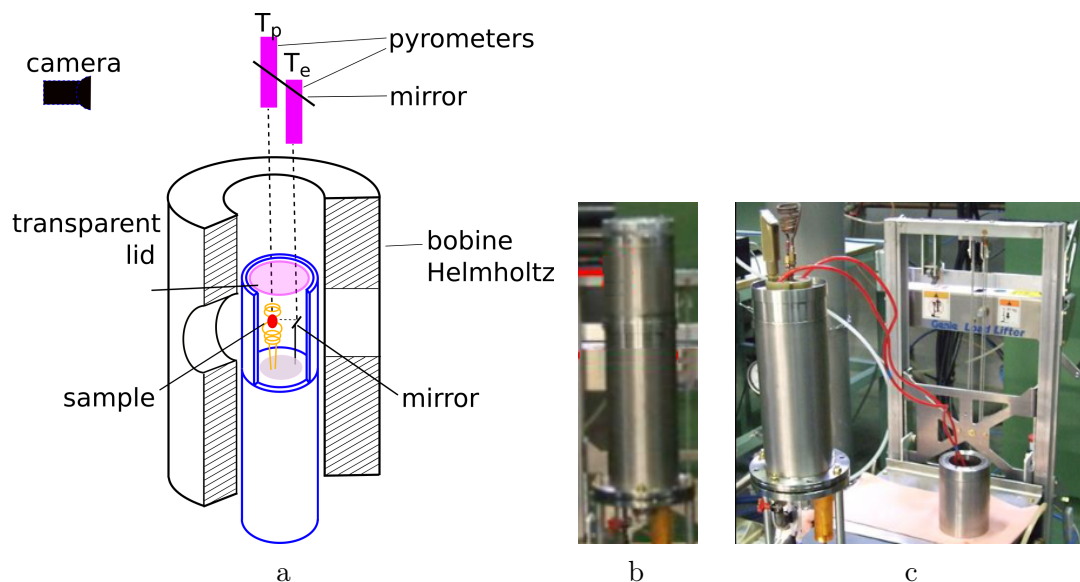


Figure 4.9: Scheme of the AEXAM set-up, first version: a) Complete installation with the Helmholtz coil providing DC magnetic field up to 5 T directed horizontally and the double-wall water cooled vacuum chamber inserted in the coil; b) Photo of the vacuum chamber which consisted of 2 parts and c) Photo of the opened vacuum chamber to show the ELM inductor, mirror and tubes for water cooling

Yet, when the attempt was made to reproduce these results with sample visualization throughout the whole experiment (duration above 1 hour), we observed multiple artifacts related to the unstable levitation of the droplet [80]. The conclusion was that the construction of the chamber which contained the electromagnetic coil for levitation had to be modified to be more ergonomic and to allow one to have better reproduction of the experimental results, this operation is ongoing (note that this text is written in 2021).

4.3 Conclusion

The chapter 4 with the two examples of the application of the monophasic AC magnetic field completes the present Thesis.

To our knowledge, in the study performed for the PIVIC process, the application of the electromagnetic field in the process with two liquids of significantly different properties was considered for the first time. A strong deformation of the surface of the metal was considered in the presence of the glass overlaid the metal. A simple theoretical model for the height of the dome of the metal was proposed and was proved correct up to a certain amount of the glass. Numerical results were obtained for different parameters that could be controlled during the process: power inputs, frequency of the AC current, and quantity of glass. In particular it was interesting to observe the difference between the expectations according to the theory and actual effects of the one or another parameter. This was related to:

- (i) the low frequency of the AC current in the system – the approximation and the reasoning in the limit of the thin electromagnetic skin depth was not correct
- (ii) the fact that the variation of the position of the metal surface was taken into account: then the distance between the load and the inductor changes and affects the force in the load.

As indicated above, it would be interesting to consider the interaction between the metal and the glass in the presence of the turbulence and to give attention to the air entrainment at the triple point, which was observed numerically.

Regarding the problem of the measurement of the thermophysical properties of liquid metals with use of the electromagnetic levitation, both the numerical and experimental ways of study continue. It was demonstrated that the results for the oscillation frequency of the droplet surface obtained with the numerical model of levitation were not too far from the theoretical ones. However, the origin of this – minor – difference is not clear. Concerning the measurements in terrestrial conditions, both the modeling and further development of the set-up are foreseen.

4.3.1 The author's contribution

Regarding the PIVIC process, the author co-supervised the Thesis of Rémi Bourrou, which was devoted to the development of the numerical model for the process. Further, the author participated in the analysis of the various aspects of the effect of the electromagnetic forces.

Numerical simulation for the electromagnetic levitation presented in the section 4.2 was performed by the author as well as the analysis of the obtained results. Further numerical studies are planned.

Chapter 5

Conclusion, ongoing projects and perspectives

In this work the projects related to the solidification of alloys, to the treatment of the nuclear wastes and to the measurement of the thermophysical properties of the liquid metals were presented. The accent was made upon the various types of electromagnetic fields used for a particular process and on the effect which the latter brings for the process. Thus, examples of application of the three types of the electromagnetic field – polyphase AC, monophasic AC and DC magnetic field – were considered. It should be underlined that EMF fields were considered as a tool to achieve a required result in a particular process. Consequently, activity of the author of this work was related to the development of the numerical and analytical models for the processes which were affected (at some extent) by the EMF. However, the proper treatment of the transport processes or/and kinetics of the phase transition implicit for the processes was of ultimate and primary importance. For each problem considered in the present work further directions for research can be rather easily indicated and these possibilities were actually evoked in conclusions for respective chapters. Let us briefly remind them.

Solidification of alloys and effect of the electromagnetic stirring

Regarding the modeling of solidification of alloys, an obvious continuation would be related to the development of a columnar-equiaxed model able to treat solidification both in columnar and equiaxed structures including the transition between these two regimes. Very few such models exist nowadays and, to our knowledge, they were not actually verified with experimental benchmark processes. That gives another possible direction for the research work on solidification related to the development and realization of experimental benchmarks, similar to Hebditch-Hunt and AFRODITE experiments, but with even better control of the boundary conditions and probably more data collected during the experiment. Moreover, development of the benchmark is interesting and seems to be really necessary accounting for the possibility of the use of Neural Networks for the prediction of the results of various processes. Since any Neural Networks should be trained on a large ensemble of the results, benchmark experiments is an appropriate tool which can provide them.

If electromagnetic stirring is applied during solidification, additional questions arise. For example, estimation of the effect related to the variation of electromagnetic properties due to phase transition on the resulting force would be of interest. Then, one can assume that interaction between the floating grains can be altered by the additional force. Yet, the most important ques-

tion is related to the interaction of the solid and the liquid phase accounting for the turbulent flow which appears inevitably once the electromagnetic stirring is applied.

Effect of DC fields on solidification of alloys

As it was already indicated, analytical solutions for different configurations of the systems with circulation of the thermoelectric current would be extremely helpful for better understanding of various results observed in multiple experiments on solidification. Furthermore, it has been demonstrated by other authors that the models which treat solidification processes at the scale of a dendrite (Phase-field, level-set) are, generally, capable to account for the magneto-thermoelectric force acting both in the solid and in the liquid. However, to our knowledge, comparison of numerical solutions obtained with these models for simple configurations with known analytic results have never been done while this step is of great importance because numerical simulation in this case are extremely mesh-sensitive. Examples of configurations which would be interesting to treat theoretically and to compare with numerical modelling are shown in fig.5.1.

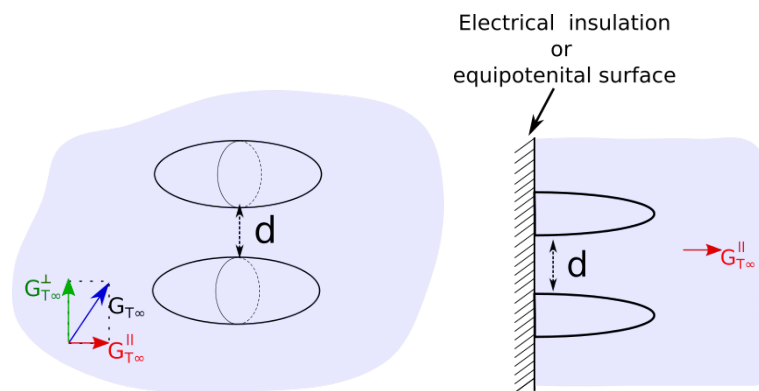


Figure 5.1: Example of configurations for the theoretical study of the thermoelectric problems: first step toward the effect of particles' interaction on the thermoelectric current

Consideration of such configurations would be helpful for the eventual development of the averaged macros-scale models where the thermoelectric current would be accounted properly.

Interaction of two liquids with different properties under electromagnetic stirring

This is a fundamental question issued from the study performed for the PIVIC process in which the melted glass overlays the liquid metal and the system is subjected to the electromagnetic stirring. The study of interaction of the two fluids would be related to the definition of the characteristics of the turbulent flow which arises due to the Lorentz force acting near the surface of the metal whose effect can be presented via shear stress and pressure. Since there is no wall between the two liquids, the turbulence seems to penetrate to the highly viscous glass where it is dissipated. This study would require some theoretical consideration for the characteristics of turbulent flow, while an experiment with the direct observation of the behaviour of the liquids near the interface would be of a high interest. Unfortunately, the latter seems to be hardly realizable.

Use of electromagnetic levitation as environment for measurements

This subject is extremely vast for further theoretical, modeling and experimental studies, it is foreseen to be the primary activity of the author and is described below.

5.1 Ongoing projects

Development of the AEXAM set-up with electromagnetic levitation

Development of the experimental set-up AEXAM for the measurements of thermophysical properties of liquid metals in Terrestrial conditions, was presented in the chapter 4, section 4.2. As it was mentioned above, the development of the experimental set-up AEXAM consists not only in the proper instrumentation of the set-up, but also in finding and application of novel procedures of measurements and treatment of the data issued from these measurements. For example, for the measurement of the thermal properties of the alloy it has been proposed to use the heating of the sample modulated with pseudo white noise instead of generally adopted sinusoidal heating [68]. Measurement of the temperature should be made at the pole and equator of the sample. Then, the theory of signal processing allows one to extract the so-called Transfer Functions which relates variation of the power released in the sample with variation of the temperature. The properties of the alloy can be almost readily obtained from the Transfer Functions if amount of the energy dissipated in the sample is known. This concept was verified during an experimental campaign with use of Ni samples and the possibility to obtain the expected data was demonstrated. Yet, to optimize and to fix the measurement protocol the experiments with samples of various materials are required. We got other ideas related to a specific control over the whole system which would provide one the ability to identify other properties of the materials, the work is ongoing. The possibility of coupling of numerical modeling of levitation in Terrestrial conditions with adapted data treatment seems to be very attractive, and some steps are made toward accounting for the 3D geometry of the inductor (fig.5.2). Yet, three-dimensional simulations remain challenging, in particular, a proper treatment of the shape of the sample seems hardly possible at the current stage.

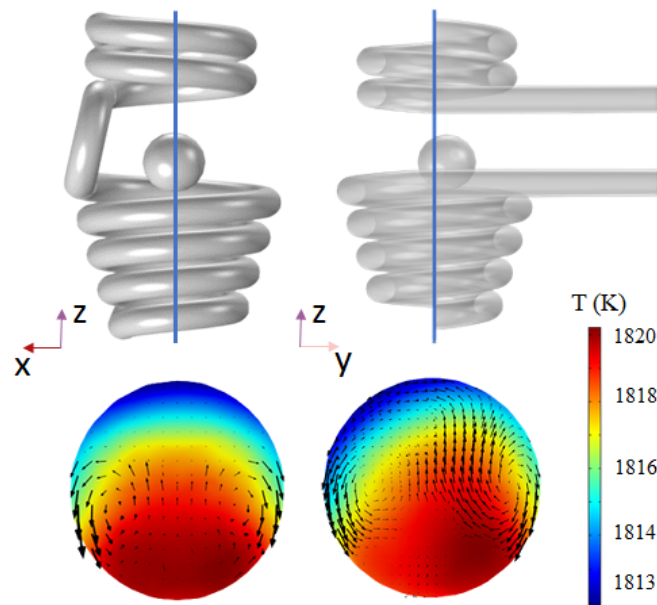


Figure 5.2: Effect of the geometry of the inductor on the flow in a levitating droplet studied with COMSOL[®] Multiphysics[®], sample deformation is not taken into account, by R. Pons at el., submitted to Magneto hydrodynamics

On the other hand, three-dimensional simulations similar to the one presented in the section 4.2.1

seem to be feasible, although extremely demanding in resources since a fine mesh is required to describe the sample (fig.5.3). However, other limitation exist regarding the shape of the inductor that can be treated and also some problems of accounting for a heat transfer with thermal radiation as a principal mode.

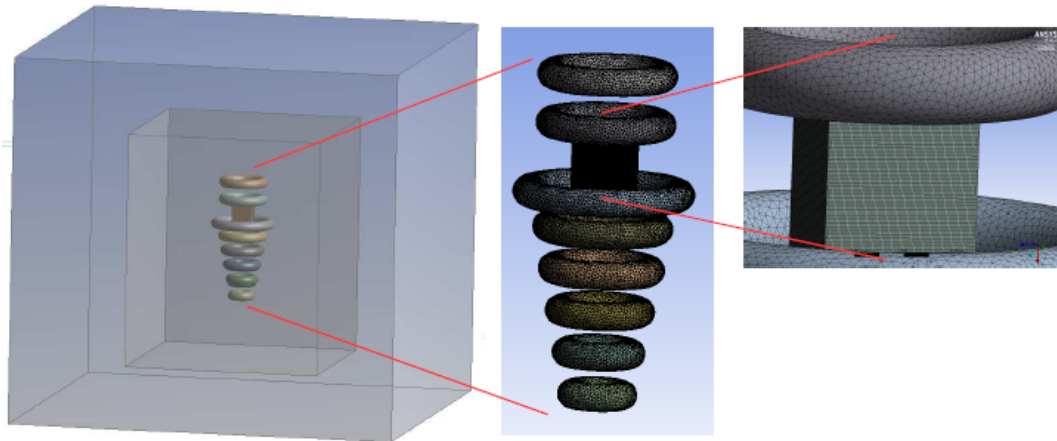


Figure 5.3: Example of a three-dimensional geometry for a levitation problem with modeling in ANSYS® Fluent® software

Consequently, the author plans to continue to work over the numerical models to be able to reproduce numerically the measurement procedure in microgravity and in the terrestrial conditions.

Solidification of multicomponent alloys

This project presents collaboration of the author with the Helmholtz-Zentrum Dresden-Rossendorf, Institute of Fluid Dynamics, Magnetohydrodynamics department¹. The collaboration is based on the large experience of the HZDR with in-situ observation of solidification of alloys with use of the laboratory source of X-Rays. Contribution of the group EPM/SIMAP is related to the expertise of the effect of convection on solidification and to the calculation of the phase diagram of a ternary alloy.

The work was initiated during the one month research stay of the author at the HZDR in the frame of a DAAD program². During this period several experiments with multicomponent low-temperature alloys were performed, their results are currently under processing and abstracts have been submitted to the International Conference on Advanced Solidification Processes, ICASP-6, which is planned for 20–24 June 2022, Le Bischenberg, France.

Further continuation of the work is seen via using of another ternary alloy to in experiments with in-situ observations. A challenge is to find an eutectic alloy which could be proceeded

¹The Helmholtz-Zentrum Dresden-Rossendorf is member of the Helmholtz Association of German Research Centres. As registered, non-profit institution supported by the authorities of the Federal Government and the Free State of Saxony the HZDR pursues interdisciplinary research in the fields of Energy, Health, and Matter, <https://www.hzdr.de/db/Cms?pNid=175>

²German Academic Exchange Service <https://www.daad.de/en/study-and-research-in-germany/plan-your-studies/help-and-advice/>

both in the set-up of HZDR with in-situ observation and in the "AFRODITE-type" set-up with post-mortem characterisation. All these actions are under discussion.

5.2 More distant future...

Eventual development of the former and actual activity of the author are indicated above. Currently, the priority is the activity related to the study of materials' properties with use of levitation technique. Actually, this is supposed to be a long-term project since multiple actions can be foreseen. In particular, a project where classical treatment of the experimental data, numerical modeling and methods of Deep Learning and Artificial Intelligence are combined seems to be very attractive. Yet, although this idea is already under discussion in the group, the time is needed to "let it ripen".

Otherwise, the author has possibility to strengthen and to develop the competence in electromagnetic fields and to study their applications to high-temperature and low-temperature multiphase fluids as well as to composite materials. The idea would be to study the effect of the EMF at different spatial scales. In fact, solidification is a good example because even in a laboratory experiment one deals with a scale which corresponds to the scale of the process and a much smaller one that corresponds to the characteristic size of the structures which appear. Keeping this idea of multiscale, the author would like to participate in studies over other materials and even the treatment of gas-fluids mixtures may be also concerned.

To sum up, the author would be interested to persuade both directions, the one related to the materials science and the second with the electromagnetic fields and fluids, electrically conductive or not, as the principles actors.

Bibliography

- [1] A. SMACS, [Solidification benchmark](#).
URL <https://benchmark-solidification.ijl.univ-lorraine.fr/>
 - [2] M. Bellet, H. Combeau, Y. Fautrelle, D. Gobin, M. Rady, E. Arquis, O. Budenkova, B. Dussoubs, Y. Duterrail, A. Kumar, C. Gandin, B. Goyeau, S. Mosbah, M. Založnik, Call for contributions to a numerical benchmark problem for 2d columnar solidification of binary alloys", *International Journal of Thermal Sciences* 48 (11) (2009) 2013 – 2016. [doi:10.1016/j.ijthermalsci.2009.07.024](https://doi.org/10.1016/j.ijthermalsci.2009.07.024).
 - [3] X. Wang, R. Moreau, J. Etay, Y. Fautrelle, A periodically reversed flow driven by a modulated traveling magnetic field: Part ii. theoretical model, *Metallurgical and Materials Transactions B* 40 (1) (2009) 104–113. [doi:10.1007/s11663-008-9210-2](https://doi.org/10.1007/s11663-008-9210-2).
 - [4] D. J. Hebditch, J. D. Hunt, Observations of Ingot Macrosegregation on Model Systems., *Metall. Trans.* 5 (7) (1974) 1557–1564.
 - [5] L. Ratke, S. Steinbach, G. Müller, M. Hainke, A. Roósz, Y. Fautrelle, M. Dupouy, G. Zimmermann, A. Weiß, H.-J. Diepers, J. Lacaze, R. Valdes, G. Grün, H.-P. Nicolai, H. Gerke-Cantow, Microstructure formation in casting of technical alloys under diffusive and magnetically controlled convective conditions, in: *Solidification and Gravity IV*, Vol. 508 of *Mater. Sci. Forum*, Trans Tech Publications Ltd, 2006, pp. 131–144.
 - [6] S. Steinbach, L. Ratke, G. Zimmermann, L. Sturz, A. Roosz, J. Kovács, Y. Fautrelle, O. Budenkova, J. Lacaze, S. Dost, G.-U. Grün, N. Warnken, M. Wu, W. Sillekens, Investigation of the effect of fluid flow on microstructure evolution in al-si-fe alloys: The micast project, in: *Proceedings of the 6th Decennial International Conference on Solidification Processing*, Old Windsor, July 2017, 2017, pp. 267–271.
 - [7] S. Steinbach, L. Ratke, G. Zimmermann, O. Budenkova, Formation of intermetallic phases in AlSi7Fe1 alloy processed under microgravity and forced fluid flow conditions and their influence on the permeability, *IOP Conference Series: Materials Science and Engineering* 117 (2016) 012019. [doi:10.1088/1757-899x/117/1/012019](https://doi.org/10.1088/1757-899x/117/1/012019).
 - [8] O. Budenkova, F. Baltaretu, S. Steinbach, L. Ratke, A. Roósz, A. Rónaföldi, J. Kovács, A. M. Bianchi, Y. Fautrelle, Modelling of al-7with a rotating magnetic field, in: *Solidification and Gravity VI*, Vol. 790 of *Materials Science Forum*, Trans Tech Publications Ltd, 2014, pp. 46–51. [doi:10.4028/www.scientific.net/MSF.790-791.46](https://doi.org/10.4028/www.scientific.net/MSF.790-791.46).
 - [9] P. Marty, W. L. Martin, P. Trombetta, T. Tomasino, J. P. Garandet, *On the Stability of Rotating MHD Flows*, Springer Netherlands, Dordrecht, 1999, pp. 327–343. [doi:10.1007/978-94-011-4764-4_23](https://doi.org/10.1007/978-94-011-4764-4_23).
-

- [10] S. Eckert, B. Willers, P. Nikrityuk, K. Eckert, U. Michel, G. Zouhar, Application of a rotating magnetic field during directional solidification of pb–sn alloys: Consequences on the cet, *Materials Science and Engineering: A* 413-414 (2005) 211 – 216, international Conference on Advances in Solidification Processes. doi:[10.1016/j.msea.2005.09.014](https://doi.org/10.1016/j.msea.2005.09.014).
- [11] O. Budenkova, A. Noepfel, J. Kovács, A. Rónaföldi, A. Roósz, A. M. Bianchi, F. Baltaretu, M. Medina, Y. Fautrelle, Comparison between simulation and experimental results of the effect of rmf on directional solidification of al-7wt.649 of *Materials Science Forum*, Trans Tech Publications Ltd, 2010, pp. 269–274. doi:[10.4028/www.scientific.net/MSF.649.269](https://doi.org/10.4028/www.scientific.net/MSF.649.269).
- [12] S. Steinbach, L. Ratke, Melt flow in a mushy zone – barrier effect of intermetallic phases, *International Journal of Cast Metals Research* 22 (1-4) (2009) 290–293. doi:[10.1179/136404609X367920](https://doi.org/10.1179/136404609X367920).
- [13] C. Nagy, Modélisation numérique multiphysique et multi-échelles de la solidification des alliages sous la convection forcée, Ph.D. thesis, Université Grenoble Alpes et University of Miskolc (Hongrie) (2018).
- [14] C. Nagy, O. Budenkova, Y. Du Terrail, A. Rónaföldi, A. Roósz, Numerical simulation series for the investigation and validation of the lorenz force field in bidirectional travelling magnetic field via thermal gradient shift effect, in: *Solidification and Gravity VII - 2018*, Hungarian Academy of Sciences – University of Miskolc, Materials Science Research Group Miskolc Committee of Hungarian Academy of Sciences, 2018, pp. 173–178.
- [15] A. Noepfel, A. Ciobanas, X. D. Wang, K. Zaidat, N. Mangelinck, O. Budenkova, A. Weiss, G. Zimmermann, Y. Fautrelle, Influence of forced/natural convection on segregation during the directional solidification of al-based binary alloys, *Metallurgical and Materials Transactions B* 41 (1) (2010) 193–208. doi:[10.1007/s11663-009-9311-6](https://doi.org/10.1007/s11663-009-9311-6).
- [16] A. I. Ciobanas, Y. Fautrelle, Ensemble averaged multiphase eulerian model for columnar/equiaxed solidification of a binary alloy: I. the mathematical model, *Journal of Physics D: Applied Physics* 40 (12) (2007) 3733–3762. doi:[10.1088/0022-3727/40/12/029](https://doi.org/10.1088/0022-3727/40/12/029).
- [17] A. Noepfel, O. Budenkova, G. Zimmermann, L. Sturz, N. Mangelinck-Noël, H. Jung, H. Nguyen-Thi, B. Billia, C.-A. Gandin, Y. Fautrelle, Numerical modelling of columnar to equiaxed transition – application to microgravity experiments, *International Journal of Cast Metals Research* 22 (1-4) (2009) 34–38. doi:[10.1179/136404609X367272](https://doi.org/10.1179/136404609X367272).
- [18] C. Beckermann, C. Wang, Multiphase/-scale modeling of alloy solidification, *Annual Review of Heat Transfer* 6 (1995).
- [19] H. Combeau, M. Založnik, S. Hans, P. E. Richy, Prediction of macrosegregation in steel ingots: Influence of the motion and the morphology of equiaxed grains, *Metallurgical and Materials Transactions B* 40 (3) (2009) 289–304. doi:[10.1007/s11663-008-9178-y](https://doi.org/10.1007/s11663-008-9178-y).
- [20] W.-s. Li, H.-f. Shen, B.-c. Liu, Numerical simulation of macrosegregation in steel ingots using a two-phase model, *International Journal of Minerals, Metallurgy, and Materials* 19 (9) (2012) 787–794. doi:[10.1007/s12613-012-0629-8](https://doi.org/10.1007/s12613-012-0629-8).

-
- [21] J. Li, M. Wu, A. Ludwig, A. Kharicha, Simulation of macrosegregation in a 2.45-ton steel ingot using a three-phase mixed columnar-equiaxed model, *International Journal of Heat and Mass Transfer* 72 (2014) 668–679. doi:10.1016/j.ijheatmasstransfer.2013.08.079.
- [22] R. Boussaa, L. Hachani, O. Budenkova, V. Botton, D. Henry, K. Zaidat, H. B. Hadid, Y. Fautrelle, Macroseggregations in sn-3wt % pb alloy solidification: Experimental and 3d numerical simulation investigations, *Int. J. Heat Mass Transf.* 100 (2016) 680–690.
- [23] L. Hachani, K. Zaidat, Y. Fautrelle, Experimental study of the solidification of sn-10wt.%pb alloy under different forced convection in benchmark experiment, *Int. J. Heat Mass Transf.* 85 (2015) 438 – 454.
- [24] X. Wang, R. Moreau, J. Etay, Y. Fautrelle, A periodically reversed flow driven by a modulated traveling magnetic field: Part II. theoretical model, *Metall. Mater. Trans. B* 40 (1) (2009) 104–113.
- [25] L. Hachani, Study of the influence of natural and forced convection on the solidification of a binary metal alloy, Phd thesis, Université de Grenoble (2013).
- [26] T. Wang, Rôle des grains équiaxes dendritiques dans la formation de macroségrégation: modélisation numérique des benchmarks laboratoires et solidification de lingot industrielle, Phd thesis, Université Grenoble Alpes (2021).
- [27] T. Wang, L. Hachani, Y. Fautrelle, Y. Delannoy, E. Wang, X. Wang, O. Budenkova, Numerical modeling of a benchmark experiment on equiaxed solidification of a sn–pb alloy with electromagnetic stirring and natural convection, *International Journal of Heat and Mass Transfer* 151 (2020) 119414. doi:10.1016/j.ijheatmasstransfer.2020.119414.
- [28] T. Wang, S. Semenov, E. Wang, Y. Delannoy, Y. Fautrelle, O. Budenkova, Effect of diffusion length in modeling of equiaxed dendritic solidification under buoyancy flow in a configuration of hebditch–hunt experiment, *Metallurgical and Materials Transactions B* 50 (6) (2019) 3039–3054. doi:10.1007/s11663-019-01703-z.
- [29] A. Mikelson, Y. K. Karklin, Control of crystallization processes by means of magnetic fields, *Journal of Crystal Growth* 52 (1981) 524–529.
- [30] C. Vives, C. Perry, Effects of magnetically damped convection during the controlled solidification of metals and alloys, *International Journal of Heat and Mass Transfer* 30 (3) (1987) 479 – 496. doi:10.1016/0017-9310(87)90263-8.
- [31] Y. Kishida, K. Takeda, I. Miyoshino, E. Takeuchi, Anisotropic effect of magnetohydrodynamics on metal solidification, *ISIJ International* 30 (1) (1990) 34–40. doi:10.2355/isijinternational.30.34.
- [32] O. Laskar, Phénomènes thermoélectriques et magnétohydrodynamiques en solidification des alliages métalliques, Ph.D. thesis, Institut National Polytechnique de Grenoble (1994).
- [33] A. Thierry, Magnétohydrodynamique et ségrégation solutale en croissance bridgman horizontale, Ph.D. thesis, Institut National Polytechnique de Grenoble (1994).
- [34] P. Lehman, Stabilité d’un front de solidification en présence d’effets thermoélectriques et magnétohydrodynamiques, Ph.D. thesis, Institut National Polytechnique de Grenoble (1996).

- [35] X. Li, Solidification en présence de champs magnétiques intenses, Ph.D. thesis, Grenoble, INPG (2007).
- [36] I. Kaldre, Effet thermoélectrique dans les métaux liquides sous champ magnétique, Ph.D. thesis, Université de Grenoble (2013).
- [37] J. Wang, Etude de l'effet thermoélectrique magnétique en solidification directionnelle d'alliages al-cu, Ph.D. thesis, Université de Grenoble (2013).
- [38] G. Salloum-Abou-Jaoude, In situ investigation by x-ray radiography of microstructure evolution during solidification of binary alloys, Ph.D. thesis, Université d'Aix-Marseille (2014).
- [39] L. Abou-Khalil, Study of the influence of external fields on solidification microstructures formation by x-ray radiography, Ph.D. thesis, Université d'Aix-Marseille (2017).
- [40] C. Wei, J. Wang, Y. He, J. Li, E. Beaugnon, Solidification of immiscible alloys under high magnetic field: A review, *Metals* 11 (3) (2021). doi:10.3390/met11030525.
- [41] R. Zhao, J. Gao, A. Kao, K. Pericleous, Measurements and modelling of dendritic growth velocities of pure fe with thermoelectric magnetohydrodynamics convection, *Journal of Crystal Growth* 475 (2017) 354–361. doi:10.1016/j.jcrysgro.2017.07.020.
- [42] A. Kao, B. Cai, P. Lee, K. Pericleous, The effects of thermoelectric magnetohydrodynamics in directional solidification under a transverse magnetic field, *Journal of Crystal Growth* 457 (2017) 270–274. doi:10.1016/j.jcrysgro.2016.07.003.
- [43] A. Kao, N. Shevchenko, S. He, P. D. Lee, S. Eckert, K. Pericleous, Magnetic effects on microstructure and solute plume dynamics of directionally solidifying ga-in alloy, *JOM* 72 (10) (2020) 3645–3651. doi:10.1007/s11837-020-04305-2.
- [44] M. Tanaka, Stabilité d'un front de solidification en présence d'effets thermoélectriques et magnétohydrodynamiques, Ph.D. thesis, Institut National Polytechnique de Grenoble (1994).
- [45] P. B. Nagy, A. H. Hayfeh, On the thermoelectric magnetic field of spherical and cylindrical inclusions, *Journal of Applied Physics* 87 (2000) 7481–7490.
- [46] F. Baltaretu, J. Wang, S. Letout, Z. Ren, X. Li, O. Budenkova, Y. Fautrelle, Thermoelectric effects on electrically conducting particles in liquid metal, *Magnetohydrodynamics* 51 (1) (2015) 45–55.
- [47] O. Budenkova, N. Bernabeu, S. Rukolaine, Y. Du Terrail Couvat, A. Gagnoud, R. Tarpagkou, Y. Fautrelle, Thermoelectric problem for an axisymmetric ellipsoid particle in the liquid metal: Analytical solution and numerical modeling, *Applied Mathematical Modelling* 45 (2017) 590–605. doi:10.1016/j.apm.2017.01.016.
- [48] D. Leenov, A. Kolin, Theory of electromagnetophoresis. i. magnetohydrodynamic forces experienced by spherical and symmetrically oriented cylindrical particles, *The Journal of Chemical Physics* 22 (4) (1954) 683–688. doi:10.1063/1.1740149.
- [49] J. A. Shercliff, Thermoelectric magnetohydrodynamics, *Journal of Fluid Mechanics* 91 (2) (1979) 231–251. doi:10.1017/S0022112079000136.

-
- [50] N. Bernabeu, O. Budenkova, A. Gagnoud, S. Rukolaine, Y. D. T. Couvat, Y. Fautrelle, Modelling of coupled convective and magneto-thermoelectric phenomena for a sphere immersed in liquid metal using finite element method and adaptive meshes, *Magnetohydrodynamics*.
- [51] P. Saramito, *Efficient C++ finite element computing with Rheolef* (2016).
- [52] R. Moreau, *Magnetohydrodynamics*, SPRINGER-SCIENCE+BUSINESS MEDIA, B.V., 1990. doi:10.1007/978-94-015-7883-7.
- [53] J.-M. Ducoulombier, B. Lantes, M. Bordier, Low and intermediate level waste management in edf pwr's, *Nuclear Engineering and Design* 176 (1) (1997) 27–34. doi:10.1016/S0029-5493(96)01328-3.
- [54] H.-W. Seo, D.-H. Lee, D. S. Kessel, C.-L. Kim, Proposal for the management strategy of metallic waste from the decommissioning of kori unit 1 by using melting and segmentation technology, *Annals of Nuclear Energy* 110 (2017) 633–647. doi:10.1016/j.anucene.2017.06.056.
- [55] R. Boen, P. Charvin, F. Lemont, A. Russello (2 2015).
- [56] P. Charvin, F. Lemont, A. Russello, Nuclear waste treatment by induction heating and stirring of a metal/glass bath: the PIVIC process, *IOP Conference Series: Materials Science and Engineering* 424 (2018) 012063. doi:10.1088/1757-899x/424/1/012063.
- [57] R. Bourrou, Développement d'un modèle numérique magnéto-thermo-hydrodynamique pour un procédé de fusion par induction d'un mélange métal-verre, Phd thesis, Université Grenoble Alpes (ComUE) (2019).
- [58] R. Bourrou, O. Budenkova, P. Charvin, C. Lafon, F. Lemont, A. Gagnoud, Numerical study of the hydrodynamics in a two-phase induction melter for nuclear waste treatment under various operating parameters, *European Journal of Mechanics - B/Fluids* 79 (2020) 181–189. doi:10.1016/j.euromechflu.2019.09.005.
- [59] K. Sene, Air entrainment by plunging jets, *Chemical Engineering Science* 43 (10) (1988) 2615–2623. doi:10.1016/0009-2509(88)80005-8.
- [60] I. Egry, G. Lohoefer, G. Jacobs, Surface tension of liquid metals: Results from measurements on ground and in space, *Phys. Rev. Lett.* 75 (1995) 4043–4046. doi:10.1103/PhysRevLett.75.4043.
- [61] H. Kobatake, H. Fukuyama, I. Minato, T. Tsukada, S. Awaji, Noncontact measurement of thermal conductivity of liquid silicon in a static magnetic field, *Applied Physics Letters* 90 (9) (2007) 094102. doi:10.1063/1.2710220.
- [62] M. Adachi, Y. Yamagata, M. Watanabe, S. Hamaya, M. Ohtsuka, H. Fukuyama, Composition dependence of normal spectral emissivity of liquid ni–al alloys, *ISIJ International* 61 (3) (2021) 684–689. doi:10.2355/isijinternational.ISIJINT-2020-233.
- [63] M. Mohr, D. C. Hofmann, H.-J. Fecht, Thermophysical properties of an fe57.75ni19.25mo10c5b8 glass-forming alloy measured in microgravity, *Advanced Engineering Materials* 23 (3) (2021) 2001143. doi:10.1002/adem.202001143.

- [64] M. Mohr, R. K. Wunderlich, K. Zweiacker, S. Prades-Rödel, R. Sauget, A. Blatter, R. Logé, A. Dommann, A. Neels, W. L. Johnson, et al., Surface tension and viscosity of liquid pd43cu27ni10p20 measured in a levitation device under microgravity, *npj Microgravity* 5 (1) (2019) 1–8. doi:10.1038/s41526-019-0065-4.
- [65] H. Lamb, *Hydrodynamics*, Cambridge University Press, 1975.
- [66] H. J. Fecht, W. L. Johnson, A conceptual approach for noncontact calorimetry in space, *Review of Scientific Instruments* 62 (5) (1991) 1299–1303. doi:10.1063/1.1142488.
- [67] T. Tsukada, H. Fukuyama, H. Kobatake, Determination of thermal conductivity and emissivity of electromagnetically levitated high-temperature droplet based on the periodic laser-heating method: Theory, *International Journal of Heat and Mass Transfer* 50 (15) (2007) 3054–3061. doi:10.1016/j.ijheatmasstransfer.2006.12.026.
- [68] P. Schetelat, J. Etay, A new approach for non-contact calorimetry: system identification using pseudo-white noise perturbation, *Heat and mass transfer* 47 (7) (2011) 759–769. doi:doi.org/10.1007/s00231-010-0711-6.
- [69] E. Becker, W. J. Hiller, T. A. Kowalewski, Experimental and theoretical investigation of large-amplitude oscillations of liquid droplets, *Journal of Fluid Mechanics* 231 (1991) 189–210. doi:10.1017/S0022112091003361.
- [70] S. R. Berry, R. W. Hyers, L. M. Racz, B. Abedian, Surface oscillations of an electromagnetically levitated droplet, *International Journal of Thermophysics* 26 (5) (2005) 1565–1581. doi:10.1007/s10765-005-8104-7.
- [71] O. Budenkova, Y. Delannoy, A. Gagnoud, Numerical simulations of turbulent flow in an electromagnetically levitated metallic droplet using $k\text{-}\Omega$ sst and reynolds stress models, *Magnetohydrodynamics c/c of Magnitnaia Gidrodinamika* 56 (2-3) (2020) 203–214.
- [72] D. L. Cummings, D. A. Blackburn, Oscillations of magnetically levitated aspherical droplets, *Journal of Fluid Mechanics* 224 (1991) 395–416. doi:10.1017/S0022112091001817.
- [73] M. E. Fraser, W. K. Lu, A. E. Hamielec, R. Murarka, Surface tension measurements on pure liquid iron and nickel by an oscillating drop technique, *Metallurgical Transactions* 2 (3) (1971) 817–823. doi:10.1007/BF02662741.
- [74] H. Fukuyama, H. Higashi, H. Yamano, Thermophysical properties of molten stainless steel containing 5 mass % b4c, *Nuclear Technology* 205 (9) (2019) 1154–1163. doi:10.1080/00295450.2019.1578572.
- [75] M. Watanabe, M. Adachi, H. Fukuyama, Normal spectral emissivity and heat capacity at constant pressure of fe–ni melts, *Journal of Materials Science* 52 (16) (2017) 9850–9858. doi:10.1007/s10853-017-1122-6.
- [76] M. Adachi, Y. Yamagata, M. Watanabe, S. Hamaya, M. Ohtsuka, H. Fukuyama, Composition dependence of normal spectral emissivity of liquid ni–al alloys, *ISIJ International* 61 (3) (2021) 684–689. doi:10.2355/isijinternational.ISIJINT-2020-233.
- [77] K. PERICLEOUS, V. BOJAREVICS, A. ROY, Modeling of eml in combined ac/dc magnetic fields as the basis for microgravity experiments, *International Journal of Microgravity Science and Application* 30 (1) (2013) 56. doi:10.15011/jasma.30.1.56.

- [78] A. Diarra, Mesures de propriétés thermiques des métaux par procédé électromagnétique, Theses, Université Grenoble Alpes (Jul. 2016).
- [79] J. Etay, A. Diarra, A. Gagnoud, C. Garnier, S. Massucci, M. Al Amir, A. Sulpice, S. Rivoirard, Measuring thermal conductivity and heat capacity of molten metallic alloys by electromagnetic levitation in dc field., *Magnetohydrodynamics (0024-998X)* 53 (2) (2017).
- [80] O. Budenkova, M. Milgravis, C. Garnier, A. Gagnoud, Y. Delannoy, S. Semenov, P. Chometon, S. Rivoirard, M. Alamir, J. Etay, Application of modulated calorimetry to the liquid metals using electromagnetic levitation and static magnetic field, *IOP Conference Series: Materials Science and Engineering* 424 (2018) 012004. [doi:10.1088/1757-899x/424/1/012004](https://doi.org/10.1088/1757-899x/424/1/012004).

Appendix A

Curriculum Vitae

BUDENKOVA Olga

CNRS researcher from 2011

Professional address:

SIMAP laboratory

1340 rue de la piscine

38402 Saint Martin d'Herès, France

EDUCATION AND CAREER

DIPLOMA:

2005: PhD in Physics, Ioffe Institute of Russian Academy of Science, Saint-Petersburg¹, Russia

1997: MD/Engineer in Thermal Physics, Department of Physics and Mechanics at State Polytechnic University of Saint-Petersburg², Russia

PREVIOUS ACTIVITY

2007-2011: Postdoc at SIMAP UMR5266³, France

1997-2007: Researcher at Ioffe Institute of Russian Academy of Science, Saint-Petersburg, Russia

RESEARCH

RESEARCH AREA

Multiscale numerical simulation :

- transport processes and phase transition in multiphase flow: solidification of alloys
- modeling of electromagnetic systems, application of electromagnetic forces in physical processes

Experimental activity:

- measurement of physical properties of metals by modulated calorimetry in electromagnetic levitation
- conception and study of electromagnetic system

¹http://www.ioffe.ru/index_en.html

²<https://english.spbstu.ru/>

³Science et Ingénierie des Matériaux et Procédés, <https://simap.grenoble-inp.fr/>

COLLABORATIONS WITH ACADEMIC PARTNERS

- Invited researcher of Helmholtz-Zentrum Dresden-Rossendorf, Germany, via DAAD scholarship, 2019
Study of solidification of multicomponents alloy, the action is on-going
- Project leader Défi CNRS Instrumentation aux limites in 2017
Collaboration with IM2NP, UMR CNRS 7334, study of the possibility of adding a stirrer in a furnace used for in-situ observation of solidification of high temperature alloys
- Project leader (from French side) for French - Hungarian collaboration via CNRS PICS 2014-2016
Collaboration with Miskolc University on the effect of electromagnetic stirring in solidification of Al-based alloys, the project allowed better supervision of the theses of C. Nagy, 2013-2018
- Project leader (from French side) for OSMOSE HPC Campus France 2015-2017
Collaboration with the laboratory of MHD Technology of Institute of Physics of University of Latvia on the use of electromagnetic impulses for enhancement of the physical processes at the surface of the liquid metals;
- Collaboration with Key EPM laboratory of the Ministry of Education at Northeastern University of Shenyang, Chine
The PhD Thesis of Tao Wang, 2017-2021 was realized in the frame of this collaboration;
- Collaboration with the laboratory of Applied Mathematics and Mathematical Physics at Ioffe Institute of Russian Academy of Sciences, Saint-Petersbourg, Russia
The joint work allowed us to consider theoretically some thermoelectric problems and to publish results in 2 papers.

ACADEMIC AND INDUSTRIAL CONTRACTS

ACADEMIC CONTRACTS

- CNES⁴ research support via program Material Sciences in Microgravity, 2018-2021
CNES provides the access to the data obtained in experiments performed in Space and supports projects related to the experiments in microgravity or to those which “mimics” the microgravity experiments, the latter is the case of the AEXAM set-up described in the section 4.2.2
- ESA⁵ – MAP ThermoProp, 2017-2019 coordinator for the group EPM–SIMAP
In the ThermoProp project EPM was responsible for numerical simulation of electromagnetic levitation, this is described in the section 4.2.1
- ESA – MAP MICAST AO-99-031, 2015-2018
The MICAST⁶ project, presented in the section 2.1, has been supported by ESA during several decades, the EPM was responsible for simulations related to the effect of electromagnetic stirring on solidification.

⁴National Center for Research in Space – Centre National d’Etudes Spatiales, <https://cnes.fr/en>

⁵European Space Agency, https://www.esa.int/Space_in_Member_States/France

⁶https://www.esa.int/Science_Exploration/Human_and_Robotic_Exploration/Blue_dot/Materials

INDUSTRIAL CONTRACTS

- CEA⁷ research contract on the study of the thermo-hydrodynamic coupling in a system of liquid metal and glass heated by low frequency induction
The project concerned development of a novel technology for the treatment of the nuclear wastes of weak activity, see section 4.1 for details. Continuation is foreseen via the guidance of a PostDoc.
- METALOR⁸ research contract on the study of the thermo-electrical properties of multiphase materials
Simulation of a complex 3D structure is required for estimation of the properties of a material, details are confidential.

SUPERVISION

THESIS SUPERVISION

Ongoing Thesis:

Romain Pons, financement from MESR

Supervised by O. Budenkova (55%) and DR CNRS Didier Chaussende (45%), both SIMAP

Thesis Subject: Development of the set-up for the measurements of the properties of liquid metals using electromagnetic levitation.

The subject of the Thesis is described in the section 4.2.2

Defended Thesis:

Tao Wang defended 1 June 2021, co-supervised by Grenoble INP, France and Northeastern University, Shenyang, China

Supervisors: O. Budenkova (40%), Prof. Y. Delannoy, SIMAP (30%), and Prof. E. Wang, Northeastern University (30%)

Actual position: PostDoc at Shanghai Jiao Tong University

Abstract: This thesis concerns the solidification of alloys and more particularly the modeling of macrosegregation in metallurgical ingots due to the growth of equiaxed grains in motion within the liquid phase. The development of a numerical model based on volume average method is presented, followed by tests on benchmark experiments and by an application to the casting of an industrial ingot. First, a modernized three-phase multiscale equiaxed solidification model has been developed, in which a new expression of the diffusion length required in the equation of grain growth has been introduced. The drastic effect of the diffusion length model has been demonstrated through simulations for solidification of Sn-5 wt% Pb alloy that mimics the Hebditch-Hunt experiment. Then, the reliability of that new equiaxed solidification model has been tested using a numerical simulation of the AFRODITE benchmark experiment on solidification of Sn-10 wt% Pb alloy with electromagnetic stirring. The predicted distributions of temperature during the solidification and of the final macro-segregation agreed well with experimental results. Finally, the equiaxed solidification model developed in this work has been used to study the formation of macrosegregation in a 2.45 ton industrial steel ingot. The formation

⁷Commissariat à l'énergie atomique et aux énergies alternatives – French Alternative Energies and Atomic Energy Commission

⁸<https://metalor.com/heritage/>

mechanism of macrosegregation in the ingot has been analyzed and the effect of cooling intensity has been studied. In addition, the effect of electromagnetic stirring on solidification process and macrosegregation formation in the ingot has been investigated through a series of simulations.

Rémi Bourrou defended 04 December 2019

Supervisors: O. Budenkova (33%), DR CNRS A. Gagnoud, SIMAP (33%), and C. Lafont, CEA (33%)

Abstract: In the PIVIC process, aimed to package mixed technological nuclear wastes, a metal-glass bath is melted by electromagnetic induction. The electrical conductivity of the glass being relatively low, the Lorentz forces and the Joule heating are present only in the metal. The glass is therefore put in motion and heated by its contact with the metallic phase, which complicates the control of the process, especially when this material starts to freeze. The goal of this thesis is to study the magneto-thermo-hydrodynamic coupling in the process to understand the freezing mechanism in order to avoid it. To this end, several numerical modelling tools are used in order to represent the thermal, hydrodynamic, and electromagnetic phenomena in the process. An essential point to take into account is the deformation of the metal's free surface by the magnetic pressure, producing a dome that can emerge from the glass phase. For the first stage of the numerical modelling, the heat transfers are discarded. The model developed consists in a coupling between COMSOL[®] Multiphysics[®] (EM induction) and ANSYS[®] Fluent[®] (turbulent fluid flow). In order to represent the deformation of the interfaces between the fluids, a three phase Volume Of Fluid (VOF) model is used. The results of the numerical model are compared to the measures performed on the prototype of the process. The study highlights the parameters having the most impact on the process and also raises an air entrainment phenomenon between the liquids. At the second stage, thermal phenomena are added to the numerical model. A separate model is developed to represent radiative heat transfers at the free surface of the liquids with the VOF model. The repartition of the cooling fluxes and the temperature inside the crucible are compared between this numerical model and the prototype. Finally, the impact of the glass mass in the crucible on the thermal behavior of the process is studied.

Csaba Nagy defended 7 September 2018, co-supervised by Grenoble INP, France and Miskolc University, Hungary

Supervisors: O. Budenkova (40%), IR Yves Du Terrail Couvat, SIMAP (30%), and Prof. A. Roozs Université de Miskolc, Hongrie, (30%)

Actual position: Engineering Team Leader - Series production support for generators at SEG Automotive, Hungary

Abstract: Aluminium and aluminium-based alloys are widely in industry due to the corrosion passivity, lighter weight, yet – in several cases – comparable strength with steel. Often, the material is used “as-cast“, that means that composition, macro- and microstructure of the material emerged during the casting defines its behaviour under different loads. Yet, convective flows generally arise in casting processes performed on-ground because of gravity and modify local solidification conditions, and, consequently, solute distribution and affect properties of material. To understand and to be able to control such phenomena, detailed experimental and numerical work has been needed. Two Bridgman-type furnaces were constructed in the University of Miskolc, Hungary, by MTA-ME Materials Science Research Group in the framework of the ESA funded MICAST project for experimental study of the effect of convective flow in solidification of alloys. These facilities were equipped with electromagnetic systems capable to generate rotating and travelling magnetic fields of various intensities. Multiphase models developed at SIMaP/EPM,

Grenoble, France, were applied for numerical study of the solidification of binary and ternary aluminium alloys under electromagnetically generated convective flow. Solidification of a binary Al-Si alloy under RMF stirring was done with Euler-Euler ensemble averaging and lever rule mesoscale models coupled with the macroscale transport both in 2D and 3D geometries. Further, effect of various modes of TMF stirring during solidification of a ternary alloys was studied in 3D geometry with lever rule based macroscopic model. Results of numerical simulations well explain the segregation observed in the experimental samples.

POST-DOC SUPERVISION:

Roza Tarpagkou, supervisors: O. Budenkova (35%), Y. Du Terrail Couvat (35%), A. Gagnoud (30%), the work on the development of a Finite Element Code for simulations of the thermoelectric effect in solidification of alloys, presented in the section [3.3](#)

Noe Bernabeu, supervisors: O. Budenkova (50%) and A. Gagnoud (50%), the work on the numerical simulation of the coupled convective and thermoelectric problem, presented in the section [3.3](#)

Sergey Semenov, supervisor: O. Budenkova (100%), the development of the equiaxed model of solidification – collaboration with Tao Wang, presented in the section [2.2](#).

STUDENT INTERNSHIP SUPERVISION

Regular supervision of 1-2 internship students per year since 2014. Exception: academic year 2020-2021.

PARTICIPATION IN THE PHD COMMITTEE

- Tao Wang Bourrou, Grenoble INP, defended on 1 June 2021, co-supervisor, invited
- Jérémy Chaulet, Université de Lorraine, defended on 11 May 2021, examiner
- Rémi Bourrou, Grenoble INP, defended on 4 December 2019, co-supervisor, invited
- Shambhavi Nandan, l'Université Aix-Marseille, defended on 20 December 2019, examiner
- Csaba Nagy, Grenoble INP – Université de Miskolc, defended on 7 September 2018, co-supervisor, examiner
- Elénore Letty, INSA – Lyon, defended on 19 October 2017, examiner
- Anne Noeppel, Grenoble INP, defended on 06 April 2009, examiner

TEACHING

- Méthodes numériques, Master 2, PHELMA, Grenoble INP, 2021/2022, 21 hours
- Rayonnement, Master 2, PHELMA, Grenoble INP, annual course from 2018, 12 hours
- Heat Transfer, “International Bachelor” (equiv. Bac+3), at PHELMA, Grenoble INP: annual course of 30 hours in 2010-2019, actually interrupted because of COVID-19
- Mathématiques : bases; “International Bachelor” (equiv. Bac+3), PHELMA, Grenoble INP, 4 hours, in 2017/2018
- Laboratory Engineering and Processes, 1st year, PHELMA, Grenoble INP, 24 hours, 2016/2017 and 2017/2018
- Supervision of students’ industrial projects, ENSE3, Grenoble INP in 2015/2016 and 2017/2018

EXPERTISE AND EDITORIAL WORK

EXPERTISE

Member of the Working group Material Sciences which assists the CNES Scientific Programs Committee, nomination for the period 2020-2025

Project reviewer for general ANR call, year 2018-2019 and 2020-2021

Project reviewer for the DFG, the German Research Foundation, in 2020 and in 2021

EDITORIAL WORK

Associated editor of Comptes Rendus Mécanique since 2019

Reviewer for various international journal, provide about 16 reviews/year

Appendix B

List of publications

Book Chapter:

Olga Budenkova, Bachir Saadi, Alexandru Ciobanas, Xiaodong Wang, Yves Fautrelle, *Chapitre 3, Transition Colonnaire-Equiaxe*, pp.281 – 297 in **Les changements de phase solide-liquide-vapeur, Vol.2 Vaporisation- Condensation- Fusion-Solidification**, Sous la direction de Hervé Combeau et Lounès Tadrist, CNRS Editions, 2016

Referred journals

- [J1] R. Pons, A. Gagnoud, D. Chaussende, and O. Budenkova, *Design of a coil for electromagnetic levitation: comparison of numerical models and coil realization*, **Magneto hydrodynamics**, submitted
- [J2] T. Wang, E. Wang, Y. Delannoy, Y. Fautrelle, O. Budenkova, *Effect of vertical electromagnetic stirring on solute distribution in billet continuous casting process*, **J. Iron and Steel Research International**, under review
- [J3] Xinming Xing, Takeshi Yoshikawa, Olga Budenkova, Didier Chaussende, *A sessile drop approach for studying 4H-SiC liquid silicon high-temperature interface reconstructions*, **J. Materials Science**, under review
- [J4] T. Wang, E. Wang, Y. Delannoy, Y. Fautrelle, O. Budenkova, *Numerical Simulation of Macrosegregation Formation in a 2.45 ton Steel Ingot Using a Three-Phase Equiaxed Solidification Model*, **Metals**, **2021**, 11 (2), 262, doi.org/10.3390/met11020262
- [J5] O. Budenkova, Y. Delannoy, A. Gagnoud, *Numerical simulations of turbulent flow in an electromagnetically levitated metallic droplet using $k-\Omega$ SST and Reynolds stress models*. **Magneto hydrodynamics**, **2020**, 56 (2-3), pp. 203-214, <http://www.mhd.sal.lv/contents/2020/2/MG.56.2.12.R.html>
- [J6] Tao Wang, Lakhdar Hachani, Yves Fautrelle, Yves Delannoy, Engang Wang, Xiaodong Wang, Olga Budenkova, *Numerical modeling of a benchmark experiment on equiaxed solidification of a Sn-Pb alloy with electromagnetic stirring and natural convection*, **Int. J. Heat and Mass Transfer**, **2020**, 151, 119114, [10.1016/j.ijheatmasstransfer.2020.119414](https://doi.org/10.1016/j.ijheatmasstransfer.2020.119414)

- [J7] R. Bourrou, O. Budenkova, C. Lafon, and A. Gagnoud, *Numerical modelling of heat transfers between inductively heated metallic and dielectric phases*, **COMPEL - The international journal for computation and mathematics in electrical and electronic engineering**, 2020, 39 (1), 108-116, <https://www.emerald.com/insight/content/doi/10.1108/COMPEL-05-2019-0218/full/html>
- [J8] R. Bourrou, O. Budenkova, P. Charvin, C. Lafon, F. Lemont, A. Gagnoud, *Numerical study of the hydrodynamics in a two-phase induction melter for nuclear waste treatment under various operating parameters*, **European Journal of Mechanics-B/Fluids**, 2020, 79, 181-189, [10.1016/j.euromechflu.2019.09.005](https://doi.org/10.1016/j.euromechflu.2019.09.005)
- [J9] T. Wang, S. Semenov, E. Wang, Y. Delannoy, Y. Fautrelle, O. Budenkova, *Effect of Diffusion Length in Modeling of Equiaxed Dendritic Solidification under Buoyancy Flow in a Configuration of Hebditch–Hunt Experiment*, **Metallurgical and Materials Transactions B**, 2019, 50 (6), 3039-3054, [10.1007/s11663-019-01703-z](https://doi.org/10.1007/s11663-019-01703-z)
- [J10] O. Budenkova, N. Bernabeu, S. Rukolaine, Y. Du Terrail Couvat, A. Gagnoud, R. Tarpagkou, Y. Fautrelle, *Thermoelectric problem for an axisymmetric ellipsoid particle in the liquid metal: Analytical solution and numerical modeling*, **Applied Mathematical Modelling**, 2017, 45, 590-605, [10.1016/j.apm.2017.01.016](https://doi.org/10.1016/j.apm.2017.01.016)
- [J11] N. Bernabeu, O. Budenkova, A. Gagnoud, S. Rukolaine, Y. Du Terrail Couvat, Y. Fautrelle, *Modelling of coupled convective and magneto-thermoelectric phenomena for a sphere immersed in liquid metal using finite element method and adaptive meshes*, **Magnetohydrodynamics**, 2017, 53 (1), 149-158, <http://mhd.sal.lv/contents/2017/1/MG.53.1.16.R.html>
- [J12] R. Boussaa, L. Hachani, O. Budenkova, V. Botton, D. Henry, K. Zaidat, H. Ben Hadid, Y. Fautrelle, *Macroseggregations in Sn-3 wt%Pb alloy solidification: Experimental and 3D numerical simulation investigations*, **Int. J. Heat and Mass Transfer**, 2016, 100, 680-690, [10.1016/j.ijheatmasstransfer.2016.04.120](https://doi.org/10.1016/j.ijheatmasstransfer.2016.04.120)
- [J13] F. Baltaretu, J. Wang, S. Letout, Z.-M. Ren, X. Li, O. Budenkova, Y. Fautrelle, *Thermoelectric effects on electrically conducting particles in liquid metals*, **Magnetohydrodynamics**, 2015, 51 (1), 45-55, <http://mhd.sal.lv/contents/2015/1/MG.51.1.6.R.html>
- [J14] S. Ganina, V. Ginkin, O. Budenkova, B. Saadi, L. Hachani and Y. Fautrelle, *Modelling of the crystallization of binary alloys based on the results of numerical and experimental benchmarks*, **VANT: Mathematical modelling of physical processes**, 2012, 3, 45-57, in Russian
- [J15] A. Noeppel, A. Ciobanas, X. D. Wang, K. Zaidat, N. Mangelinck, O. Budenkova, A. Weiss, G. Zimmermann and Y. Fautrelle, *Influence of Forced/Natural Convection on Segregation During the Directional Solidification of Al-Based Binary Alloys*, **Metallurgical Materials Transactions B**, 2010, 41 (1), 193-208, [10.1007/s11663-009-9311-6](https://doi.org/10.1007/s11663-009-9311-6)
- [J16] A. Noeppel, O. Budenkova, G. Zimmermann, L. Sturz, N. Mangelinck-Noel, H. Jung, H. Nguyen-Thi, B. Billia, C.-A. Gandin and Y. Fautrelle, *Numerical modelling of columnar to equiaxed transition – application to microgravity experiments*, **Int. J. Cast Metals Research**, 2009, 22 (1-4), 34-38, [10.1179/136404609X367272](https://doi.org/10.1179/136404609X367272)

- [J17] A. Noeppel, O. Budenkova, Y. Fautrelle, *Numerical investigation of the influence of forced convection induced by a travelling magnetic field during solidification of metallic alloys*, **Magneto-hydrodynamics**, **2009**, 45 (4), 497-504, <http://mhd.sal.lv/contents/2009/4/MG.45.4.2.R.html>
- [J18] M. Bellet, H. Combeau, Y. Fautrelle, D. Gobin, M. Rady, E. Arquis, O. Budenkova, B. Dussoubs, Y. Duterrail, A. Kumar, C.A. Gandin, B. Goyeau, S. Mosbah and M. Založnik *Call for contributions to a numerical benchmark problem for 2D columnar solidification of binary alloys*, **Int. Journal of Thermal Science**, **2009**, 48(11), 2013-2016, [10.1016/j.ijthermalsci.2009.07.024](https://doi.org/10.1016/j.ijthermalsci.2009.07.024)
- [J19] X. Li, A. Noeppel, B. Saadi, O. Budenkova, K. Zaidat, A. Ciobanas, Z. Ren and Y. Fautrelle, *Solidification of Metallic Alloys under Magnetic Field*, **Trans. Indian Institute of Metals**, **2009**, 62 (4-5), 465-467, [10.1007/s12666-009-0062-5](https://doi.org/10.1007/s12666-009-0062-5)
- [J20] O. N. Budenkova, M. G. Vasiliev, V. S. Yuferev, I. A. Ivanov, A. M. Bul'kanov, and V. V. Kalaev, *Investigation of the Variations in the Crystallization Front Shape during Growth of Gadolinium Gallium and Terbium Gallium Crystals by the Czochralski Method*, **Crystallogr. Reports**, **2008**, 53, No. 7, 1181-1190, [10.1134/S106377450807016X](https://doi.org/10.1134/S106377450807016X)
- [J21] O. Budenkova, M. Vasiliev, V. Yuferev and V. Kalaev, *Effect of internal radiation on the solid-liquid interface shape in low and high thermal gradient Czochralski growth*, **J. Crystal Growth**, **2007**, 303, 156-160, [10.1016/j.jcrysgro.2006.12.055](https://doi.org/10.1016/j.jcrysgro.2006.12.055)
- [J22] O. N. Budenkova, M. G. Vasiliev, V. N. Shlegel, N. V. Ivannikova, R. I. Bragin, V. V. Kalaev *Comparative analysis of the heat transfer processes during growth of $Bi_{12}GeO_{20}$ and $Bi_4Ge_3O_{12}$ crystals by the Low-Thermal-Gradient Czochralski technique*, **Crystallography Reports**, **2005**, 49, Suppl.1, S.100-106, [10.1134/1.2133982](https://doi.org/10.1134/1.2133982)
- [J23] V. Bermudez, O. N. Budenkova, V. S. Yuferev, M. G. Vasiliev, E. N. Bystrova, V. V. Kalaev, J. C. Rojo, E. Dieguez, *Effect of the shouldering angle on the shape of the solid-liquid interface and temperature fields in sillenite-type crystals growth*, **J. Crystal Growth**, **2005**, 279, 82-87, [10.1016/j.jcrysgro.2004.12.181](https://doi.org/10.1016/j.jcrysgro.2004.12.181)
- [J24] M. G. Vasiliev, O. N. Budenkova, V. S. Yuferev, V. V. Kalaev, V. N. Shlegel, N. V. Ivannikova, Ya. V. Vasiliev, V. M. Mamedov. *Effect of heat shield on the shape of the solid/liquid interface and temperature fields in the BGO-eulithine LTG Cz growth*, **J. Crystal Growth**, **2005**, 275, e745-e750, [10.1016/j.jcrysgro.2004.11.087](https://doi.org/10.1016/j.jcrysgro.2004.11.087)
- [J25] O. N. Budenkova, V. S. Yuferev, M. G. Vasiliev, V. V. Kalaev, *Peculiarities of the temperature fields in semitransparent oxide crystals being grown by Cz technique*, **J. Crystal Growth**, **2005**, 275, e727-e731, [10.1016/j.jcrysgro.2004.11.218](https://doi.org/10.1016/j.jcrysgro.2004.11.218)
- [J26] O. N. Budenkova, M. G. Vasiliev, V. S. Yuferev, E. N. Bystrova, V. V. Kalaev, V. Bermudez, E. Dieguez and Yu. N. Makarov, *Simulation of global heat transfer in the Czochralski process for BGO sillenite crystals*, **J. Crystal Growth**, **2004**, 266, 103-108 [10.1016/j.jcrysgro.2004.02.035](https://doi.org/10.1016/j.jcrysgro.2004.02.035)
- [J27] O. N. Budenkova, V. M. Mamedov, M. G. Vasiliev, V. S. Yuferev, Yu. N. Makarov, *Effect of internal radiation on the crystal-melt interface shape in Czochralski oxide growth*, **J. Crystal Growth**, **2004**, 266, 92-102, [10.1016/j.jcrysgro.2004.02.034](https://doi.org/10.1016/j.jcrysgro.2004.02.034)

- [J28] O. N. Budenkova, M. G. Vasilyev, S. A. Rukolaine, V. S. Yuferev, *Radiative heat transfer in axisymmetric domains of complex shape with Fresnel boundaries*, **J. Quant. Spectroscopy and Rad. Transfer**, **2004**, 84, 451-463, [10.1016/S0022-4073\(03\)00262-0](https://doi.org/10.1016/S0022-4073(03)00262-0)
- [J29] V. S. Yuferev, O. N. Budenkova, M. G. Vasiliev, S. A. Rukolaine, V. N. Shlegel, Ya. V. Vasiliev, A. I. Zhmakin, *Variations of solid-liquid interface in the BGO low thermal gradients Cz growth for diffuse and specular crystal side surface*, **J. Crystal Growth**, **2003**, 253, 383-397, [10.1016/S0022-0248\(03\)01110-2](https://doi.org/10.1016/S0022-0248(03)01110-2)
- [J30] V. V. Bat'kovich, O. N. Budenkova, V. B. Konstantinov, O. L. Sadvov, E. A. Smirnova, *Determination of the temperature distribution in liquids and solids using holographic interferometry*, **Technical Physics**, **1999**, 44 (6), 704-708, [10.1134/1.1259446](https://doi.org/10.1134/1.1259446)

Conference Proceedings with the Review Committee

- [PC1] T. Wang, S. Semenov, E. Wang, Y. Delannoy, Y. Fautrelle, O. Budenkova, *Comparison of two-phase and three-phase macroscopic models of equiaxed grain growth in solidification of binary alloy with electromagnetic stirring*, **IOP Conference Series: Materials Science and Engineering**, **2020**, 861, 012026, [doi:10.1088/1757-899X/861/1/012026](https://doi.org/10.1088/1757-899X/861/1/012026)
- [PC2] T. Wang, E. Wang, Y. Delannoy, Y. Fautrelle, O. Budenkova, *Three-phase numerical modeling for equiaxed solidification of Sn-10 wt.%Pb alloy under forced convection driven by electromagnetic force*, **IOP Conference Series: Materials Science and Engineering**, **2019**, 529 (1), 012030, [10.1088/1757-899X/529/1/012030](https://doi.org/10.1088/1757-899X/529/1/012030)
- [PC3] O. Budenkova, M. Milgravis, Ch. Garnier, A. Gagnoud, Y. Delannoy, S. Semenov, P. Chometon, S. Rivoirard, M. Alamir, J. Etay, *Application of modulated calorimetry to the liquid metals using electromagnetic levitation and static magnetic field*, **IOP Conference Series: Materials Science and Engineering**, **2018**, 424 (1), 012004, [10.1088/1757-899X/424/1/012004](https://doi.org/10.1088/1757-899X/424/1/012004)
- [PC4] R. Bourrou, A. Gagnoud, O. Budenkova, P. Charvin, C. Lafon, *Numerical simulation of surface deformations in a three-fluid process stirred by low frequency magnetic field*, **IOP Conf. Series: Materials Science and Engineering**, **2018** 424 (1) 012030, [doi:10.1088/1757-899X/424/1/012030](https://doi.org/10.1088/1757-899X/424/1/012030)
- [PC5] A. Gagnoud, Y. Du Terrail-Couvat, O. Budenkova, *3D Numerical Modeling for Inductive Processes*, **IOP Conf. Series: Materials Science and Engineering**, **2018**, 424(1) 012045, [doi:10.1088/1757-899X/424/1/012045](https://doi.org/10.1088/1757-899X/424/1/012045)
- [PC6] O Budenkova, A Gagnoud, Y Delannoy, *Numerical Simulations of Turbulent Flow in the Electromagnetically levitated metallic droplet*, **Proc. 11th PAMIR International Conference Fundamental and Applied MHD, 1- 5 July, Reims, France, 2018**
- [PC7] C. Nagy, O. Budenkova, Y. Du Terrail, A. Ronafodli, A. Roos, *Numerical simulation series for the investigation and validation of the Lorenz force field in bidirectional travelling magnetic field via thermal gradient shift effect*, **Proc. Solidification and Gravity VII, Sep 2018, Miskolc, Hungary, 173 - 178**
- [PC8] T. Wang, O. Budenkova, Y. Delannoy, Y. Fautrelle, E. Wang, *A 3-phase equiaxed solidification numerical model for binary alloy coupling macroscopic transport and grain growth*, **Proc. Solidification and Gravity VII, Sep 2018, Miskolc, Hungary, 179 - 184**

- [PC9] O. Budenkova, C. Nagy, Y. Du Terrail Couvat, S. Steinbach, A. Roosz, Y. Fautrelle, *Comparison of 2D and 3D simulations of solidification of binary and ternary Al-based alloys under RMF*, **Proc. 6th Decennial Int. Conf. on Solidification Processing, 25th-28th July 2017, Beaumont Estate, Old Windsor, UK**
- [PC10] S.Steinbach, O. Budenkova, C. Nagy, Y. Du Terrail Couvat, S. Steinbach, A. Roosz, Y. Fautrelle, *Comparison of 2D and 3D simulations of solidification of binary and ternary Al-based alloys under RMF*, **Proc. 6th Decennial Int. Conf. on Solidification Processing, 25th-28th July 2017, Beaumont Estate, Old Windsor, UK**
- [PC11] R. Tarpagkou, Y. Du Terrail Couvat, A. Gagnoud, O. Budenkova, Y. Fautrelle, *Finite Element Multigrid Approach to Numerical Simualtions related to Magneto-Thermoelectric Effects in Solidification of Metals*, **Proc. 10th PAMIR Int. Conf., Fundamental and Applied MHD, June 20-24, 2016, Cagliari, Italy**
- [PC12] S. Steinbach, L. Ratke, G. Zimmermann and O. Budenkova, *Formation of intermetallic phases in AlSi7Fe1 alloy processed under microgravity and forced fluid flow conditions and their influence on the permeability*, **IOP Conf. Series: Materials Science and Engineering, 2016, 117, 012019, doi:10.1088/1757-899X/117/1/012019**
- [PC13] J. Wang, G. S. Abou-Jaoude, O. Budenkova, G. Reinhart, N. Mangelinck, X. Li, H. Nguyen-Thi, Z-M. Ren, Y. Fautrelle, *Convection and solidification influenced by thermo-electric effect*, **IOP Conf. Series: Materials Science and Engineering, 2016, 117, 012051, 10.1088/1757-899X/117/1/012051**
- [PC14] N. Bernabeu, A. Gagnoud, Y. Du Terrail Couvat, O. Budenkova, Y. Fautrelle, *Simulation of magneto-thermoelectric phenomena coupled with convection around a particle using finite element method and adaptive meshes*, **Proc. 10th PAMIR Int. Conf., Fundamental and Applied MHD, June 20-24, 2016, Cagliari, Italy**
- [PC15] N. Csaba, O.Budenkova, Y. Du Terrail Couvat, Y. Fautrelle, A. Roósz, *Effect of electromagnetic stirring on the solidification of Al-7wt%Si alloy: experiment and simulation*, **Proc. 8 Int. Conf. Electromagnetic processing of materials, EPM 2015, 12-16 October 2015, Cannes, France, 77-80**
- [PC16] Y. Du Terrail Couvat, O. Budenkova, A. Gagnoud, G. Salloum Abou Jaoude, H. Nguyen-Thi, G. Reinhart, J. Wang, Z-M. Ren, Y. Fautrelle, *Modeling of the effect of a thermoelectric magnetic force onto conducting particles immersed in the liquid metal*, **IOP Conf. Series: Materials Science and Engineering, 2015, 84, 012019, 10.1088/1757-899X/84/1/012019**
- [PC17] Ya. Fan, Y. Fautrelle, Z.-R. Ren, O. Budenkova, C. Li, W. Ren, *A new method for calculating thermoelectric current during the solidification of alloys*, **Proc. 8 Int. Conf. Electromagnetic processing of materials, EPM 2015, 12-16 October 2015, Cannes, France, 101-104**
- [PC18] Y. Du Terrail Couvat, A. Gagnoud, D. Brasiliano, O. Budenkova, Y. Fautrelle, *Numerical modelling of thermoelectric magnetic effects in solidification*, **Proc. 8 Int. Conf. Electromagnetic processing of materials, EPM 2015, 12-16 October 2015, Cannes, France, 133-136**

- [PC19] O. Budenkova, F. Baltaretu, S. Steinbach, L. Ratke, A. Roósz, A. Rónaföldi, J. Kovács, A-M. Bianchi and Y. Fautrelle, *Modeling of Al-7wt%Si-1wt%Fe ternary alloy: application to space experiments with a rotating magnetic fields*, **Materials Science Forum**, **2014**, 790-791, 46-51, <https://www.scientific.net/MSF.790-791.46>
- [PC20] L. Hachani, J. Wang, I. Kaldre, G. Salloum Abou-Jaoude, O. Budenkova, G. Reinhart, K. Zaidat, N. Mangelinck-Noel, X. Li, H. Nguyen-Thi, A. Bojarevics, Z.-M. Ren, L. Buligins and Y. Fautrelle, *Magnetic Fields, Convection and Solidification*, **Materials Science Forum**, **2014**, 790-791, 375-383, <https://www.scientific.net/MSF.790-791.375>
- [PC21] H. Nguyen-Thi, J. Wang, G. Salloum Abou-Jaoude, G. Reinhart, I. Kaldre, N. Mangelinck, Z.-M. Ren, L. Buligins, A. Bojarevics, Y. Fautrelle, O. Budenkova and T. Lafford, *In-situ and real-time analysis of TEM forces induced by a permanent magnetic field during solidification of Al-4wt%Cu*, **Materials Science Forum**, **2014**, 790-791, 420-425, <https://www.scientific.net/MSF.790-791.420>
- [PC22] Csaba Nagy, Yves Fautrelle, Olga Budenkova, Arnold Rónaföldi, András Roósz, *Numerical simulation of the RMF stirring of molten Ga-In alloy using RANS $k-\varepsilon$ and LES turbulence models*, **Materials Science Forum**, **2014**, 790-791, 402-407, <https://www.scientific.net/MSF.790-791.402>
- [PC23] R. Boussaa, O. Budenkova, L. Hachani, X-D. Wang, B. Saadi, K. Zaidat, H. Ben Hadid, Y. Fautrelle, *2D and 3D Numerical Modeling of Solidification Benchmark of Sn-3Pb%wt. Alloy under Natural Convection*, **Proc. 141st TMS Annual Meeting and Exhibition, Conf. EPD 2012, 11-15 March, Orlando, Florida, USA**, Ed. JOHN WILEY & SONS 2012, ISBN:978-1-11829-140-5,537-544
- [PC24] R. Boussaa, O. Budenkova, L. Hachani, X-D. Wang, B. Saadi, K. Zaidat, H. Ben Hadid, Y. Fautrelle, *2D and 3D Numerical Modeling of Solidification Benchmark of Sn-3Pb (%wt.) Alloy under Natural Convection*, **Proc. 141st TMS Annual Meeting and Exhibition, Symp. CFD Modeling and Simulation in Materials Processing, 11-15 March, Orlando, Florida, USA**, Ed. JOHN WILEY & SONS 2012, ISBN:978-1-11829-615-8,163-170
- [PC25] LI Xi, REN Zhongming, GAGNOUD Annie, BUDENKOVA Olga, BOJAREVICS Andris, FAUTRELLE Yves, *Thermo-electric motions and structures generated by static magnetic fields during the solidification of metallic alloys*, **Proc. Electromagnetic Processing of Materials, EPM2012 dans J. Iron and Steel Research, Vol.19, Suppl.1, 2012, 9-17**
- [PC26] Kader Zaïdat, Mircea Cablea, Abdallah Nouri, Ghatfan Hassan, Bachir Saadi, Olga Budenkova, Annie Gagnoud, Yves Delannoy, *Impact of the Travelling Magnetic Field on the Metallic Impurities During the Crystallization of Photovoltaic Silicon*, **Proc. Electromagnetic Processing of Materials, EPM2012 dans J. Iron and Steel Research, Vol.19, Suppl.1, 2012, 243-247**
- [PC27] S. Ganina, V. Ginkin, O. Budenkova, B. Saadi, L. Hachani and Y. Fautrelle, *Comparison of Two Models for Simulation of Binary Alloy Solidification*, **Defect and Diffusion Forum**, **2012**, 326-328,599-604, [doi:10.4028/www.scientific.net/DDF.326-328.599](https://doi.org/10.4028/www.scientific.net/DDF.326-328.599)
- [PC28] O. Budenkova, F. Baltaretu, J. Kovács, A. Roósz, A. Rónaföldi, A-M. Bianchi and Y. Fautrelle, *Simulation of a directional solidification of a binary Al-7wt%Si and a ternary alloy Al-7wt%Si-*

1wt%Fe under the action of a rotating magnetic field, **IOP Conf. Series: Mater. Science and Engineering**, 2012, 33, 012046 doi:10.1088/1757-899X/33/1/012046

- [PC29] H. Combeau, M. Bellet, Y. Fautrelle, D. Gobin, E. Arquis, O. Budenkova, B. Dussoubs, Y. Du Terrail, A. Kumar, C.-A. Gandin, B. Goyeau, S. Mosbah, T. Quatravaux, M. Rady and M. Založnik, *Analysis of a numerical benchmark for columnar solidification of binary alloys*, **IOP Conf. Series: Materials Science and Engineering**, 2012, 33, 012086, doi: 10.1088/1757-899X/33/1/012086
- [PC30] H. Combeau, M. Bellet, Y. Fautrelle, D. Gobin, E. Arquis, O. Budenkova, B. Dussoubs, Y. Duterrail, A. Kumar, B. Goyeau, S. Mosbah, T. Quatravaux, M. Rady, C.-A. Gandin, M. Založnik, *A Numerical Benchmark on the Prediction of Macrosegregation in Binary Alloys*, **Proc. 2011 TMS Annual Meeting & Exhibition, Frontiers in Solidification Science, Vol 2 MATERIALS FABRICATION, PROPERTIES, CHARACTERIZATION, AND MODELING**, 2011, 755-762
- [PC31] R. Mooney, D. J. Browne, O. Budenkova, Y. Fautrelle, L. Froyen, A. Kartavykh, S. Mc Fadden, S. Rex, B. Schmitz, D. Voss, *Review of the MAXUS 8 sounding rocket experiment to investigate solidification in a Ti-Al-Nb alloy*, **Proc. 20th ESA Symposium on European Rocket and Balloon Programmes and Related Research**, 22-26 May, Hyeres, France 2011, 453-458
- [PC32] O. Budenkova, A. Noepfel, J. Kovács, A. Rónaföldi, A. Roósz, A.-M. Bianchi, F. Baltaretu, M. Medina and Y. Fautrelle, *Numerical investigation of directional solidification of Al-7%wt Si under the action of RMF*, **Materials Science Forum**, 2010, 649, 269-274, <https://www.scientific.net/MSF.649.269>
- [PC33] F. Lemoisson, S. Mc Fadden, M. Rebow, D.J. Browne, L. Froyen, D. Voss, D.J. Jarvis, A. Kartavykh, S. Rex, W. Herfs, D. Groethe, J. Lapin, O. Budenkova, J. Etay and Y. Fautrelle, *The Development of a Microgravity Experiment involving Columnar to Equiaxed Transition for Solidification of a Ti-Al based Alloy*, **Materials Science Forum**, 2010, 649, 17-23, <https://www.scientific.net/MSF.649.17>
- [PC34] Valentin Yuferev, V.B. Konstantinov and O.N. Budenkova, *Numerical and Experimental Study of Thermal Convection under Quasi-static Component of Microgravity Field*, **Proc. 1 Int. Symp. on Microgravity Research & Applications in Physical Sciences & Biotechnology 2002**, 167-174
- [PC35] V. V. Batkovich, O. N. Budenkova, O. L. Sadov, E. A. Smirnova, *Extraction of fringe skeleton and data organization using n-ary trees in automatic interferogram processing*, **Proc. SPIE 2001.-Vol.4680, P.244**
- [PC36] O. N. Budenkova, *Numerical simulation of speckle patterns under different conditions of their observation*, **Proc. SPIE**, 2001, 4680, 238-243

Seminars, Workshop, Collocs

- [C1] Olga Budenkova, Yves Delannoy, Annie Gagnoud, Didier Chaussende, *Application de la calorimétrie modulée aux métaux liquides en lévitation électromagnétique*, **Colloque Annuel du GDR MFA 2799**, Octobre 2020, en ligne

- [C2] Olga Budenkova, Yves Delannoy, Annie Gagnoud, *Application de la calorimétrie modulée aux métaux liquides en lévitation électromagnétique*, **Colloque Annuel du GDR MFA 2799, Octobre 2019, La Rochelle, France**
- [C3] Olga Budenkova, Mikus Milgravis, Christian Garnier, Annie Gagnoud, Yves Delannoy, Paul Chometon, Sophie Rivoirard, Mazen Alamir, *Application de calorimétrie modulée aux métaux liquide en lévitation avec un champ continue surimposé*, **Colloque Annuel du GDR MFA 2799, Nov 2018, Marseille, France**
- [C4] Lucas Dubald, Christian Garnier, Olga Budenkova, A. Gagnoud, Yves Delannoy, et al., *Measurement of thermophysical properties by modulated calorimetry in electromagnetic levitation: experimental results for Ni and Al-7wt%Si alloy*. **Colloque annuel du GDR MFA 2799, Nov 2017, Fréjus, France**
- [C5] Y. Du Terrail Couvat, N. Bernabeu, R. Tarpagkou, A. Gagnoud, O. Budenkova, Y. Fautrelle, *Finite element multigrid and adaptive mesh approaches to numerical simulations of the coupled phenomena related to magneto-thermoelectric effects in solidification of metals*, **Colloque « La Métallurgie, quel avenir ! », Réseau National de la Métallurgie / SF2M, June 27th to July 1st, 2016, Saint-Étienne, France**
- [C6] O. Budenkova, Y. Fautrelle, S. Steinbach, *Numerical and experimental results in solidification of a ternary alloy Al-7wt%Si-1wt%Fe obtained within MICAST project*, **Colloque du GDR MFA Micropesanteur Fondamentale et Appliquée, Ballaruc-Les-Bains, 10-13 Novembre 2015**
- [C7] F. Baltaretu, O. Budenkova, M. Dumont, A. Ciobanas, A. M. Bianchi, Y. Fautrelle, *Thermal phenomena in processes with liqui-solid phase changes; Thermique mise en jeu dans les procedes de changement de phase liquide-solide*, **Proc. 6th Colloquium on Energy-Environment-Economy and Thermodynamics COFRET 2012, Jun 2012, Sozopol, Bulgaria.**
- [C8] Yves Fautrelle, Olga Budenkova, Kader Zaidat, *Mise en place des structures et formation des macro et mésoségrégations dans les procédés de solidification*, **colloque annuelle du GDR 3328 Solidification des Alliages Metalliques, Ecole des Mines de Nancy, 12-14 Septembre 2012**
- [C9] Hervé Combeau, Michel Bellet, Yves Fautrelle, Dominique Gobin, Mohamed A. Rady, Eric Arquis, Olga Budenkova, Bernard Dussoubs, Yves Du Terrail, Arvind Kumar, Charles-André Gandin, Benoit Goyeau, Salem Mosbah, Miha Zaloznik, *Benchmark sur la simulation des macroségrégations lors de la solidification d'un alliage: première synthèse*, **Proc. Congrès de la Société Française de Thermique, 25-28 Mai 2010, Le Touquet, France** http://www.sft.asso.fr/Local/sft/dir/user-3775/documents/actes/Congres_2010/communications/203.pdf
- [C10] Hervé Combeau, Michel Bellet, Yves Fautrelle, Dominique Gobin, Mohamed A. Rady, Eric Arquis, Olga Budenkova, Bernard Dussoubs, Yves Du Terrail, Arvind Kumar, Charles-André Gandin, Benoit Goyeau, Salem Mosbah, Miha Zaloznik, *Formation de macroségrégations pendant la solidification d'un alliage Sn-Pb: Synthèse des premiers résultats d'un benchmark*, **Proc. Matériaux, 18-22 October 2010, Nantes, France**
- [C11] O. Budenkova, M. Dumont, Y. Fautrelle, J. Etay, S. Rex, U. Hecht, S. McFadden, A. Kartavykh, D. Voss, *Solidification of Ti-Al alloys in microgravity in MAXUS-8 sounding rocket*, **colloque**

annuels de GDR 2799 Micropesanteur Fondamentale et Appliquée, Antibes 17-20 October 2010

- [C12] O.Budenkova, Y. Fautrelle, *Numerical modelling of the directional solidification of metallic alloys: applications to micro- and hyper-gravity situations*, **colloque annuels de GDR 2799 Micropesanteur Fondamentale et Appliquée, Balaruc Les Bains, 22-25 November 2009**